SPECTRAL METHODS FOR LIMITED AREA MODELS

Submitted by

Scott R. Fulton

Department of Atmospheric Science

In partial fulfillment of the requirements

for the Degree of Doctor of Philosophy

Colorado State University

Fort Collins, Colorado

Fall 1984

COLORADO STATE UNIVERSITY

6 November 19 84

WE HEREBY RECOMMEND THAT THE THESIS PREPARED UNDER OUR SUPERVISION

BY Scott R. Fulton

ENTITLED Spectral Methods for Limited Area Models

BE ACCEPTED AS FULFILLING IN PART REQUIREMENTS FOR THE DEGREE OF

Doctor of Philosophy

Committee on Graduate Work

Gerald P. Taylor

David A. Krueger

Duane E. Stevens

Richard H. Johnson

Wayne H. Schubert

Adviser

Department Head

ABSTRACT OF DISSERTATION

SPECTRAL METHODS FOR LIMITED AREA MODELS

This study investigates the usefulness of Chebyshev spectral methods in limited area atmospheric modeling. Basic concepts of spectral methods and properties of Chebyshev polynomials are reviewed. Chebyshev spectral methods are illustrated by applying them to the linear advection equation in one dimension. Numerical results demonstrate the high accuracy obtained compared to finite difference methods.

The nonlinear shallow water equations on a bounded domain in two dimensions are then considered as a more realistic prototype model. Characteristic boundary conditions based on Reimann invariants are developed, and contrasted with wall conditions and boundary conditions based on the assumption of balanced flow. Chebyshev tau and collocation methods are developed for this model. Results from one-dimensional tests show the superiority of the characteristic conditions in most situations. Results from two-dimensional tests are also presented. Comparison of the tau and collocation methods shows that each has its own advantages and both are practical.

Time differencing schemes for Chebyshev spectral methods are studied. The stability condition obtained with explicit time differencing, often thought to be "severe", is shown to be less severe than the corresponding condition for finite difference methods. Numerical results and asymptotic estimates show that time steps may in

fact be limited by accuracy rather than stability, in which case simple explicit time differencing is practical and efficient. Two modified explicit schemes are reviewed, and implicit time differencing is also discussed.

A Chebyshev spectral method is also used to solve the vertical structure problem associated with vertical normal mode transforms in a hydrostatic atmosphere. Numerical results demonstrate the accuracy of the method, and illustrate the aliasing which can occur unless the vertical levels at which data is supplied are carefully chosen. Vertical transforms of observed forcings of tropical wind and mass fields are presented.

The results of this study indicate that Chebyshev spectral methods are a practical alternative to finite difference methods for limited area modeling, especially when high accuracy is desired. Spectral methods require less storage than finite difference methods, are more efficient when high enough accuracy is desired, and are at least as easy to program.

Scott R. Fulton
Department of Atmospheric Science
Colorado State University
Fort Collins, CO 80523
Fall 1984

ACKNOWLEDGMENTS

I would like to thank my adviser, Professor Wayne H. Schubert, for his guidance and support during this work and throughout my tenure as a graduate student. Many thanks also go to the other members of my advisory committee, Professors Duane E. Stevens, Richard H. Johnson, Gerald D. Taylor and David A. Krueger, for their careful review of this dissertation. I have benefitted greatly from discussions with Mark DeMaria, James J. Hack and Pedro L. Silva Dias, and thank them for their comments and suggestions. I am also grateful to Roger Daley for his interest in this work, and to Michio Yanai for supplying the data used in chapter 5.

A special note of thanks goes to Odilia Panella, who typed this dissertation. She completed this difficult and intimidating task expertly and efficiently, and her cheerful help is gratefully acknowledged.

This work was supported by the National Science Foundation under Grant ATM-8207563 and the Office of Naval Research under Contract N00014-84-C-0591. Acknowledgment is also made to the National Center for Atmospheric Research, which is sponsored by the National Science Foundation, for computer time used in this research.

TABLE OF CONTENTS

TABLE OF CONTENTS continued

CHAPTER 1

INTRODUCTION

With the advent of large digital computers, numerical modeling has taken an important place in atmospheric science. Numerical models allow the researcher to study in detail various physical processes which would be difficult or impossible to observe directly, and to perform "experiments" which could never be carried out in the real atmosphere. In addition, numerical models already play a central role in operational weather forecasting, and their importance in this area will no doubt continue to grow as modeling techniques and computer performance improve.

Constructing a numerical model involves an interplay between physical and mathematical considerations. The first step is to formulate a set of governing equations in continuous form which represents the physical processes of interest. This step is primarily a "physics" problem, although the form which the equations take may be guided by mathematical considerations. The second step is to discretize the governing equations so they may be solved on a computer. This step is primarily a "mathematics" problem, although the discretization may be guided by physical considerations. The third step is to construct appropriate parameterizations, i.e. implicit representations of physical processes which cannot be resolved explicitly in the numerical solution. These parameterizations may be based on physical or mathematical theories or on empirical results, and their formulation often

constitutes a major part of the effort of constructing the model. A comprehensive overview of these aspects of numerical modeling may be found in Haltiner and Williams (1980). In this thesis we will concentrate primarily on the second step mentioned above: the construction of appropriate discretizations and the efficient solution of the resulting discrete equations.

The earliest numerical models of the atmosphere were based on finite differences, and this discretization method remains perhaps the most common to this day. In it, the continuous fields such as wind, temperature, and pressure are represented by their values at a finite set of points which form the computational grid. Discrete analogues of the governing equations are then formed using finite difference approximations to the derivatives. Finite difference methods have been widely used for years, and in general are reasonably efficient, reasonably accurate and reasonably well-understood.

Recently, new discretization methods have been introduced, primarily by the engineering community, including finite element and spectral methods. In both of these methods the dependent variables are represented by truncated series of known basis functions, with the series coefficients determined by an appropriate projection of the governing equations (e.g., Galerkin or collocation projection). Choosing basis functions which are local (i.e., nonzero over only a small part of the computational domain) leads to finite element methods. These methods are reasonably efficient and often more accurate than finite difference methods. Choosing basis functions which are global (i.e., nonzero over essentially the whole computational domain) leads to spectral methods. These methods are extremely accurate; in particular,

they result in little or no phase error (computational dispersion) and hence are well suited to the accurate simulation of wave processes such as those which occur in the atmosphere. Since they allow very good approximations to be obtained with relatively few degrees of freedom, spectral methods require relatively little storage and are potentially very efficient.

Atmospheric models can be divided into two primary classes: global models and limited area models. As the name implies, a global model represents large-scale circulation features over the entire globe, and thus has no lateral boundaries. With present computer capabilities, however, global models cannot achieve sufficient resolution for the detailed study or prediction of smaller-scale phenomena such as fronts and tropical cyclones. One way to achieve the needed resolution is to restrict the computational domain to less than the entire globe, resulting in a limited area model. Such a model invariably has computational boundaries, i.e. boundaries of the computational domain which have no physical counterparts. A fundamental problem in limited area modeling is to minimize the impact of these computational boundaries on the solution.

Although spectral methods have been used with great success in global atmospheric models (e.g. Bourke et al., 1977; Machenhauer, 1979), their uses in limited area atmospheric models have been few. Haidvogel et al. (1980) compared spectral, finite element and finite difference discretizations for limited area ocean models based on the barotropic vorticity equation. DeMaria and Schubert (1984) used spectral techniques in a primitive equation hurricane model with the simplifying but unrealistic assumption of periodicity in both horizontal directions.

Spectral methods based on normal mode expansions have also been used in hurricane modeling (Schubert and DeMaria, 1984); this technique is promising but requires boundary conditions which reflect propagating gravity waves. More general spectral techniques, based on Chebyshev polynomial expansions, have been developed by the applied mathematics community (e.g. Orszag, 1971a,b; Orszag and Israeli, 1974; Gottlieb and Orszag, 1977). The purpose of this thesis is to investigate the usefulness of such techniques in limited area atmospheric modeling.

Chapter 2 consists of an overview of the basic concepts of spectral models as appropriate for limited area problems. A brief discussion of discretization schemes is followed by an examination of the choice of appropriate basis functions, using the convergence properties of Sturm-Liouville series to motivate the use of Chebyshev polynomials. Galerkin, tau, and collocation projections are then defined and contrasted. These ideas are all illustrated by applying them to the one-dimensional linear advection equation. The numerical results presented demonstrate the high accuracy of the spectral method in comparison to two simple finite difference schemes.

In Chapter 3 these concepts are extended to the two-dimensional nonlinear shallow-water equations. Some of the properties of the continuous form of this model are examined first and used in constructing appropriate boundary conditions for limited area simulations. Chebyshev spectral methods are then formulated using both the tau and collocation projections. The results presented for simple test cases illustrate the differences obtained by using different boundary conditions, projections and forms of the governing equations.

Time differencing for Chebyshev spectral methods is addressed in Chapter 4. Explicit schemes, which are the easiest to implement, are discussed first. The related questions of accuracy, stability and efficiency are discussed, and numerical results and asymptotic estimates are presented which indicate that explicit time differencing may be practical and efficient. Two modified explicit schemes which have been proposed for use with spectral methods are also examined. In some cases implicit time differencing may give greater efficiency; the implementation of implicit schemes is outlined for the tau and collocation methods.

In Chapter 5 a Chebyshev spectral method is used to solve the vertical structure problem associated with vertical normal mode transforms in a hydrostatic atmosphere; these transforms are a means of separating the vertical and horizontal dependence of the wind and mass fields. First the theory of vertical transforms is reviewed, and then their numerical implementation is discussed. Atmospheric data is generally obtained only at discrete levels in the vertical; numerical results are presented which demonstrate the effects of the choice of data levels. Spectral space profiles of observed tropical forcings of the wind and mass fields are also presented.

Chapter 6 summarizes the principal conclusions of this study and includes recommendations for further work.

CHAPTER 2

BASIC CHEBYSHEV SPECTRAL TECHNIQUES

Spectral methods are techniques for constructing highly accurate discretizations of problems involving differential equations. In a spectral discretization the dependent variables are approximated by truncated series expansions in terms of global basis functions, using a projection to relate the expansions to the problem to be solved. In this chapter we discuss these ideas in the context of limited area problems. In section 2.1 the basic concept of spectral discretization is reviewed. We examine the choice of basis functions in section 2.2, using the convergence of Sturm-Liouville series to motivate the use of Chebyshev polynomials and then reviewing their properties. In section 2.3, three projections are described and contrasted. These ideas are illustrated in section 2.4 by applying them to the linear advection equation.

2.1 Discretization Schemes

The problems to be considered in this study consist of differential equations of the general form

$$\frac{\partial u(x,t)}{\partial t} + L\, u(x,t) = f(u,x,t) \qquad (2.1)$$

coupled with appropriate initial and boundary conditions. Here x and t represent space and time coordinates, u is the unknown, L is a linear

operator involving spatial derivatives, and f represents nonlinear terms and/or specified forcing. Problems in more than one spatial dimension and systems of equations also fit the same general form with x and u, respectively, interpreted as vectors. When the continuous problem (2.1) cannot be solved analytically in closed form, one looks for ways to discretize it so it may be solved on a computer. In this section we consider spatial discretization schemes; time discretization will be discussed in chapter 4.

In one class of discretization schemes the unknown u is represented by its values at discrete points (gridpoints) in space and the derivatives in L are approximated by finite differences. Such finite difference schemes exhibit algebraic convergence, i.e. the error in the approximation is asymptotically proportional to N^{-r}, where N is the number of degrees of freedom (gridpoints) and r is a fixed positive number (usually r=2 or r=4). Finite difference methods have been used extensively in atmospheric models and are relatively easy to formulate and program.

A second class of discretization schemes is based on approximating the unknown u by a truncated series expansion of the form

$$u_N(x,t) = \sum_{n=0}^{N} \hat{u}_n(t)\, \phi_n(x) , \qquad (2.2)$$

where $\phi_0(x),\ldots,\phi_N(x)$ are fixed basis functions and N is a positive integer. The coefficients $\hat{u}_0(t),\ldots,\hat{u}_N(t)$ in the expansion are determined by requiring that (2.1) be approximately satisfied with u replaced by u_N ; in mathematical terms this amounts to a projection of the true solution u into the space spanned by the basis $\phi_0,\ldots,\phi_N$. In

this approach Lu_N may be computed exactly since L is linear and the functions $\phi_n(x)$ are known.

If the basis functions chosen are local, i.e. each nonzero over only a small part of the computational domain, the series expansion method above is called a finite element method (Strang and Fix, 1973). Such schemes are similar to higher-order finite difference schemes in terms of complexity and efficiency, and in particular exhibit algebraic convergence. As their principal advantage seems to lie in the ease of treating problems in complex geometries (e.g. flow over an airfoil or around a missile), their use in atmospheric science has been limited (Cullen, 1974; Staniforth and Mitchell, 1977).

In contrast, if the basis functions chosen are global, i.e. each nonzero over basically the whole computational domain, the series expansion method above is called a spectral method. A properly formulated spectral method exhibits exponential convergence, i.e. the error in the approximation goes to zero faster than N^{-r} for any finite r as N increases. Thus spectral discretizations can provide highly accurate approximations with far fewer degrees of freedom than required by finite difference or finite element methods. The price one pays for this high accuracy is the additional complexity introduced by the use of global basis functions. However, with the proper choices of basis functions and projections, spectral methods can be quite efficient. We examine these choices in the following sections.

2.2 Basis Functions

Spectral methods have been used for some time now in global atmospheric models (i.e., models of the circulation over the entire

globe), and the basis functions for such models have been studied in detail (Orszag, 1974; Boyd, 1978). In contrast, limited area modeling using spectral techniques has been confined primarily to the engineering community, and the basis functions appropriate to such models are less well known. As these functions are usually the solutions of a Sturm-Liouville problem, we examine the convergence of expansions based on these solutions in section 2.2.1. In section 2.2.2 we describe the particular basis functions most useful for limited area modeling, namely, the Chebyshev polynomials.

2.2.1 Sturm-Liouville expansions. The general Sturm-Liouville equation is

$$L_{SL}\phi(x) = -[p(x)\phi'(x)]' + q(x)\phi(x) = \lambda\, w(x)\phi(x) \ , \qquad (2.3)$$

where primes denote differentiation with respect to x. We seek solutions of this equation on a finite interval [a,b] which corresponds to the limited domain on which a problem of the form (2.1) is to be solved. With suitable boundary conditions and restrictions on the functions p, q, and w, (2.3) has a countably infinite set of solutions $\{\phi_n(x)\}_{n=o}^{\infty}$ corresponding to discrete eigenvalues $\{\lambda_n\}_{n=o}^{\infty}$ with $\lambda_n < \lambda_{n+1}$ and $\lambda_n \to \infty$ as $n \to \infty$. These eigenfunctions are orthonormal in the inner product

$$(f,g)_w = \int_a^b f(x)g(x)w(x)\, dx \ , \qquad (2.4)$$

that is, $(\phi_m, \phi_n)_w = \delta_{mn}$ ($\delta_{mn}=1$ if m=n and 0 otherwise). Furthermore, they form a complete set in the sense that any suitably smooth function u(x) may be expanded as

$$u(x) = \sum_{n=0}^{\infty} \hat{u}_n \, \phi_n(x) \tag{2.5}$$

where

$$\hat{u}_n = (u,\phi_n)_w \, . \tag{2.6}$$

This completeness property says that the true solution u of (2.1) may be expressed exactly as an infinite series of such eigenfunctions. However, their usefulness as basis functions for a spectral method depends on how many terms must be retained in a finite series in order to adequately approximate u.

To address this question let $u_N(x)$ denote the series (2.5) truncated after n=N. Following Gottlieb and Orszag (1977), we use the Parseval relation to write the error $u-u_N$ in the norm $\|f\|_w = \sqrt{(f,f)_w}$ generated by the inner product (2.4) as

$$\left\|u-u_N\right\|_w^2 = \left\| \sum_{n=N+1}^{\infty} \hat{u}_n \, \phi_n \right\|_w^2 = \sum_{n=N+1}^{\infty} \hat{u}_n^2 \, . \tag{2.7}$$

Thus the rate at which the error $u-u_N$ decreases with increasing N is governed by the rate at which the coefficients $\hat{u}_n$ decrease with increasing n. In particular, if $\hat{u}_n = O(n^{-r})$ as $n \to \infty$ for some $r > \frac{1}{2}$ then it is easily shown from (2.7) that $\|u-u_N\|_w = O(N^{-r})$ as $N \to \infty$. To estimate $\hat{u}_n$ we substitute for ϕ_n in (2.6) from (2.3) and integrate by parts twice (assuming u is sufficiently smooth so that this is valid) to obtain

$$\hat{u}_n = \frac{1}{\lambda_n} \left(u, \frac{L_{SL}\phi_n}{w}\right)_w = \frac{1}{\lambda_n} \left[(v,\phi_n)_w + B(u,\phi_n)\right] \, . \tag{2.8}$$

Here $v=(1/w)\ L_{SL}u$ and

$$B(u,\phi_n) = \left\{p(x)\ [u'(x)\phi_n(x)-u(x)\phi_n'(x)]\right\}\Big|_{x=a}^{x=b} . \qquad (2.9)$$

The term $(v,\phi_n)_w$ in (2.8) is bounded independent of n, since by the Cauchy-Schwartz inequality $\left|(v,\phi_n)_w\right| \leq \|v\|_w \|\phi_n\|_w$ and $\|\phi_n\|_w=1$. The value of the boundary term $B(u,\phi_n)$ depends in general on the behavior of both the function u and the eigenfunctions ϕ_n at the boundaries.

If $p(a)\neq 0$ and $p(b)\neq 0$ in (2.3) and appropriate linear homogeneous boundary conditions are applied, the Sturm-Liouville problem is said to be <u>regular</u> at both endpoints. Examples of appropriate boundary conditions include periodicity and the unmixed conditions

$$\left.\begin{aligned} \phi(a)\cos\alpha - \phi'(a)\sin\alpha &= 0 \\ \phi(b)\cos\beta + \phi'(b)\sin\beta &= 0 \end{aligned}\right\} , \qquad (2.10)$$

where α and β are specified constants. In this case the eigenvalues and eigenvectors have the asymptotic behavior $\lambda_n = O(n^2)$, $\phi_n(x) = O(1)$, $\phi_n'(x) = O(n)$ as $n\to\infty$ (Courant and Hilbert, 1953). If u does not satisfy the boundary conditions applied to the Sturm-Liouville problem, then $B(u,\phi_n) = O(n)$ and $\hat{u}_n = O(n^{-1})$ [$B(u,\phi_n) = O(1)$ and $\hat{u}_n = O(n^{-2})$ if $u(a) = u(b)=0$]. This slow convergence is a reflection of the Gibbs phenomenon associated with u not satisfying the boundary conditions satisfied by the expansion functions ϕ_n; this phenomenon is discussed in detail in Gottlieb and Orzag (1977). If u does satisfy the boundary conditions, $B(u,\phi_n)$ vanishes and the integration by parts argument may be repeated (again assuming u is sufficiently smooth) to obtain

$$\hat{u}_n = \frac{1}{\lambda_n^2}\left[(z,\phi_n)_w + B(v,\phi_n)\right] \quad , \tag{2.11}$$

where $z=(1/w)\ L_{SL}v$. Again $(z,\phi_n)_w = O(1)$ and $B(v,\phi_n) = O(n)$, so $\hat{u}_n = O(n^{-3})$ and the convergence is faster. However, in general the argument may not be repeated again since $B(v,\phi_n) \neq 0$. Thus we see that the rate of convergence of expansions based on eigenfunctions of a <u>regular</u> Sturm-Liouville problem depends both on the smoothness of the function being expanded and on its behavior at the boundaries.

If $p(a)=p(b)=0$ in (2.3) the Sturm-Liouville problem is said to be <u>singular</u> at both endpoints. In this case $B(u,\phi_n)=0$ for any bounded function u, so the integration by parts may be repeated as long as the function being integrated is smooth enough. Therefore, if u is infinitely differentiable then $\hat{u}_n < O(n^{-r})$ for all $r>0$ so the convergence is exponential. (Exponential convergence may also be obtained in the regular case with periodic boundary conditions, but only if u is also periodic.) We conclude that the rate of convergence of expansions based on eigenfunctions of a singular Sturm-Liouville problem depends only on the smoothness of the function being expanded and not on its behavior at the boundaries. Such expansions are therefore appropriate for limited area spectral models in which the behavior of the solution at the boundary is not artificially restricted by applying periodicity or wall conditions.

The actual choice of basis functions is guided by some practical considerations in addition to those described above. Polynomials are particularly convenient as basis functions, especially since their derivatives are again polynomials and thus exactly expressible in terms

of the basis. Two sets of common orthogonal polynomials satisfy Sturm-Liouville problems which are singular at finite endpoints as discussed above: the Legendre polynomials $P_n(x)$, for which $[a,b]=[-1,+1]$, $p(x)=1-x^2$, $q(x)=0$ and $w(x)=1$, and the Chebyshev polynomials $T_n(x)$, for which $[a,b]=[-1,+1]$, $p(x)=(1-x^2)^{\frac{1}{2}}$, $q(x)=0$ and $w(x)=(1-x^2)^{-\frac{1}{2}}$. Although Legendre series may give better approximations than Chebyshev series at the endpoints (Lanczos, 1973), the latter are usually preferred for the following three reasons. First, Chebyshev series give somewhat better (global) approximations than do Legendre series for the same number of terms. In fact, the Chebyshev approximation of degree N of a function is very nearly equal to the best approximation which can be obtained by <u>any</u> polynomial of degree N, in the sense of minimizing the maximum pointwise error (Rivlin, 1969). Second, Chebyshev series converge faster than Legendre series when the function being expanded is not smooth (Gottlieb and Orszag, 1977). Third, and perhaps most important, Chebyshev series can be evaluated very efficiently using the Fast Fourier Transform (FFT) algorithm (Brigham, 1974). This point will be addressed in the next section, in which we discuss the properties of Chebyshev polynomials.

2.2.2 <u>Chebyshev polynomials.</u> Much has been written about the Chebyshev polynomials and their many uses in applied mathematics. Here we present only the main properties which will be needed in this study; more complete discussions may be found in Snyder (1966) and Fox and Parker (1968). For our purposes we regard the Chebyshev polynomials $T_n(x)$ as being defined on the interval $-1 \leq x \leq 1$ by

$$T_n(\cos\theta) = \cos(n\theta) \tag{2.12}$$

where $x=\cos\theta$. From (2.12) we immediately have $T_0(x)=1$ and $T_1(x)=x$, and the trigonometric identity $\cos(n\theta) = 2\cos\theta\cos[(n-1)\theta]-\cos[(n-2)\theta]$ yields the recurrence relation

$$T_n(x) = 2x\,T_{n-1}(x) - T_{n-2}(x)\ . \tag{2.13}$$

The first five Chebyshev polynomials are shown in Fig. 1, from which it is evident that the extrema of $T_n(x)$ all have absolute value 1. In fact, from (2.12) the zeros of $T_n(x)$ occur at

$$\tilde{x}_j^{(n)} = \cos\left[(j+\tfrac{1}{2})\,\frac{\pi}{n}\right] \qquad (j=0,\ldots,n-1) \tag{2.14}$$

and the extrema at

$$\bar{x}_j^{(n)} = \cos\left(\frac{j\pi}{n}\right) \qquad (j=0,\ldots,n) \tag{2.15}$$

with $T_n(\bar{x}_j^{(n)})=(-1)^j$. In particular, $T_n(1)=1$ and $T_n(-1)=(-1)^n$ for $n=0,1,2,\ldots$. Note that both the zeros and the extrema have spacing $O(\frac{1}{n})$ near $x=0$ and $O(\frac{1}{n^2})$ near $x=\pm1$.

The Chebyshev polynomials are orthogonal (but not normalized) in the Chebyshev inner product

$$\langle f,g\rangle = \int_{-1}^{1} \frac{f(x)g(x)}{(1-x^2)^{\frac{1}{2}}}\,dx \tag{2.16}$$

with

$$\langle T_m,T_n\rangle = \frac{\pi}{2}\,c_n\,\delta_{mn}\ , \qquad c_n = \begin{cases} 2 & n=0 \\ 1 & n>0 \end{cases}\ . \tag{2.17}$$

Thus the coefficients in the Chebyshev series

$$u(x) = \sum_{n=0}^{\infty} \hat{u}_n\,T_n(x) \tag{2.18a}$$

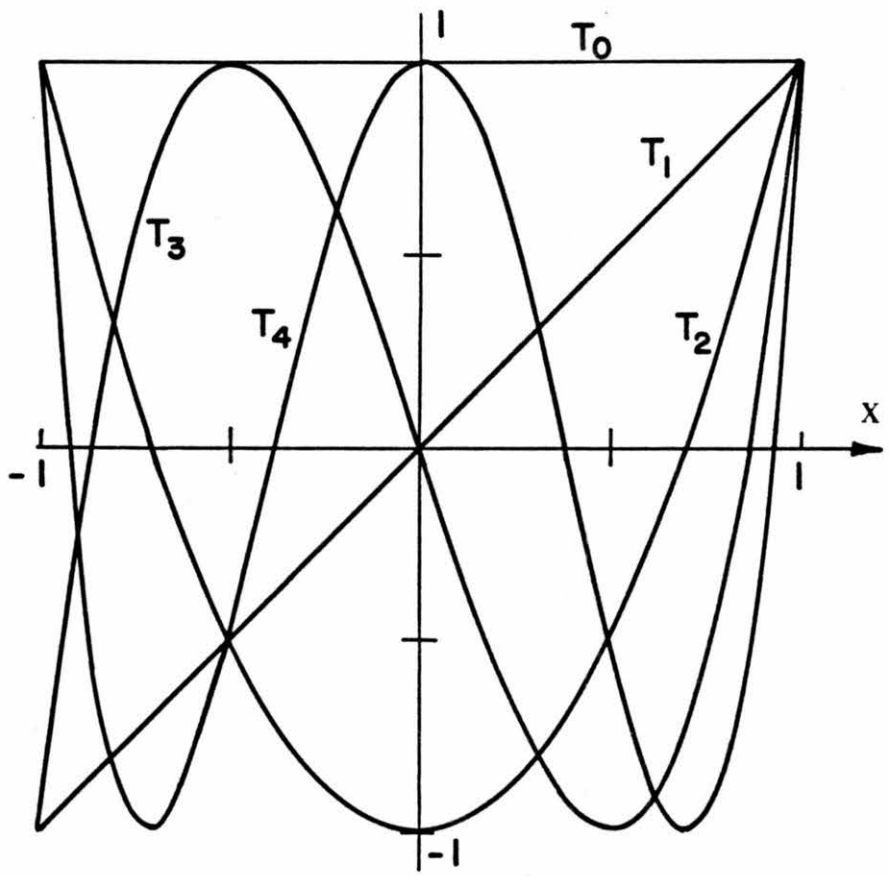

Figure 1. The first five Chebyshev polynomials $T_n(x)$.

are

$$\hat{u}_n = \frac{2}{\pi c_n} \langle u, T_n \rangle \quad . \tag{2.18b}$$

Equations (2.18) constitute the continuous Chebyshev transform pair. Substituting $x=\cos\theta$ and using (2.12) and (2.16) this pair becomes

$$u(\cos\theta) = \sum_{n=0}^{\infty} \hat{u}_n \cos(n\theta) \ , \tag{2.19a}$$

$$\hat{u}_n = \frac{2}{\pi c_n} \int_0^{\pi} u(\cos\theta)\cos(n\theta)\, d\theta \ , \tag{2.19b}$$

showing that the Chebyshev series in x for a function $u(x)$ is precisely the Fourier cosine series in θ for the function $u(\cos\theta)$. Thus the change of variable $x=\cos\theta$ introduces periodicity into the (possibly nonperiodic) function u, so provided only that u is sufficiently smooth the series converges quickly, regardless of the behavior of u at $x=\pm 1$.

For the truncated series

$$u_N(x) = \sum_{n=0}^{N} \hat{u}_n T_n(x) \tag{2.20}$$

the transform pair (2.18) has the discrete analogue

$$\bar{u}_j = \sum_{n=0}^{N} \hat{u}_n T_n(\bar{x}_j) \ , \tag{2.21a}$$

$$\hat{u}_n = \frac{2}{N\bar{c}_n} \sum_{j=0}^{N} \frac{1}{\bar{c}_j} \bar{u}_j T_n(\bar{x}_j) \ . \tag{2.21b}$$

Here $\bar{x}_j = \bar{x}_j^{(N)}$ $(j=0,\ldots,N)$ are the points at which $T_N(x)$ has extrema,

$\bar{u}_j = u_N(\bar{x}_j)$, and $\bar{c}_n = 2$ for n=0 and n=N and 1 otherwise. This discrete Chebyshev transform pair may be written as the discrete cosine transform pair

$$\bar{u}_j = \sum_{n=0}^{N} \hat{u}_n \cos\left(\frac{jn\pi}{N}\right), \tag{2.22a}$$

$$\hat{u}_n = \frac{2}{N\bar{c}_n} \sum_{j=0}^{N} \frac{1}{\bar{c}_j} \bar{u}_j \cos\left(\frac{jn\pi}{N}\right), \tag{2.22b}$$

either member of which may be evaluated in O(N log N) operations via the FFT algorithm for real symmetric data (Cooley et al., 1970). Note that (2.22b) amounts to approximating (2.19b) by trapezoidal quadrature (with a factor of 2 difference when n=N).

Many common operations on functions represented by Chebyshev series can be calculated easily in terms of the spectral coefficients. For example, if u(x) is given by (2.18a) then the derivative is

$$u'(x) = \sum_{n=0}^{\infty} \hat{u}_n^{(1)} T_n(x) \tag{2.23}$$

where

$$\hat{u}_n^{(1)} = \frac{2}{c_n} \sum_{\substack{m=n+1 \\ m+n \text{ odd}}}^{\infty} m \hat{u}_m . \tag{2.24}$$

Similarly,

$$xu'(x) = \sum_{n=0}^{\infty} [n\hat{u}_n + \hat{u}_n^{(1,x)}] T_n(x) \tag{2.25}$$

where

$$\hat{u}_n^{(1,x)} = \frac{2}{c_n} \sum_{\substack{m=n+2 \\ m+n \text{ even}}}^{\infty} m\hat{u}_m \ . \tag{2.26}$$

For the truncated series (2.20), (2.24) and (2.26) yield the recurrence formulas

$$c_{n-1}\, \hat{u}_{n-1}^{(1)} - \hat{u}_{n+1}^{(1)} = 2n\, \hat{u}_n \tag{2.27}$$

and

$$c_{n-1}\, \hat{u}_{n-1}^{(1,x)} - \hat{u}_{n+1}^{(1,x)} = 2(n+1)\, \hat{u}_{n+1} \tag{2.28}$$

for $n=1,\ldots,N-1$ with the starting values $\hat{u}_{N+1}^{(1)}=\hat{u}_N^{(1)}=\hat{u}_{N+1}^{(1,x)}=\hat{u}_N^{(1,x)}=0$. Thus the spectral coefficients for $u_N'(x)$ and $xu_N'(x)$ may be obtained from those for $u_N(x)$ in $O(N)$ operations.

2.3 Projections

Having discussed the basis functions in terms of which the dependent variables in a spectral model are to be expanded, we turn now to the approximation methods which relate those expansions to the problem to be solved. Such methods are known as projections, since they project the true solution into the space spanned by the basis functions. Substituting the spectral approximation $u_N(x,t)$ as given by (2.2) for the true solution $u(x,t)$ in (2.1) results in the expression $\tau_N(x,t)= \partial u_N/\partial t + Lu_N - f$, known as the truncation error, which in general is nonzero. The three projections in common use seek to make the truncation error approximately zero; they differ in the sense of approximation used.

The Galerkin projection (Galerkin, 1915) is the classical approximation used in spectral models in spherical geometry (Machenhauer, 1979). It defines u_N by requiring the truncation error to be orthogonal to each of the basis functions $\phi_0,\ldots,\phi_N$ in some inner product (,), so the truncation error is approximately zero in the sense that it has no projection onto the basis functions used in the model. Thus the Galerkin equations are

$$\left(\frac{\partial u_N}{\partial t} + L u_N \, , \, \phi_n \right) = (f,\phi_n) \qquad (n=0,\ldots,N \,; \quad t>0) \quad , \tag{2.29a}$$

$$(u_N \, , \, \phi_n) = (U,\phi_n) \qquad (n=0,\ldots,N \,; \quad t=0) \quad , \tag{2.29b}$$

where $U(x)$ is the initial value of $u(x,t)$. If the basis functions are orthonormal in the chosen inner product then (2.29) simplifies to

$$\frac{d\hat{u}_n}{dt} + \sum_{m=0}^{N} (L\,\phi_m,\phi_n)\,\hat{u}_m = (f,\phi_n) \qquad (n=0,\ldots,N \,; \quad t>0) \quad , \tag{2.30a}$$

$$\hat{u}_n = (U,\phi_n) \qquad (n=0,\ldots,N \,; \quad t=0) \quad . \tag{2.30b}$$

Solution of these equations is facilitated by choosing the basis functions ϕ_n and inner product (,) so that the summation in (2.30a) involves relatively few terms. In particular, if the ϕ_n are the normal modes of the system (i.e., the eigenfunctions of L) then (2.30a) reduces to

$$\frac{d\hat{u}_n}{dt} + \lambda_n \hat{u}_n = (f,\, \phi_n) \qquad (n=0,\ldots,N) \tag{2.31}$$

where $L\phi_n=\lambda_n\phi_n$. In this manner the equations are decoupled, except for possible coupling through nonlinear terms represented by f.

In the Galerkin projection the boundary conditions of the problem are handled implicitly by building them into the basis functions. That is, the basis functions must be chosen so that they individually satisfy the boundary conditions; these conditions in turn must be linear and homogeneous so they will be satisfied by the linear combination u_N. Since suitable basis functions which individually satisfy open boundary conditions can seldom be found, the Galerkin approximation is not well suited to many limited area problems. However, a simple modification removes this difficulty, leading to the tau projection of Lanczos (1938, 1956). In the tau approximation the basis functions need not individually satisfy the boundary conditions of the problem; rather, these conditions are applied explicitly to the truncated series u_N as a whole. With M as the number of independent boundary conditions to be applied, these equations simply replace the last M of equations (2.29a). Thus the tau equations are

$$\left.\begin{aligned}\left(\frac{\partial u_N}{\partial t} + L\,u_N,\ \phi_n\right) &= (f,\ \phi_n) \quad (n=0,\ldots,N-M\ ;\ \ t>0)\\ (u_N,\ \phi_n) &= (U,\ \phi_n) \quad (n=0,\ldots,N\ ;\ \ t=0)\end{aligned}\right\}, \tag{2.32}$$

together with the M boundary conditions applied to u_N for $t>0$. If the basis functions are orthonormal then (2.32) simplifies to the form of (2.30) as before.

The third projection in common use is collocation. In this approximation the truncation error is required to vanish at selected points known as collocation points. Usually it is most convenient to

choose basis functions which do not satisfy the boundary conditions of the problem, and then apply these conditions explicitly as in the tau method. Thus the collocation equations are

$$\left.\begin{aligned} \frac{du_N}{dt} + L\,u_N &= f \quad \text{at} \quad x=\bar{x}_j \quad (j=0,\ldots,N-M; \quad t>0) \\ u_N &= U \quad \text{at} \quad x=\bar{x}_j \quad (j=0,\ldots,N \quad ; \quad t=0) \end{aligned}\right\}, \tag{2.33}$$

where $\bar{x}_0,\ldots,\bar{x}_{N-M}$ denote the collocation points, together with the M boundary conditions applied to u_N for $t>0$. In this method the dependent variables are the boundary values of u_N and the values $\bar{u}_j(t)=u_N(\bar{x}_j,t)$ at the collocation points, rather than the spectral coefficients $\hat{u}_0,\ldots,\hat{u}_N$, with the series expansion (2.2) used only in evaluating Lu_N. Thus the collocation projection leads to equations much like those of finite difference methods but of very high accuracy. The collocation projection has been used extensively with local basis functions in finite element methods; when used with global basis functions the resulting methods are often called pseudospectral (Merilees and Orszag, 1979). This terminology emphasizes the connection with classical spectral (Galerkin and tau) methods -- in particular, the use of global basis functions and the resulting exponential convergence -- and de-emphasizes the connection with finite element collocation methods. As we shall see, the collocation projection is often extremely easy to implement, even when the problem to be solved is highly nonlinear.

2.4 Application to the Linear Advection Equation

To illustrate the concepts and methods discussed above we apply them to the one-dimensional linear advection equation

$$\frac{\partial u}{\partial t} + c\,\frac{\partial u}{\partial x} = f(x,t) \quad (-1 < x \leq 1\ ,\ \ t > 0\ ) \tag{2.34a}$$

with the boundary and initial conditions

$$u(-1,t) = g(t) \quad (t > 0)\ , \tag{2.34b}$$

$$u(x,t) = U(x) \quad (t = 0)\ . \tag{2.34c}$$

Here c is a positive constant, f represents specified forcing, and g and U are specified boundary and initial values. This problem is the simplest prototype of a limited area model involving wave or advective processes. When f=0 it has the analytical solution

$$u(x,t) = \left\{ \begin{array}{ll} U(x-ct) & x-ct \geq -1 \\ g(t-(x+1)/c) & x-ct < -1 \end{array} \right\}\ , \tag{2.35}$$

representing propagation or advection in the +x direction with speed c.

Following the discussion in the preceeding sections we seek an approximate solution in the form of the Chebyshev expansion

$$u_N(x,t) = \sum_{n=0}^{N} \hat{u}_n(t)\ T_n(x)\ . \tag{2.36}$$

The spectral (tau) approximation to (2.34) is defined by

$$\left.\begin{array}{ll} \left\langle \frac{\partial u_N}{\partial t} + c\,\frac{\partial u_N}{\partial x}\ ,\ T_n \right\rangle = \langle f, T_n \rangle & (n=0,\ldots,N-1\ ;\ t>0) \\ u_N(-1,t) = g(t) & (t>0) \\ \langle u_N, T_n \rangle = \langle U, T_n \rangle & (n=0,\ldots,N\ ;\ t=0) \end{array}\right\} \tag{2.37}$$

where $\langle\ ,\ \rangle$ denotes the Chebyshev inner product (2.16). Substituting

from (2.36) for u_N and using the orthogonality property (2.17) and the property $T_n(-1)=(-1)^n$, the tau equations (2.37) reduce to

$$\frac{d\hat{u}_n}{dt} + c\,\hat{u}_n^{(1)} = \hat{f}_n \qquad (n=0,\ldots,N-1\ ;\ t>0) \quad , \tag{2.38a}$$

$$\sum_{n=0}^{N} (-1)^n\,\hat{u}_n = g \qquad (t>0) \quad , \tag{2.38b}$$

$$\hat{u}_n = \frac{2}{\pi c_n}\,\langle U, T_n\rangle \qquad (n=0,\ldots,N\ ;\ t=0) \quad , \tag{2.38c}$$

where $\hat{f}_n = \frac{2}{\pi c_n}\langle f, T_n\rangle$ and $\hat{u}_n^{(1)} = \frac{2}{\pi c_n}\langle \frac{\partial u_N}{\partial x}\ , T_n\rangle$ as given by (2.24). Methods for solving this coupled system of ordinary differential equations in t for the spectral coefficients $\hat{u}_0(t),\ldots,\hat{u}_N(t)$ will be discussed in detail in chapter 4. Here we simply note that with explicit time differencing, such as the forward (Euler) scheme, (2.38a) can be used to predict new values of $\hat{u}_0,\ldots,\hat{u}_{N-1}$ from those at the previous time level, and then $\hat{u}_N$ can be diagnosed from (2.38b). Using the recurrence relation (2.27) to compute the spectral coefficients $\hat{u}_n^{(1)}$ of the derivative this procedure takes only O(N) operations per time step, in spite of the global nature of the spectral approximation.

We note in passing that the reason for the excellent error properties of this approximation can be readily seen from (2.37). Indeed, expanding the truncation error τ_N in the Chebyshev series

$$\tau_N(x,t) = \frac{\partial u_N}{\partial t} + c\,\frac{\partial u_N}{\partial x} - f = \sum_{n=0}^{\infty} \hat{\tau}_n(t)\,T_n(x)\ , \tag{2.39}$$

we obtain immediately from (2.36) and (2.37) that

$$\hat{\tau}_n = \begin{cases} 0 & 0 \le n < N \\ \frac{2}{\pi c_n} \langle \tau_n, T_n \rangle & n = N \\ -\hat{f}_n & N < n \end{cases} . \qquad (2.40)$$

Thus if f is smooth enough that the coefficients $\hat{f}_n$ decay rapidly as $n \to \infty$, then for sufficiently large N (i.e., N large enough to resolve the behavior of u as forced by f) the truncation error τ_N is dominated by the term $\hat{\tau}_N(t)T_N(x)$. Since $T_N(x)$ oscillates with equal amplitude on the interval [-1,1], the truncation error is distributed equally across the domain, resulting in a good approximation in a global sense. The use of the symbol "τ" by Lanczos for the expansion coefficients of the truncation error is the source of the name "tau method."

For the pseudospectral (collocation) approximation to (2.34) we choose as collocation points the points $\bar{x}_j = \bar{x}_j^{(N)} = \cos(j\pi/N)$ (j=0,...,N) at which $T_N(x)$ has extrema. Since $\bar{x}_N = -1$ is the boundary point, the collocation equations are

$$\left.\begin{aligned} \frac{\partial u_N}{\partial t} + c\,\frac{\partial u_N}{\partial x} &= f \quad \text{at} \quad x = \bar{x}_j \qquad (j=0,\ldots,N-1 \ ; \ t>0) \\ u_N(-1,t) &= g(t) \qquad\qquad\qquad (t>0) \\ u_N(\bar{x}_j,t) &= U(\bar{x}_j) \qquad\qquad (j=0,\ldots,N \ ; \ t=0) \end{aligned}\right\} , \qquad (2.41)$$

which may be written as

$$\frac{d\bar{u}_j}{dt} + c\,\bar{u}_j^{(1)} = \bar{f}_j \qquad (j=0,\ldots,N-1 \ ; \ t>0) \quad , \qquad (2.42a)$$

$$\bar{u}_N = g \qquad (t>0) \quad , \qquad (2.42b)$$

$$\bar{u}_j = U(\bar{x}_j) \qquad (j=0,\ldots,N \ ; \ t=0) \quad , \qquad (2.42c)$$

where $\bar{u}_j(t)=u_N(\bar{x}_j,t)$, $\bar{f}_j(t)= f(\bar{x}_j,t)$ and $\bar{u}_j^{(1)}(t)= \frac{\partial u_N}{\partial x}(x_j,t)$. With explicit time differencing, this coupled system of ordinary differential equations for the values $\bar{u}_0(t),\ldots,\bar{u}_N(t)$ may be solved by using (2.42a) to predict new values $\bar{u}_0,\ldots,\bar{u}_{N-1}$ from those at the previous time level and then using (2.42b) to obtain $\bar{u}_N$. In computing the derivative values $\bar{u}_j^{(1)}$ we make use of the spectral representation (2.36) as follows. First, the spectral coefficients $\hat{u}_0,\ldots,\hat{u}_N$ are obtained from the values $\bar{u}_0,\ldots,\bar{u}_N$ via the discrete Chebyshev transform (2.21b) (note that these coefficients will be different than those in the tau approximation). Next, the recurrence relation (2.27) is used to compute the spectral coefficients $\hat{u}_0^{(1)},\ldots,\hat{u}_N^{(1)}$ of the derivative. Finally, these coefficients are used to compute the derivative values $\bar{u}_0^{(1)},\ldots,\bar{u}_N^{(1)}$ via the inverse transform (2.21a). Referring to the values $\bar{u}_j$ and coefficients $\hat{u}_n$ as "physical space" and "spectral space" representations of u_N, respectively, this calculation can be described as transforming u_N from physical to spectral space, computing the derivative there, and transforming the result back to physical space. Using the FFT algorithm in the transforms, this whole procedure takes only O(N log N) operations.

To illustrate the accuracy of the methods described above we compare them with simple finite difference methods. Specifically, we consider the first-order upstream difference scheme

$$\frac{d\tilde{u}_j}{dt} + c\,\frac{\tilde{u}_j - \tilde{u}_{j-1}}{\Delta x} = \tilde{f}_j \qquad (2.43)$$

and the second-order centered difference scheme

$$\frac{d\tilde{u}_j}{dt} + c\,\frac{\tilde{u}_{j+1} - \tilde{u}_{j-1}}{2\Delta x} = \tilde{f}_j\ , \tag{2.44}$$

where $(\tilde{\ })_j$ denotes values at the gridpoints $\tilde{x}_j = -1+j\Delta x$ $(j=0,\ldots,N)$ with $\Delta x=2/N$. For the results presented here we use initial conditions and forcing given by

$$\left.\begin{aligned} U(x) &= \exp\left[-\left(\frac{x-a}{b}\right)^2\right] \\ f(x,t) &= 0 \\ g(t) &= U(-1-ct) \end{aligned}\right\}\ , \tag{2.45}$$

with $a= -0.5$, $b=0.2$ and $c=1$. The analytical solution corresponding to (2.45) is

$$u(x,t) = U(x-ct) = \exp\left[-\left(\frac{x-ct-a}{b}\right)^2\right]. \tag{2.46}$$

Figure 2 shows the approximate solutions at $t=1.0$ obtained by the Chebyshev-tau method and the two finite difference methods using $N=8$, 16 and 32, along with the corresponding analytical solution. Chebyshev-collocation results are not shown, since they are practically identical to the tau results for this problem. The spectral method clearly gives a much better approximation than do the difference methods, even for small N. In particular, the spectral solution does not exhibit the computational dispersion which broadens both difference solutions and introduces spurious oscillations in the centered difference method. The corresponding error $u-u_N$ at $t=1.0$, measured in the L_2 norm

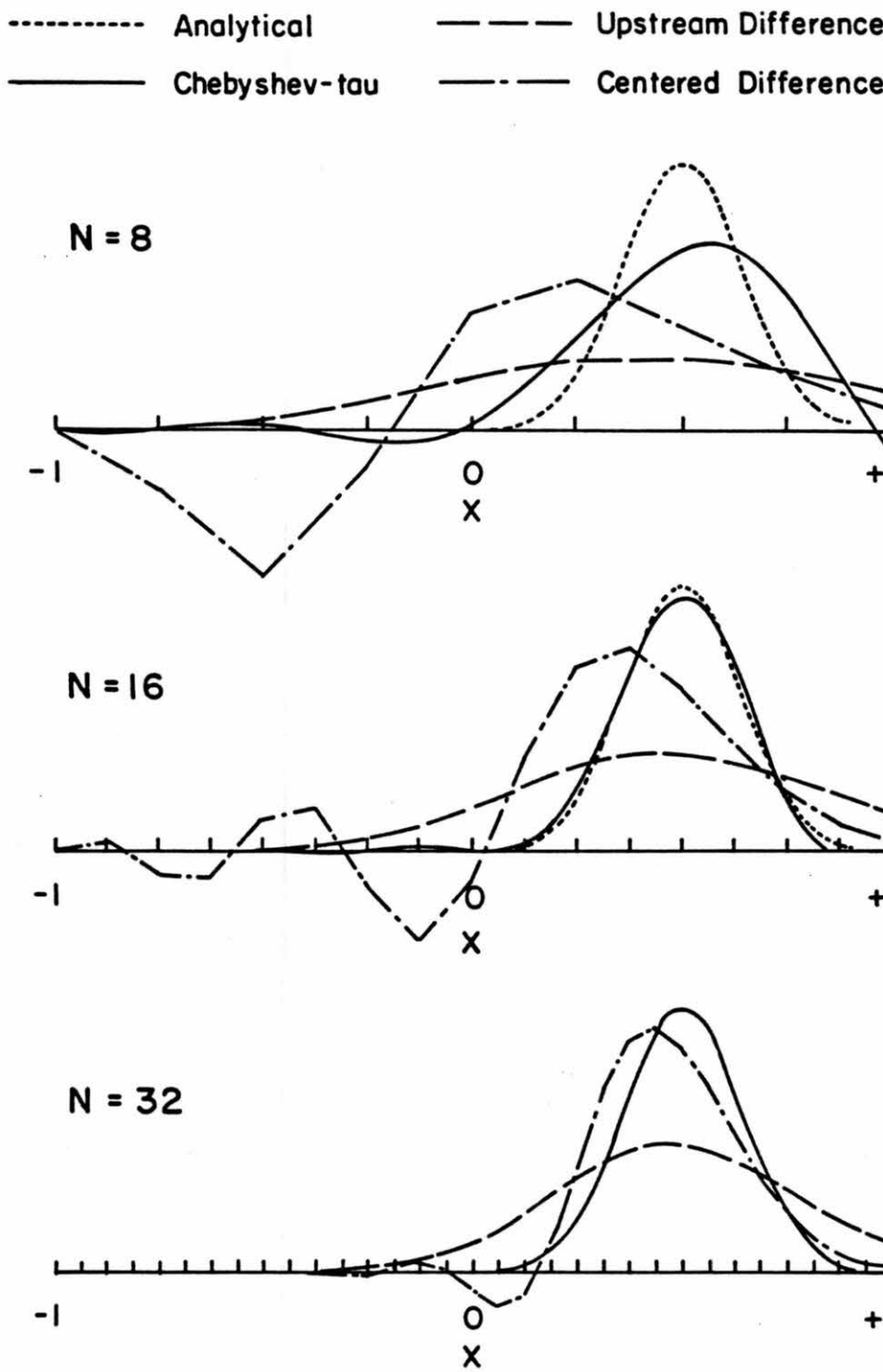

Figure 2. Analytical and numerical solutions of the linear advection equation at t=1.0.

$$\|u - u_N\|_2 = \left\{ \tfrac{1}{2} \int_{-1}^{1} [u(x)-u_N(x)]^2 \, dx \right\}^{\frac{1}{2}} , \qquad (2.47)$$

is shown in Figure 3 as a function of N. As N approaches 32 the error in the spectral solution is decreasing like $10^{-N/4}$, while the upstream and centered difference errors are only beginning to approach their asymptotic rates of decrease N^{-1} and N^{-2}, respectively.

The above results show that when modest accuracy is desired Chebyshev spectral methods require fewer degrees of freedom than do finite difference methods, and that this advantage increases dramatically as the accuracy desired is increased. This fact has immediate implications for the amount of computer storage required to obtain accurate solutions. However, the question of the relative efficiency of the methods is more difficult, as it depends on the method chosen for solving the spectral equations. In particular, the time step required for stability with explicit time differencing is $O(N^{-2})$ for the Chebyshev methods but only $O(N^{-1})$ for the finite difference schemes; this is due to the higher resolution of the Chebyshev series near the boundaries. We will discuss the questions of time differencing and efficiency in detail in chapter 4. Before that, however, we consider in the next chapter how to extend the simple methods discussed so far to more complicated problems.

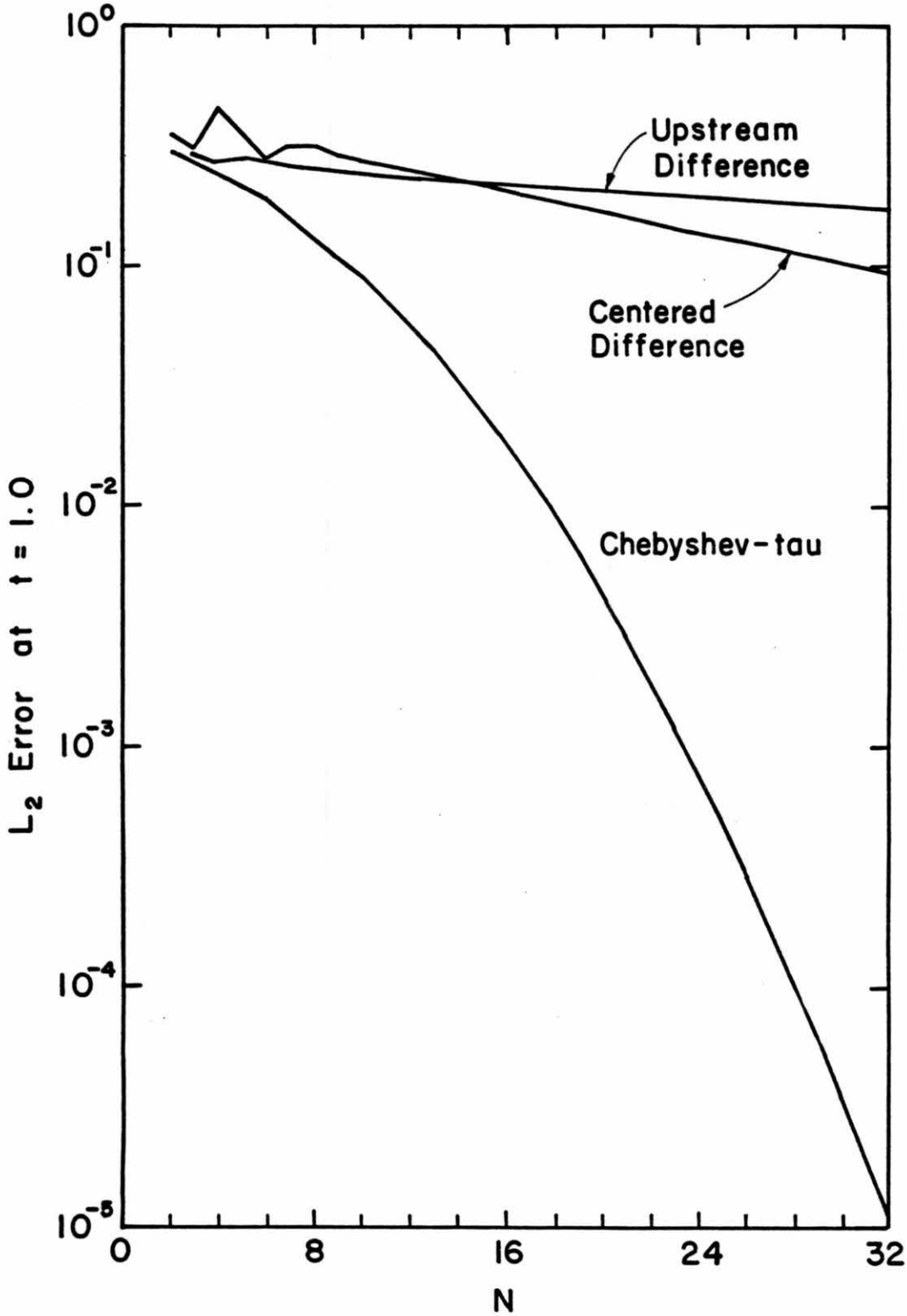

Figure 3. Errors in the numerical solution of the linear advection equation as a function of the number of degrees of freedom N.

CHAPTER 3

APPLICATION OF CHEBYSHEV SPECTRAL TECHNIQUES

Actual numerical models used in practice are invariably more complicated than the simple advection model considered in the previous chapter. Nonlinear terms, non-trivial boundary conditions and coupled systems of equations are among the complications that a numerical method must be able to handle in order to be practical. In this chapter we consider how the spectral methods described above may be extended to deal with such complications. We use the nonlinear shallow water equations as a simple prototype model embodying many of the important features of the "primitive" meteorological equations. In section 3.1 we present the governing equations and discuss some basic properties of their solutions. In section 3.2 suitable boundary conditions are examined. Chebyshev tau and collocation methods for this model are formulated in sections 3.3 and 3.4, respectively, with model results presented in section 3.5.

3.1 Properties of the Shallow Water Model

The nonlinear shallow water equations are

$$\left.\begin{aligned} &\frac{\partial u}{\partial t} + u\frac{\partial u}{\partial x} + v\frac{\partial u}{\partial y} - fv + \frac{\partial \phi}{\partial x} = F \\ &\frac{\partial v}{\partial t} + u\frac{\partial v}{\partial x} + v\frac{\partial v}{\partial y} + fu + \frac{\partial \phi}{\partial y} = G \\ &\frac{\partial \phi}{\partial t} + u\frac{\partial \phi}{\partial x} + v\frac{\partial \phi}{\partial y} + (\bar{\phi}+\phi)\left(\frac{\partial u}{\partial x} + \frac{\partial v}{\partial y}\right) = Q \end{aligned}\right\} . \qquad (3.1)$$

Here u and v are the velocity components in the x and y directions, respectively, ϕ is the deviation of the geopotential (free surface height h times the acceleration due to gravity g) from the constant positive reference value $\bar{\phi}$, f is the Coriolis parameter (assumed constant for simplicity), and F, G, and Q represent specified forcing. We will refer to (3.1) as the advective form of the model; the equivalent form

$$\left.\begin{aligned} &\frac{\partial u}{\partial t} - \left(f + \frac{\partial v}{\partial x} - \frac{\partial u}{\partial y}\right) v + \frac{\partial}{\partial x}\left[\phi + \tfrac{1}{2}(u^2+v^2)\right] = F \\ &\frac{\partial v}{\partial t} + \left(f + \frac{\partial v}{\partial x} - \frac{\partial u}{\partial y}\right) u + \frac{\partial}{\partial y}\left[\phi + \tfrac{1}{2}(u^2+v^2)\right] = G \\ &\frac{\partial \phi}{\partial t} + \frac{\partial}{\partial x}\left[(\bar{\phi}+\phi)\, u\right] + \frac{\partial}{\partial y}\left[(\bar{\phi}+\phi)\, v\right] = Q \end{aligned}\right\} , \qquad (3.2)$$

referred to as the rotational form, will also be used as a starting point for developing numerical models.

Many of the properties of the shallow water model may be understood by considering the linearized version

$$\left.\begin{aligned} &\frac{\partial u'}{\partial t} + \bar{u}\frac{\partial u'}{\partial x} + \bar{v}\frac{\partial u'}{\partial y} - fv' + \frac{\partial \phi'}{\partial x} = F' \\ &\frac{\partial v'}{\partial t} + \bar{u}\frac{\partial v'}{\partial x} + \bar{v}\frac{\partial v'}{\partial y} + fu' + \frac{\partial \phi'}{\partial y} = G' \\ &\frac{\partial \phi'}{\partial t} + \bar{u}\frac{\partial \phi'}{\partial x} + \bar{v}\frac{\partial \phi'}{\partial y} + \bar{\phi}\left(\frac{\partial u'}{\partial x} + \frac{\partial v'}{\partial y}\right) = Q \end{aligned}\right\} . \qquad (3.3)$$

Here u', v' and ϕ' represent small-amplitude perturbations from the constant basic state $\bar{u}$, $\bar{v}$, $\bar{\phi}$, with $-f\bar{v}$ and $f\bar{u}$ balancing the mean forcing $\bar{F}$ and $\bar{G}$. This system can be written in matrix form as

$$\frac{\partial w'}{\partial t} + A_1 \frac{\partial w'}{\partial x} + A_2 \frac{\partial w'}{\partial y} + Cw' = \frac{\partial W}{\partial t} , \qquad (3.4)$$

where $w' = [u', v', \phi'/c]^T$ and $\partial W/\partial t = [F', G', Q/c]^T$, with T denoting the transpose, and

$$A_1 = \begin{bmatrix} \bar{u} & 0 & c \\ 0 & \bar{u} & 0 \\ c & 0 & \bar{u} \end{bmatrix}, \quad A_2 = \begin{bmatrix} \bar{v} & 0 & 0 \\ 0 & \bar{v} & c \\ 0 & c & \bar{v} \end{bmatrix}, \quad C = \begin{bmatrix} 0 & -f & 0 \\ f & 0 & 0 \\ 0 & 0 & 0 \end{bmatrix}. \tag{3.5}$$

The homogeneous (unforced) system admits wave solutions, i.e. solutions of the form

$$w'_{k,\ell}(x,y,t) = \tilde{w}(k,\ell)\, e^{i(\underset{\sim}{k}\cdot\underset{\sim}{x}-\omega t)}, \tag{3.6}$$

where $\underset{\sim}{k} = k\hat{i}+\ell\hat{j}$ is the vector wavenumber, $\underset{\sim}{x} = x\hat{i}+y\hat{j}$, and ω is the frequency. Indeed, substituting (3.6) into (3.4) with $\partial W/\partial t$ set to zero yields (after much algebra) the solutions

$$w'^{(j)}_{k,\ell}(x,y,t) = \tilde{w}^{(j)}(k,\ell)\, e^{i\underset{\sim}{k}\cdot(\underset{\sim}{x}-\underset{\sim}{\bar{u}}t)}\, e^{-i\nu_j t} \quad (j=1,2,3). \tag{3.7}$$

Here $\underset{\sim}{u} = \bar{u}\hat{i} + \bar{v}\hat{j}$ is the mean flow,

$$\nu_1=0, \quad \nu_2=\nu, \quad \nu_3= -\nu \tag{3.8}$$

with

$$\nu = [f^2 + c^2(k^2 + \ell^2)]^{\frac{1}{2}}, \tag{3.9}$$

and

$$\tilde{w}^{(j)}(k,\ell) = \frac{c}{\gamma_j}\begin{Bmatrix} k\nu_j+i\,\ell\, f \\ \ell\nu_j-i\,k\, f \\ (\nu_j{}^2-f^2)/c \end{Bmatrix} \tag{3.10}$$

with $\gamma_1 = f\nu/c$ and $\gamma_2 = \gamma_3 = \rho\nu\sqrt{2}$, $\rho = (k^2+\ell^2)^{\frac{1}{2}}$. When $k=\ell=0$, an appropriate limit must be taken in (3.10) for j=2 and j=3; e.g., set k=0 and let $\ell \to 0$ through positive values.

The solutions (3.7) for j=1 are identified as geostrophic "waves" or modes, since they satisfy the geostrophic relations $fv' = \partial\phi'/\partial x$ and $fu' = -\partial\phi'/\partial y$; these modes do not propagate with respect to the mean flow $\underset{\sim}{\bar{u}}$. The solutions for j=2 and j=3 are identified as gravity waves (more precisely gravity-inertia waves, since the frequency ν depends not only on c, k, and ℓ but also on f); they are dispersive waves which propagate in the $+\underset{\sim}{k}$ and $-\underset{\sim}{k}$ directions, respectively, with respect to the mean flow $\underset{\sim}{\bar{u}}$. Any solution of the unforced system may be expressed as a linear combination of these geostrophic modes and gravity waves, with the coefficients in this expansion being constant. These two components of the flow have a definite separation of time scales, with the slow component (the geostrophic modes) typically being the component of interest.

For the inhomogeneous (forced) system the solution may still be expressed in terms of the waves (3.7), but in this case the expansion coefficients will depend on t. It is more instructive to express this expansion in terms of the normal modes of the system, which correspond to just the space dependence of the waves (3.7). To do so, we define for any function $\psi(x,y)$ the double Fourier transform pair

$$\psi(x,y) = \frac{1}{2\pi} \int_{-\infty}^{\infty}\int \tilde{\psi}(k,\ell)\, e^{i(kx+\ell y)}\, dk d\ell \ , \qquad (3.11a)$$

$$\tilde{\psi}(k,\ell) = \frac{1}{2\pi} \int_{-\infty}^{\infty}\int \psi(x,y)\, e^{-i(kx+\ell y)}\, dx dy \ . \qquad (3.11b)$$

Transforming (3.4) using (3.11b) yields

$$\frac{\partial \tilde{w}(k,\ell,t)}{\partial t} + A(k,\ell)\, \tilde{w}(k,\ell,t) = \frac{\partial \tilde{W}(k,\ell,t)}{\partial t} \qquad (3.12)$$

where

$$A(k,\ell) = ik\, A_1 + i\ell\, A_2 + C\ . \qquad (3.13)$$

From (3.13) A is skew-Hermitian, i.e. A*= -A, where the asterisk denotes the conjugate transpose, so its eigenvalues are pure imaginary and its eigenvectors form a complete orthogonal set. Writing the eigenproblem for A as

$$A\, \tilde{\psi}^{(j)} = i\, \omega_j\ \tilde{\psi}^{(j)} \qquad (j=1,2,3) \qquad (3.14)$$

we find that $\omega_j = k\bar{u} + \ell\bar{v} + \nu_j$ with ν_j given by (3.8), and $\tilde{\psi}^{(j)}$ is proportional to $\tilde{w}^{(j)}(k,\ell)$ as given by (3.10). Choosing $\tilde{\psi}^{(j)} = \tilde{w}^{(j)}/c$ is convenient, for then the matrix P which has $\tilde{\psi}^{(1)}$, $\tilde{\psi}^{(2)}$, $\tilde{\psi}^{(3)}$ as its columns is unitary, i.e. P*P=I, the identity matrix. Then defining

$$P^*\tilde{w} = \hat{w} = [\hat{w}_1,\ \hat{w}_2,\ \hat{w}_3]^T \qquad (3.15)$$

we have $\tilde{w}=P\hat{w}$, so from (3.11a) $\hat{w}_j$ is the amplitude of the normal mode

$$\psi^{(j)}(x,y;k,\ell) = \tilde{\psi}^{(j)}(k,\ell)\ e^{i(kx+\ell y)} \qquad (3.16)$$

in the solution w(x,y,t). Since $P^*AP = \mathrm{diag}[\omega_1,\omega_2,\omega_3]$, multiplying (3.12) on the left by P* then gives

$$\frac{\partial \hat{w}_j(k,\ell,t)}{\partial t} + i\,\omega_j(k,\ell)\,\hat{w}_j(k,\ell,t) = \frac{\partial \hat{W}_j(k,\ell,t)}{\partial t} \qquad (j=1,2,3), \quad (3.17)$$

where $\hat{W} = [\hat{W}_1, \hat{W}_2, \hat{W}_3]^T = P^*\tilde{W}$. Thus the linearized shallow water model has been reduced to the decoupled set of forced oscillation equations (3.17).

The solution of (3.17) is

$$\hat{w}_j(k,\ell,t) = e^{-i\omega_j(k,\ell)t}\,\hat{w}_j(k,\ell,0) + \int_0^t e^{-i\omega_j(k,\ell)(t-t')}\,\frac{\partial \hat{W}_j(k,\ell,t')}{\partial t'}\,dt' \,. \quad (3.18)$$

In the unforced case, $\hat{w}_j(k,\ell,t)$ has the time dependence $e^{-i\omega_j(k,\ell)t}$ and the solution $w(x,y,t)$ is therefore a superposition of the waves (3.7) as claimed above. However in the forced case the time dependence of $\hat{w}_j(k,\ell,t)$ depends not only on the internal dynamics $[\omega_j(k,\ell)]$ of the system but also on the forcing $[\partial \hat{W}_j(k,\ell,t)/\partial t]$. Thus the geostrophic modes of the solution may have a component which propagates and the gravity modes a component which propagates slowly (or not at all) in response to the forcing. In this case we can define the balanced flow to be the geostrophic ($j=1$) component of the solution $w(x,y,t)$ plus the part of the gravity mode ($j=2,3$) components for which $\partial \hat{w}_j/\partial t$ is negligible in (3.17). Thus the balanced flow consists of the "slow modes" present in the solution, and is usually of more interest than the propagating gravity waves or "fast modes." This separation based on time scales will be used in the next section in developing boundary conditions.

3.2 Boundary Conditions

To solve the shallow water model on a limited region Ω of the (x,y)-plane we must specify boundary conditions. These should be chosen so that the resulting problem is well-posed in a mathematical sense. That is, for any combination of initial conditions and forcing (the "data"), the problem should have a unique solution, and this solution should depend continuously on the data. Furthermore, the boundary conditions should be physically reasonable. Here we are particularly interested in simulating a portion of an infinite domain with a limited area model and hence seek boundary conditions which minimize the impact of the computationally imposed boundaries. In light of the discussion in the previous section, "ideal" boundary conditions would allow the slow modes of the model solution to closely approximate those of the solution on an infinite domain, and allow the outward-propagating fast modes to leave the model domain without reflecting.

Open boundary conditions, i.e. those which transmit at least some portion of the waves incident on the boundary, have been studied extensively. Such conditions are generally based on the Sommerfeld radiation condition (e.g., Pearson, 1974; Orlanski, 1976; Hack and Schubert, 1981) or the related Riemann invariants (Wurtele et al., 1971; Elvius and Sundström, 1973), both of which are discussed in Courant and Hilbert (1962, pp. 315, 430). For dispersive systems or problems in more than one space dimension such conditions are inexact. Higher-order approximations have been obtained (Engquist and Majda, 1977; Bayliss and Turkel, 1980) at the cost of increased complexity. Exact conditions have also been obtained (Bennett, 1976) but are impractical to implement. Israeli and Orszag (1981) have obtained good results by

combining open boundary conditions with absorbing boundary layers. The question of well-posedness has been investigated in detail for various systems of equations and boundary conditions by Oliger and Sundström (1978).

The derivation of appropriate boundary conditions for the shallow water model can be illustrated most easily in a single space dimension. When restricted to motions which are independent of y the linearized system (3.3) reduces to

$$\frac{\partial u'}{\partial t} + \bar{u}\frac{\partial u'}{\partial x} - fv' + \frac{\partial \phi'}{\partial x} = F \,, \tag{3.19a}$$

$$\frac{\partial v'}{\partial t} + \bar{u}\frac{\partial v'}{\partial x} + fu' = G \,, \tag{3.19b}$$

$$\frac{\partial \phi'}{\partial t} + \bar{u}\frac{\partial \phi'}{\partial x} + \bar{\phi}\frac{\partial u'}{\partial x} = Q \,. \tag{3.19c}$$

If we assume f is negligibly small then the possibility of geostrophic flow is eliminated, and (3.19) reduces to the three decoupled equations

$$\left.\begin{aligned} \frac{\partial}{\partial t}\left(u' + \frac{\phi'}{c}\right) + (c+\bar{u})\frac{\partial}{\partial x}\left(u' + \frac{\phi'}{c}\right) &= F + \frac{Q}{c} \\ \frac{\partial}{\partial t}\left(u' - \frac{\phi'}{c}\right) - (c-\bar{u})\frac{\partial}{\partial x}\left(u' - \frac{\phi'}{c}\right) &= F - \frac{Q}{c} \\ \frac{\partial v'}{\partial t} + \bar{u}\frac{\partial v'}{\partial x} &= G \end{aligned}\right\} \,. \tag{3.20}$$

From (3.20) we see that the three characteristic quantities $u'+\phi'/c$, $u'-\phi'/c$ and v' (the Riemann invariants) propagate in the x-direction with speeds $(c+\bar{u})$, $-(c-\bar{u})$ and $\bar{u}$, respectively, just as in the simple one-dimensional advection problem treated in the previous chapter. Therefore, to make the problem well-posed the boundary conditions must be formulated so they determine these quantities where they propagate

into the model domain, without determining them where they propagate out of it.

When f is negligible as assumed in (3.20), the quantities $u'+\phi'/c$ and $u'-\phi'/c$ correspond precisely to propagating gravity waves; in the typical case where $|\bar{u}|<c$ (often referred to as "subsonic") they propagate in the +x and -x directions, respectively. Assuming that the physical situation being modeled has no sources of gravity waves outside the model domain, the incoming quantity should be specified as zero at the boundary in order to simulate the infinite domain solution. On the limited domain $a \leq x \leq b$ this gives the conditions

$$\left.\begin{aligned} u' + \phi'/c = 0 \quad &\text{at} \quad x=a \\ u' - \phi'/c = 0 \quad &\text{at} \quad x=b \end{aligned}\right\} , \tag{3.21}$$

which will be referred to as homogeneous characteristic boundary conditions.

In the more general case where f is not negligible, the quantities $u'+\phi'/c$ and $u'-\phi'/c$ have contributions both from propagating gravity waves and from balanced flow. To simulate the infinite domain solution we should specify the incoming wave component as zero at the boundary, but still allow for the possibility of nonzero balanced flow there. This can be done with the conditions

$$\left.\begin{aligned} u'+\phi'/c = u'_B + \phi'_B/c \quad &\text{at} \quad x=a \\ u'-\phi'/c = u'_B - \phi'_B/c \quad &\text{at} \quad x=b \end{aligned}\right\} , \tag{3.22}$$

where the functions $u'_B(x,t)$ and $\phi'_B(x,t)$ are specified so that their boundary values closely approximate those of the balanced flow part of the infinite domain solution. The conditions (3.22) will be referred to

as inhomogeneous characteristic boundary conditions. Similarly, the quantity v' (which is not really a part of the problem unless $f \neq 0$) should be specified where there is basic state inflow by the condition

$$v' = v'_B \quad \text{at} \quad \left\{ \begin{array}{ll} x=a & \bar{u} > 0 \\ x=b & \bar{u} < 0 \end{array} \right\} , \tag{3.23}$$

where the function $v'_B(x,t)$ is specified so that its boundary value closely approximates that of the balanced flow part of the infinite domain solution. Similar inhomogeneous boundary conditions for nondispersive systems have been proposed by Bennett (1976).

One way to choose the boundary values needed for the conditions (3.22) and (3.23) is to specify the functions $u'_B(x,t)$, $v'_B(x,t)$ and $\phi'_B(x,t)$ as the solutions of the balanced model which corresponds to (3.19). This model is obtained by assuming geostrophic balance

$$fv' = \frac{\partial \phi'}{\partial x} \tag{3.24}$$

in (3.19a), with the other terms assumed to be negligible. Using (3.24), (3.19b) and (3.19c) then reduce to

$$\left(1 - \frac{c^2}{f^2} \frac{\partial^2}{\partial x^2} \right) fu' = G - \frac{1}{f} \frac{\partial Q}{\partial x} , \tag{3.25a}$$

$$\left(1 - \frac{c^2}{f^2} \frac{\partial^2}{\partial x^2} \right) \left(\frac{\partial}{\partial t} + \bar{u} \frac{\partial}{\partial x} \right) \frac{\phi'}{c} = \frac{Q}{c} - \frac{c}{f} \frac{\partial G}{\partial x} . \tag{3.25b}$$

The operator $\left(1 - \frac{c^2}{f^2} \frac{\partial^2}{\partial x^2}\right)$ in (3.25) may be inverted on the infinite domain $-\infty < x < \infty$ to give

$$\left.\begin{aligned} fu'(x,t) &= \int_{-\infty}^{\infty} \left[G(\xi,t) - \frac{1}{f} \frac{\partial Q(\xi,t)}{\partial \xi} \right] g(x;\xi)\, d\xi \\ \left(\frac{\partial}{\partial t} + \bar{u} \frac{\partial}{\partial x} \right) \frac{\phi'(x,t)}{c} &= \int_{-\infty}^{\infty} \left[\frac{Q(\xi,t)}{c} - \frac{c}{f} \frac{\partial G(\xi,t)}{\partial \xi} \right] g(x;\xi)\, d\xi \end{aligned}\right\}, \quad (3.26)$$

where

$$g(x;\xi) = \frac{f}{2c} e^{-f|x-\xi|/c} \qquad (3.27)$$

is the Green's function. Substituting (3.27) into (3.26), integrating by parts and using (3.24), we can obtain the analytical solution of the linearized balanced model from

$$\left.\begin{aligned} fu'(x,t) &= \tfrac{1}{2}(I_1+I_2)G(x,t) + \tfrac{1}{2}(I_1-I_2) \frac{Q(x,t)}{c} \\ \left(\frac{\partial}{\partial t} + \bar{u} \frac{\partial}{\partial x} \right) v'(x,t) &= [1 - \tfrac{1}{2}(I_1+I_2)]G(x,t) - \tfrac{1}{2}(I_1-I_2) \frac{Q(x,t)}{c} \\ \left(\frac{\partial}{\partial t} + \bar{u} \frac{\partial}{\partial x} \right) \frac{\phi'(x,t)}{c} &= \tfrac{1}{2}(I_1+I_2) \frac{Q(x,t)}{c} + \tfrac{1}{2}(I_1-I_2)\, G(x,t) \end{aligned}\right\}, \quad (3.28)$$

where I_1 and I_2 are the integral operators defined by

$$\left.\begin{aligned} I_1\, \psi(x) &= \frac{f}{c} \int_{\infty}^{x} \psi(\xi)\, e^{-f(x-\xi)/c}\, d\xi \\ I_2\, \psi(x) &= \frac{f}{c} \int_{x}^{\infty} \psi(\xi)\, e^{-f(\xi-x)/c}\, d\xi \end{aligned}\right\} \qquad (3.29)$$

for any function $\psi(x)$.

For the linearized two-dimensional model (3.3) a similar analysis (Oliger and Sundström, 1978) yields the boundary conditions

$$u_\perp' - \phi'/c = (u_\perp' - \phi'/c)_B \quad \text{on} \quad \partial\Omega \qquad (3.30)$$

and

$$u'_{\|} = (u'_{\|})_B \quad \text{where} \quad \bar{u}_{\perp} < 0 \quad \text{on} \quad \partial\Omega \quad , \tag{3.31}$$

where $u_{\perp}$ and $u_{\|}$ denote velocity components normal to (outward) and parallel to the boundary $\partial\Omega$, respectively, and $(\ )_B$ denotes specified boundary values. Note that the same conditions are obtained by rotating the coordinates so the y-axis is parallel to the boundary and applying the boundary conditions developed for the one-dimensional problem above; thus (3.30) effectively assumes that waves strike the boundary at normal incidence. For the full nonlinear equations (3.1) or (3.2), the conditions (3.30) and (3.31) can be implemented as

$$u_{\perp} - 2(\bar{\phi}+\phi)^{\frac{1}{2}} = [u_{\perp} - 2(\bar{\phi}+\phi)^{\frac{1}{2}}]_B \quad \text{on} \quad \partial\Omega \tag{3.32}$$

and

$$u_{\|} = (u_{\|})_B \quad \text{where} \quad u_{\perp} < 0 \quad \text{on} \quad \partial\Omega \ , \tag{3.33}$$

since if at a given boundary point both a "basic state" $u_{\perp}$, $u_{\|}$, $\bar{\phi}+\phi$ and the actual flow $u_{\perp}+u'_{\|}$, $u_{\|}+u'_{\|}$, $\bar{\phi}+\phi+\phi'$ satisfy (3.32) and (3.33) then $0 = (u_{\|}+u'_{\|})-u_{\|} = u'_{\|}$ and $0 = [(u_{\perp}+u'_{\perp})-2(\bar{\phi}+\phi+\phi')^{\frac{1}{2}}] - [u_{\perp}-2(\bar{\phi}+\phi)^{\frac{1}{2}}] \approx u'_{\perp} - \phi'/c$ with $c = (\bar{\phi}+\phi)^{\frac{1}{2}}$. These conditions yield a well-posed problem (Oliger and Sundström, 1978). The necessary boundary values could be generated from the interior forcing via the Green's function for the corresponding balanced model as above. However, in two dimensions this approach is likely to be inefficient, since it involves computing double integrals for each boundary point. In practice, suitable boundary values may be available from a coarse-resolution, large-scale model in which the fine-resolution, limited-area model is embedded.

Two other boundary conditions will also be considered in this study. The first is the balance condition, based on the assumption that near the boundaries the solution behaves like that of the corresponding

balanced model. In one dimension this condition can be derived from (3.25a) as follows. The solution u' of the homogeneous part of (3.25a) which remains bounded as $x \to -\infty$ is proportional to $e^{fx/c}$. Thus when the right-hand side of (3.25a) vanishes outside a limited region the solution on an infinite domain satisfies

$$\frac{\partial u'}{\partial x} - \frac{f}{c} u' \to 0 \quad \text{as} \quad x \to -\infty \ , \tag{3.34a}$$

and similarly

$$\frac{\partial u'}{\partial x} + \frac{f}{c} u' \to 0 \quad \text{as} \quad x \to +\infty \ , \tag{3.34b}$$

Applying (3.34) at the boundaries of the limited domain $a \leq x \leq b$ leads to the balance boundary conditions

$$\left.\begin{aligned} \frac{\partial u'}{\partial x} - \frac{f}{c} u' &= 0 \quad \text{at} \quad x=a \\ \frac{\partial u'}{\partial x} + \frac{f}{c} u' &= 0 \quad \text{at} \quad x=b \end{aligned}\right\} \ . \tag{3.35}$$

Using (3.19c) these can be written in the alternate (predictive) form

$$\left.\begin{aligned} \frac{\partial \phi'}{\partial t} + \bar{u} \frac{\partial \phi'}{\partial x} + fcu' &= Q \quad \text{at} \quad x=a \\ \frac{\partial \phi'}{\partial t} + \bar{u} \frac{\partial \phi'}{\partial x} - fcu' &= Q \quad \text{at} \quad x=b \end{aligned}\right\} \ . \tag{3.36}$$

As before, if $\bar{u} \neq 0$ then v' must be specified on inflow. Since no useful generalization of the balance condition to two dimensions in Cartesian coordinates is known, we will use this condition only in one-dimensional examples. The last boundary condition to be considered here, namely the wall boundary condition

$$u_\perp = 0 \quad \text{on} \quad \partial\Omega \ , \tag{3.37}$$

is also the simplest of the three, and yields a well-posed problem for the shallow water model (Oliger and Sundström, 1978).

The performance of the boundary conditions derived above is measured in part by their ability to transmit gravity waves. At a given boundary point $\underset{\sim}{b}$ we can write the gravity wave j=2 in (3.7) which propagates in the direction $\underset{\sim}{k}$ as

$$q'_{\theta,\rho}(x,y,t) = \begin{pmatrix} u'_\perp \\ u'_\parallel \\ \phi'/c \end{pmatrix} = \frac{\rho c}{\gamma} \begin{pmatrix} \nu\cos\theta + if\sin\theta \\ \nu\sin\theta - if\cos\theta \\ \rho c \end{pmatrix} e^{i(\underset{\sim}{k}\cdot\underset{\sim}{b}-\nu t)} \ , \tag{3.38}$$

where θ is the angle between the outward normal to the boundary and the wavenumber vector $\underset{\sim}{k}$, $\rho = |\underset{\sim}{k}| = (k^2+\ell^2)^{\frac{1}{2}}$ as before, and we have set $\bar{\underset{\sim}{u}}=0$ for simplicity. For the characteristic boundary condition (3.30) suppose that the deviation of $(u'_\perp - \phi'/c)$ from its specified value $(u'_\perp - \phi'/c)_B$ is composed of the gravity wave $q'_{\theta,\rho}$ plus the reflected wave $Rq'_{\pi-\theta,\rho}$, where R is the reflection coefficient. Applying the boundary condition (3.30) then yields

$$|R|^2 = \frac{(\nu\cos\theta - \rho c)^2 + f^2\sin^2\theta}{(\nu\cos\theta + \rho c)^2 + f^2\sin^2\theta} \ . \tag{3.39}$$

Figure 4 shows $|R|$ as a function of the dimensionless wavenumber $\rho c/f$ and the angle of incidence θ. Lower reflectivities can be achieved (e.g. Engquist and Majda, 1977) at the cost of increasingly complicated boundary conditions.

A similar analysis for the balance and wall boundary conditions (3.35) and (3.37) shows that both have unit reflectivity and hence trap

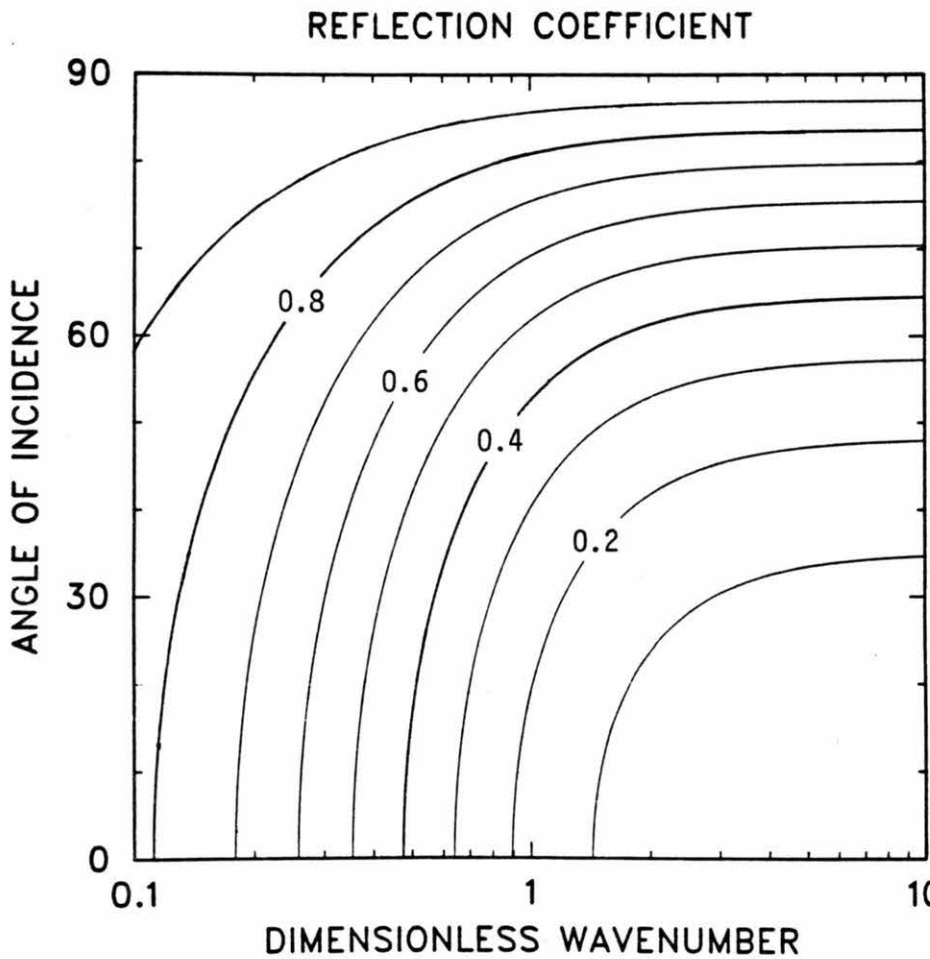

Figure 4. Reflection coefficient $|R|$ for the characteristic boundary condition as a function of the dimensionless wavenumber $\rho c/f$ and the angle of incidence θ in degrees. The contour interval is 0.1.

all gravity waves within the model domain. However, since the geostrophic modes [j=1 in (3.7)] individually satisfy (3.35) (with ℓ=0 for y-independent motion), the balance condition does not distort the geostrophic component of the flow. In addition, the balance condition allows mass flow (u) through the boundary, whereas the simpler wall condition allows neither mass flow nor wave propagation through the boundary. In the next two sections the implementation of all of these boundary conditions in Chebyshev spectral models will be discussed.

3.3 The Chebyshev-Tau Method

To apply the Chebyshev-tau method to the shallow water model we first consider the one-dimensional (y-independent) version of (3.1), namely

$$\left.\begin{aligned} \frac{\partial u}{\partial t} + u\frac{\partial u}{\partial x} - fv + \frac{\partial \phi}{\partial x} &= F \\ \frac{\partial v}{\partial t} + u\frac{\partial v}{\partial x} + fu &= G \\ \frac{\partial \phi}{\partial t} + u\frac{\partial \phi}{\partial x} + (\bar{\phi}+\phi)\frac{\partial u}{\partial x} &= Q \end{aligned}\right\} . \qquad (3.40)$$

For the model domain $a \leq x \leq b$ the dependent variables are approximated by the series expansions

$$\begin{bmatrix} u(x,t) \\ v(x,t) \\ \phi(x,t) \end{bmatrix} \approx \begin{bmatrix} u_N(x,t) \\ v_N(x,t) \\ \phi_N(x,t) \end{bmatrix} = \sum_{n=0}^{N} \begin{bmatrix} \hat{u}_n(t) \\ \hat{v}_n(t) \\ \hat{\phi}_n(t) \end{bmatrix} T_n(x') \quad , \qquad (3.41)$$

where $x' = \left(\frac{2}{b-a}\right) x - \left(\frac{b+a}{b-a}\right)$. The coefficients in (3.41) are defined by requiring the truncation error in each equation of (3.40) to be

orthogonal to most of the basis functions $T_n(x')$, using the remaining degrees of freedom to satisfy the boundary conditions. The appropriate inner product here is (2.16) with x replaced by x'. Thus the tau equations are

$$\frac{d\hat{u}_n}{dt} + \hat{A}_n - f\,\hat{v}_n + \hat{\phi}_n^{(1)} = \hat{F}_n \,, \tag{3.42a}$$

$$\frac{d\hat{v}_n}{dt} + \hat{B}_n + f\,\hat{u}_n = \hat{G}_n \,, \tag{3.42b}$$

$$\frac{d\hat{\phi}_n}{dt} + \hat{C}_n + \hat{D}_n + \bar{\phi}\,\hat{u}_n^{(1)} = \hat{Q}_n \,, \tag{3.42c}$$

where $\hat{A}_n$, $\hat{B}_n$, $\hat{C}_n$ and $\hat{D}_n$ are the spectral coefficients of the nonlinear terms

$$\left.\begin{aligned} A &= u\,\frac{\partial u}{\partial x} \,, \qquad B = u\,\frac{\partial v}{\partial x} \\ C &= u\,\frac{\partial \phi}{\partial x} \,, \qquad D = \phi\,\frac{\partial u}{\partial x} \end{aligned}\right\} \,, \tag{3.43}$$

and $\hat{u}_n^{(1)}$ and $\hat{\phi}_n^{(1)}$ denote the spectral coefficients of $\partial u/\partial x$ and $\partial \phi/\partial x$, respectively. Note that to take such derivatives in spectral space for the domain [a,b], the derivative relation (2.27) must be modified to take into account the domain length, e.g.

$$c_{n-1}\,\hat{u}_{n-1}^{(1)} - \hat{u}_{n+1}^{(1)} = 2n\left(\frac{2}{b-a}\right)\,\hat{u}_n \,. \tag{3.44}$$

The spectral coefficients of the nonlinear terms in (3.42) are related to the dependent variables $\hat{u}_n$, $\hat{v}_n$ and $\hat{\phi}_n$ as follows. For any two Chebyshev series $\sum_{n=0}^{N} \hat{a}_n T_n$ and $\sum_{n=0}^{N} \hat{b}_n T_n$ we can (with a lot of algebra) express their product directly as

$$\left(\sum_{n=0}^{N} a_n T_n\right)\left(\sum_{n=0}^{N} b_n T_n\right) =$$

$$\sum_{n=0}^{N}\left[\frac{1}{2}\sum_{m=0}^{n}\hat{a}_m\hat{b}_{n-m} + \frac{1}{2c_n}\sum_{m=n}^{N}(\hat{a}_{m-n}\hat{b}_m + \hat{a}_m\hat{b}_{m-n})\right] T_n \qquad (3.45)$$

$$+ \sum_{n=N+1}^{2N}\left(\frac{1}{2}\sum_{m=n-N}^{N}\hat{a}_m\hat{b}_{n-m}\right) T_n \ ,$$

where we have used the relation $T_m T_n = \frac{1}{2}(T_{m+n} + T_{|m-n|})$ which follows from the trigonometric identity $\cos\alpha\cos\beta = \frac{1}{2}[\cos(\alpha+\beta) + \cos(\alpha-\beta)]$ using (2.12). Using derivative relations we can express each term (3.43) as such a product and thus obtain the necessary coefficients from (3.45). For example, for the term $A=u\partial u/\partial x$ we have

$$\hat{A}_n = \frac{1}{2}\sum_{m=0}^{n}\hat{u}_m\hat{u}^{(1)}_{n-m} + \frac{1}{2c_n}\sum_{m=n}^{N}(\hat{u}_{m-n}\hat{u}^{(1)}_m + \hat{u}_m\hat{u}^{(1)}_{m-n}) \qquad (n=0,\ldots,N) \qquad (3.46)$$

where the $\hat{u}^{(1)}_n$ are related to the $\hat{u}_n$ via (3.44). Such formulas may be used to compute the spectral coefficients of the nonlinear terms directly. However, this approach, known as the interaction coefficient method, is computationally inefficient since it requires $O(N^2)$ operations.

The key to computing the nonlinear terms efficiently is the transform method, developed independently by Eliasen et al. (1970) and Orszag (1970). This method consists of transforming the necessary variables from spectral space to physical space, multiplying the resulting physical space values together at discrete points, and transforming the result back to spectral space. For example, to compute

$\hat{A}_n$ (n=0,...,N) we evaluate the Chebyshev series for u and $\partial u/\partial x$ from their coefficients $\hat{u}_n$ and $\hat{u}_n^{(1)}$, multiply these values together to obtain values of $A=u\partial u/\partial x$ at discrete points, and use these values in computing $\hat{A}_n = \frac{2}{\pi c_n} \langle A, T_n \rangle$. With the proper choice of physical space points, not only can the needed coefficients $\hat{A}_n$ (n=0,...,N) be computed exactly, but the transforms involved may be computed using the FFT algorithm so that the total work required is only O(N log N) operations.

Two reasonable choices of physical space points for the transform method can be made. Using Gauss-Chebyshev quadrature (Atkinson, 1978) the transform (2.18b) can be approximated by

$$\hat{u}_n \approx \frac{2}{(M+1)c_n} \sum_{j=0}^{M} u\left(\tilde{x}_j^{(M+1)}\right) T_n\left(\tilde{x}_j^{(M+1)}\right), \qquad (3.47)$$

where the quadrature points $\tilde{x}_j^{(M+1)}$ are the zeros of T_{M+1} as given by (2.14). This formula amounts to approximating the integral (2.19b) by the midpoint rule and is exact when u is a polynomial of degree at most 2M+1 - n. Thus for a quadratic nonlinear term such as $A=u\partial u/\partial x$ with each component a polynomial of degree at most N, we must choose

$$M \geq \frac{3N-1}{2} \qquad (3.48)$$

in order to compute $\hat{A}_n$ exactly for n=0,...,N. Using (2.12), both (3.47) and the evaluation of the series (2.18a) at the points $\tilde{x}_j^{(M+1)}$ can be written in forms computable using FFT's. However, the factor ½ in (2.14) introduces phase shifts which complicate this calculation.

A simpler approach is to use the discrete Chebyshev transform pair (2.21) with N replaced by M. Here the quadrature points $\bar{x}_j^{(M)}$ are the locations of the extrema of T_M as given by (2.15), corresponding to the

trapezoidal rule for (2.19b). As above, the spectral coefficients of quadratic nonlinear terms for n=0,...,N are computed exactly when (3.48) holds, and in this form the FFT algorithm may be used directly. Note that with either choice of quadrature points the use of the FFT requires the same number of values in physical and spectral space. Thus to compute a term like $A = u\,\partial u/\partial x$ one appends extra spectral coefficients $\hat{u}_{N+1},\ldots,\hat{u}_M$ with the value zero to $\hat{u}_0,\ldots,\hat{u}_N$ (and similarly for $\hat{u}_n^{(1)}$) and computes the transforms to get values at the M+1 physical space points. After computing the product in physical space and transforming back, the extra coefficients $\hat{A}_{N+1},\ldots,\hat{A}_M$ produced by this transform are simply dropped, since they do not enter the tau equations (in general they are also not computed exactly).

In other problems, cubic nonlinear terms can be computed exactly using the transform method with more points [$M \geq (4N-1)/2$], although the extra points may not be needed in practice (Machenhauer and Daley, 1972). For more complicated nonlinearities, such as those arising from parameterizations, one must in general give up computing the spectral coefficients of the nonlinear terms exactly, and simply use the transform method with as many points as are necessary in order to achieve sufficient accuracy.

Boundary conditions for the tau method are handled by applying them directly to the series expansions (3.41) and using the resulting equations in place of (3.42) to diagnose or predict the last mode(s) as appropriate. For example, the wall condition (3.37) applied at x=a gives

$$\sum_{n=0}^{N} (-1)^n \hat{u}_n = 0 \tag{3.49}$$

and the (linear) characteristic condition (3.22) applied at x=b gives

$$\sum_{n=0}^{N} \left(\hat{u}_n - \frac{\hat{\phi}_n}{c} \right) = u_B(b,t) - \frac{\phi_B(b,t)}{c} \quad . \tag{3.50}$$

These conditions can be used to diagnose $\hat{u}_N$ and $\hat{\phi}_N$ and thus (3.42a) and (3.42c) are applied only for n=0,...,N-1. Any other combination of the boundary conditions (3.22) and (3.35)-(3.37) can be applied in a similar manner, as can (3.32) even though it is nonlinear. To apply the inflow condition (3.33) the direction of the flow must be checked at the boundary first; this is easily accomplished by evaluating the series there directly.

The generalization of the above techniques to two dimensions is straightforward. On the rectangular domain $\Omega = [0,L_x] \times [0,L_y]$ the appropriate expansions are

$$\begin{bmatrix} u(x,y,t) \\ v(x,y,t) \\ \phi(x,y,t) \end{bmatrix} \approx \begin{bmatrix} u_{MN}(x,y,t) \\ v_{MN}(x,y,t) \\ \phi_{MN}(x,y,t) \end{bmatrix} = \sum_{m=0}^{M} \sum_{n=0}^{N} \begin{bmatrix} \hat{u}_{mn}(t) \\ \hat{v}_{mn}(t) \\ \hat{\phi}_{mn}(t) \end{bmatrix} T_m(x')T_n(y') \tag{3.51}$$

with $x'=2x/L_x-1$ and $y' = 2y/L_y-1$, and the relevant inner product is a double integral with the form (2.16) in both x' and y'. The tau equations can be written directly from (3.1) as

$$\left.\begin{aligned}
&\frac{d\hat{u}_{mn}}{dt} + \hat{A}_{mn} - f\,\hat{v}_{mn} + \hat{\phi}^{(1,0)}_{mn} = \hat{F}_{mn} \\
&\frac{d\hat{v}_{mn}}{dt} + \hat{B}_{mn} + f\,\hat{u}_{mn} + \hat{\phi}^{(0,1)}_{mn} = \hat{G}_{mn} \\
&\frac{d\hat{\phi}_{mn}}{dt} + \hat{C}_{mn} + \hat{D}_{mn} + \bar{\phi}\left(\hat{u}^{(1,0)}_{mn} + \hat{v}^{(0,1)}_{mn}\right) = \hat{Q}_{mn}
\end{aligned}\right\}, \quad (3.52)$$

where the nonlinear terms are $A = u\partial u/\partial x + v\partial u/\partial y$, $B = u\partial v/\partial x + v\partial v/\partial y$, $C = u\partial\phi/\partial x + v\partial\phi/\partial y$ and $D = \phi(\partial u/\partial x + \partial v/\partial y)$, and $\hat{(\,)}^{(1,0)}_{mn}$ and $\hat{(\,)}^{(0,1)}_{mn}$ denote the spectral coefficients of x and y derivatives, respectively. The transform method generalizes to two dimensions directly, and the application of boundary conditions is similar. In nonrectangular domains one can often use a coordinate transformation to reduce the problem to a rectangular domain (Orszag, 1980).

The tau equations (3.42) and (3.52) have been developed from the advective form (3.1), but the rotational form (3.2) can also be used. In one dimension the resulting models are similar, but in two dimensions the rotational form is preferable since it requires fewer transforms to compute the nonlinear terms than does the advective form (9 instead of 12). In either case the Chebyshev-tau equations closely parallel the continuous form of the model, and programming is easy (with explicit time differencing) once a set of routines for standard operations such as transforms and derivatives is developed. Nevertheless, Chebyshev-collocation methods are still easier, as will be seen in the next section.

3.4 The Chebyshev-Collocation Method

The formulation of the Chebyshev-collocation version of the shallow water model is extremely simple. On the domain $\Omega = [0,L_x] \times [0,L_y]$ we

again use the expansions (3.51), and introduce the collocation points $\bar{x}_j = [1 + \cos(j\pi/M)]\, L_x/2$ $(j=0,\ldots,M)$ and $\bar{y}_k = [1 + \cos(k\pi/N)]\, L_y/2$ $(k=0,\ldots,N)$. The collocation equations can then be written directly from (3.1) as

$$\left.\begin{aligned}
&\frac{d\bar{u}_{jk}}{dt} + \bar{u}_{jk}\bar{u}^{(1,0)}_{jk} + \bar{v}_{jk}\bar{u}^{(0,1)}_{jk} - f\,\bar{v}_{jk} + \bar{\phi}^{(1,0)}_{jk} &&= \bar{F}_{jk} \\
&\frac{d\bar{v}_{jk}}{dt} + \bar{u}_{jk}\bar{v}^{(1,0)}_{jk} + \bar{v}_{jk}\bar{v}^{(0,1)}_{jk} + f\,\bar{u}_{jk} + \bar{\phi}^{(0,1)}_{jk} &&= \bar{G}_{jk} \\
&\frac{d\bar{\phi}_{jk}}{dt} + \bar{u}_{jk}\bar{\phi}^{(1,0)}_{jk} + \bar{v}_{jk}\bar{\phi}^{(0,1)}_{jk} + (\bar{\phi}+\bar{\phi}_{jk})\left[\bar{u}^{(1,0)}_{jk} + \bar{v}^{(0,1)}_{jk}\right] &&= \bar{Q}_{jk}
\end{aligned}\right\}, \tag{3.53}$$

where $(\bar{\ })_{jk}$ denotes a value at the point $(\bar{x}_j,\bar{y}_k)$, and $(\ )^{(1,0)}$ and $(\ )^{(0,1)}$ denote the x and y derivatives, respectively. To compute these derivatives one uses the usual collocation procedure: transform to spectral space, take the derivative there, and transform back to physical space. A total of 12 transforms is required for (3.53), the same as for the corresponding collocation equations generated from the rotational form (3.2); these transforms are all one-dimensional and equal in length to the truncation, whereas the transforms needed in the tau method are all two-dimensional and longer than the truncation. No special treatment is needed for the nonlinear terms; other problems with more complicated nonlinearities (even transcendental ones) are handled with the same simplicity.

Boundary conditions for the collocation method are formulated exactly as in the continuous case, since the model variables $\bar{u}_{jk}$, $\bar{v}_{jk}$ and $\bar{\phi}_{jk}$ are carried at the boundary points. For example, to apply the wall condition (3.37) one simply sets the corresponding values of $\bar{u}_{jk}$ and $\bar{v}_{jk}$ to zero, such as $\bar{u}_{0,k}=0$ $(k=0,\ldots,N)$ for the boundary $x=L_x$. The

characteristic boundary condition (3.32) specifies the incoming combination $u_\perp - 2(\bar{\phi}+\phi)^{\frac{1}{2}}$ at the boundary; to determine both $u_\perp$ and ϕ there we simply require that the outgoing quantity $u_\perp + 2(\bar{\phi}+\phi)^{\frac{1}{2}}$ be unchanged from its value as predicted by the interior equations (3.53). The inflow condition (3.33) may be implemented directly in the collocation method since all model variables are in physical space. However, in one dimension the balance condition is easier to implement in the predictive form (3.36), since the diagnostic form (3.35) leads to implicit equations due to the global dependence of the derivatives.

The price one pays for the simplicity of the collocation method is the introduction of aliasing. In nonlinear processes such as advection there is often a transfer of energy between scales of motion. For example, in computing a nonlinear term such as $u\partial u/\partial x$ in the one-dimensional model (3.40) we see from (3.45) that even if u and $\partial u/\partial x$ involve only the larger scales T_n for $n=0,\ldots,N$, their product involves the smaller scales T_n for $n=N+1,\ldots,2N$ as well. In the tau method the contributions of such nonlinear terms to the resolvable scales (T_n for $n=0,\ldots,N$) are computed exactly, with the contributions to the unresolvable scales simply neglected. In the collocation method the evaluation of a term such as $\bar{u}_{jk}\bar{u}^{(1,0)}_{jk}$ in general takes the information which should go into unresolvable scales and spreads it over the resolvable scales. This phenomenon is known as aliasing (Haltiner and Williams, 1980, pp. 170-176).

The consequences of aliasing are not immediately clear. In finite difference schemes aliasing can sometimes lead to numerical instabilities (Phillips, 1959). Fox and Orszag (1973) suggest that such instabilities can be avoided in collocation methods by using rotational

forms of the equations such as (3.2). One can also make a case that aliasing need not be regarded as a type of error (Orszag, 1971c, 1972). The effects of aliasing will be examined in the next section, in which we present results from the Chebyshev models developed above.

3.5 Results

To adequately test the Chebyshev spectral models developed above we need a standard against which their solutions may be compared. No general closed-form solution of the shallow water equations on an infinite domain exists, although in the linear case the normal mode expansion developed in section 3.1 could be used. A convenient standard does exist, however, for the linear, y-independent problem (3.19), since the solution converges to that of the corresponding balanced model as $t \to \infty$ (provided the initial conditions are geostrophic and the forcing tends to zero as $t \to \infty$), and the latter solution can be computed easily from (3.28). In this section we use this comparison to investigate the accuracy of the methods and boundary conditions, and then present some simple examples of nonlinear and two-dimensional results.

The test case used for the one-dimensional results reported here consists of a separable geopotential sink

$$Q(x,t) = -\Phi(x)\,\frac{dT(t)}{dt} \tag{3.54}$$

with no forcing of the wind field (F=G=0) and the initial fields u', v' and ϕ' all zero. The space dependence of (3.54) is the Gaussian function

$$\Phi(x) = \Phi_0 \, e^{-(x/x_0)^2} , \tag{3.55}$$

where x_0 is the e-folding width, as shown in Fig. 5a. The time dependence is

$$\frac{dT(t)}{dt} = \frac{1}{t_0} \left(\frac{2t}{t_0} \right)^2 e^{-2t/t_0} , \tag{3.56}$$

where t_0 is the time of maximum forcing, as shown in Fig. 5b. This time dependence satisfies

$$T(t) = \int_0^t \frac{dT(t')}{dt'} \, dt' = 1 - \left[1 + \left(\frac{2t}{t_0} \right) + \tfrac{1}{2} \left(\frac{2t}{t_0} \right)^2 \right] e^{-2t/t_0} , \tag{3.57}$$

so that

$$\int_0^\infty Q(x,t) \, dt = - \Phi (x) . \tag{3.58}$$

With the separable forcing (3.54) the balanced model solution (3.28) with $\bar{u}=0$ reduces to

$$\left.
\begin{aligned}
u'(x,t) &= \left[\tfrac{1}{2}(I_1 - I_2) \, \frac{\Phi(x)}{c} \right] \left[\frac{1}{f} \, \frac{dT(t)}{dt} \right] \\
v'(x,t) &= -\left[\tfrac{1}{2}(I_1 - I_2) \, \frac{\Phi(x)}{c} \right] \, T(t) \\
\frac{\phi'(x,t)}{c} &= \left[\tfrac{1}{2}(I_1 + I_2) \, \frac{\Phi(x)}{c} \right] \, T(t)
\end{aligned}
\right\} . \tag{3.59}$$

Substituting (3.55) into (3.29) we can express the integrals in (3.59) as

$$\left.
\begin{aligned}
I_1 \, \Phi(x) &= \Phi_0 \, s_0 \, \sqrt{\pi} \, e^{s_0^2 - fx/c} \, \operatorname{erfc} \left(s_0 - \frac{x}{x_0} \right) \\
I_2 \, \Phi(x) &= \Phi_0 \, s_0 \, \sqrt{\pi} \, e^{s_0^2 + fx/c} \, \operatorname{erfc} \left(s_0 + \frac{x}{x_0} \right)
\end{aligned}
\right\} , \tag{3.60}$$

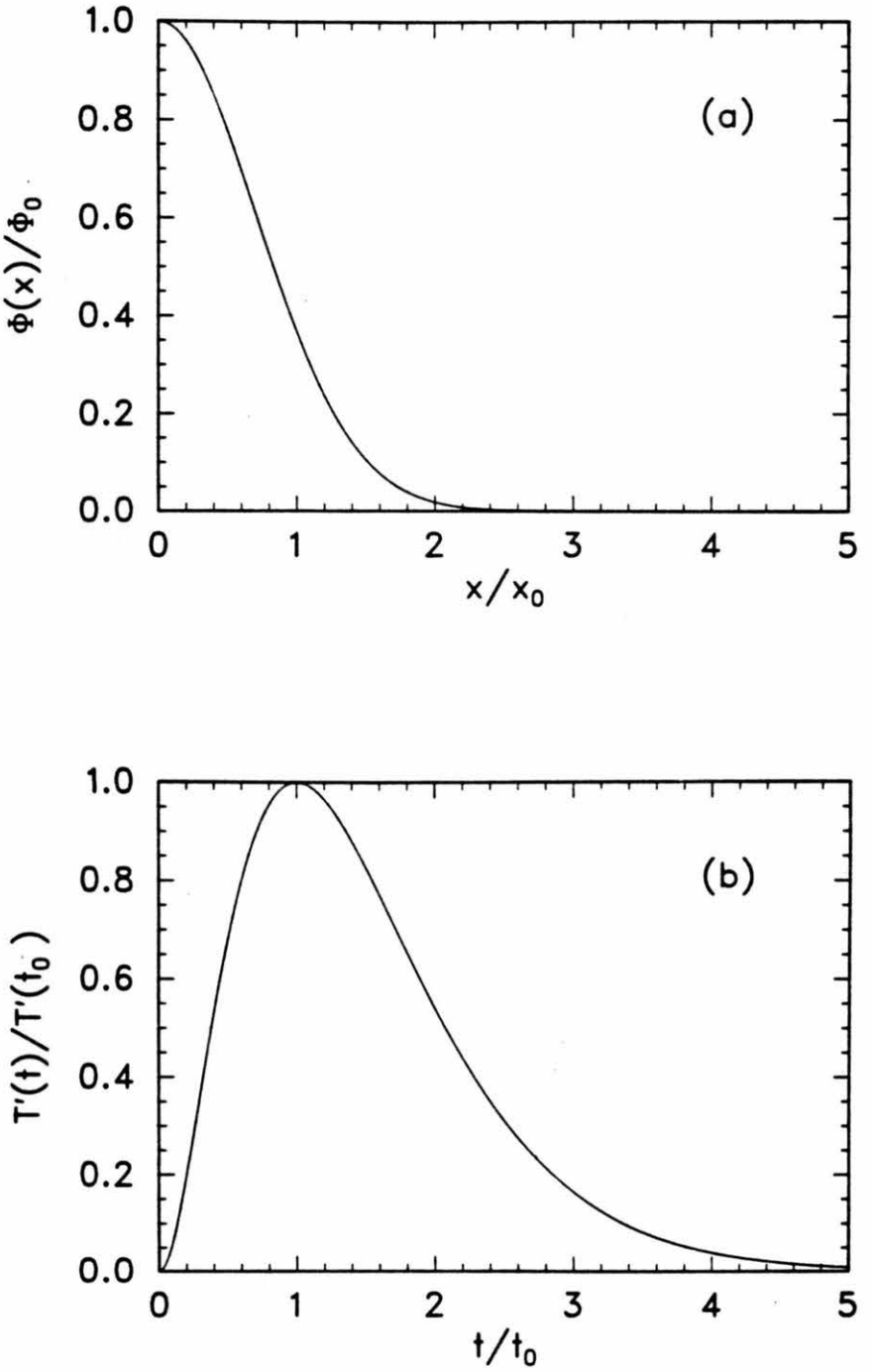

Figure 5. Space dependence (a) and time dependence (b) of the geopotential forcing.

where $s_0 = \frac{fx}{2c}$ and

$$\mathrm{erfc}(z) = \frac{2}{\sqrt{\pi}} \int_z^\infty e^{-s^2}\, ds \tag{3.61}$$

is the complementary error function (Abramowitz and Stegun, 1964, chapter 7).

For the results presented here we take advantage of the spatial symmetry of the forcing by using the domain [a,b] = [0,1000 km] with a wall at x=0. The Coriolis parameter is $f=5\times10^{-5}$ s^{-1}, corresponding to a latitude of 20°N, and the space scale of the forcing is x_0=200 km. Two forcing time scales are considered: "slow" forcing with t_0=12 hours and "fast" forcing with t_0=3 hours. The fast forcing generates more gravity waves, but in view of (3.58) the final state is the same in both cases. The spectral truncation N=16 is used unless otherwise noted, and the space-discretized equations are integrated using explicit time differencing with the time step chosen small enough that the time differencing errors are negligible. As discussed in chapter 5, the shallow water model can be related to the full "primitive equations," which govern the motions of a compressible atmosphere, through a vertical normal mode transform. For this reason we consider here three different values of c, namely 250, 50 and 10 ms^{-1}, which correspond roughly to the external, first internal and sixth internal modes of a compressible atmosphere with a lid at the pressure 100 mb. These different values of c give differing partitions of energy between gravity waves and geostrophic flow, as discussed by Schubert et al. (1980). Since the problem is linear the forcing amplitude Φ_0 is arbitrary; here we choose $\Phi_0=c^2/10$ so that the final state variables u', v' and ϕ'/c have the same order of magnitude for each of the three choices of c.

First we consider the effects of four different boundary conditions applied at x=b: the inhomogeneous characteristic condition (3.22), the homogeneous characteristic condition (3.21), the balance condition (3.35) and the wall condition (3.37). For the case c=250 ms^{-1}, which corresponds roughly to the external mode of the atmosphere, the final state is essentially reached by the time $t=8t_0$ at which the solutions are displayed below. The analytical final state as computed from the balanced model is shown in Fig. 6; in this and subsequent figures the dotted line represents u, the dashed line v and the solid line ϕ/c. With the inhomogeneous characteristic condition the numerical (Chebyshev-tau) solution is essentially the same as the analytical solution and hence is not shown. With the homogeneous characteristic condition the numerical solution in both the slow and fast forcing cases is as shown in Fig. 7; the incorrect specification of the boundary values has shifted ϕ by a constant and distorted the slope of v near the boundary. With the balance condition the numerical solution is close to the analytical solution for the slow forcing case (Fig. 8), but with fast forcing the effects of trapped gravity waves are clearly seen in both u and ϕ (Fig. 9). Similarly, the wall condition leads to v=0 at the boundary and considerable distortion of ϕ in both the slow forcing (Fig. 10) and fast forcing (Fig. 11) cases (note the change of scale for ϕ/c).

In the case c=50 ms^{-1}, corresponding roughly to the first internal mode of the atmosphere, the analytical final state shown in Fig. 12 is reached by the time t=96 hours at which the numerical results below are shown. With the inhomogeneous characteristic condition the numerical solution again is essentially the same as the analytical solution and hence is not shown. With the homogeneous characteristic condition the

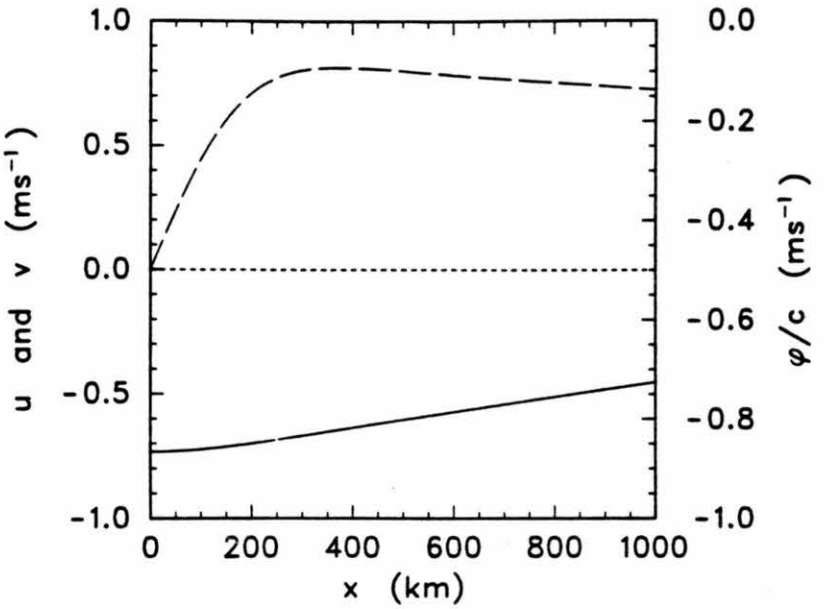

Figure 6. Analytical solution of the linear, y-independent shallow water model for the case c=250 ms^{-1}. The dotted line represents u, the dashed line v and the solid line ϕ/c.

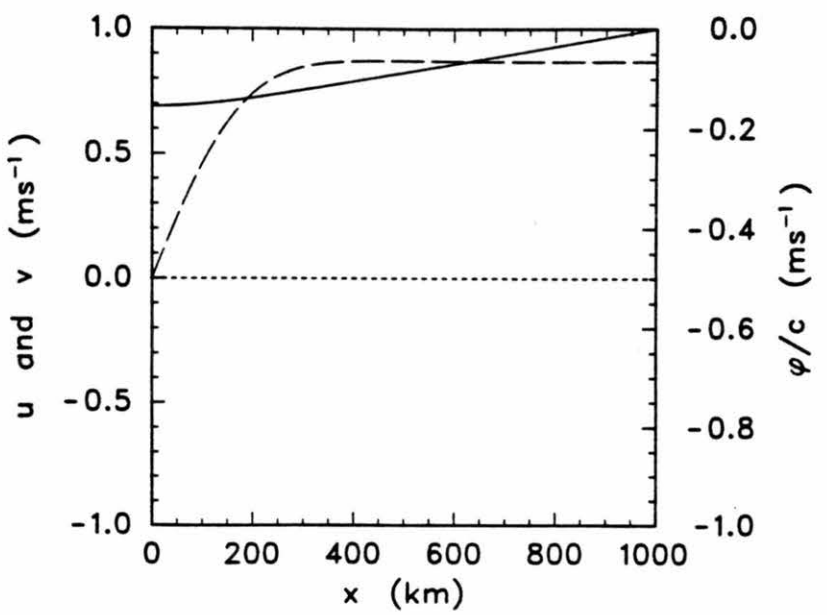

Figure 7. Numerical solution with the homogeneous characteristic condition for the case c=250 ms^{-1}.

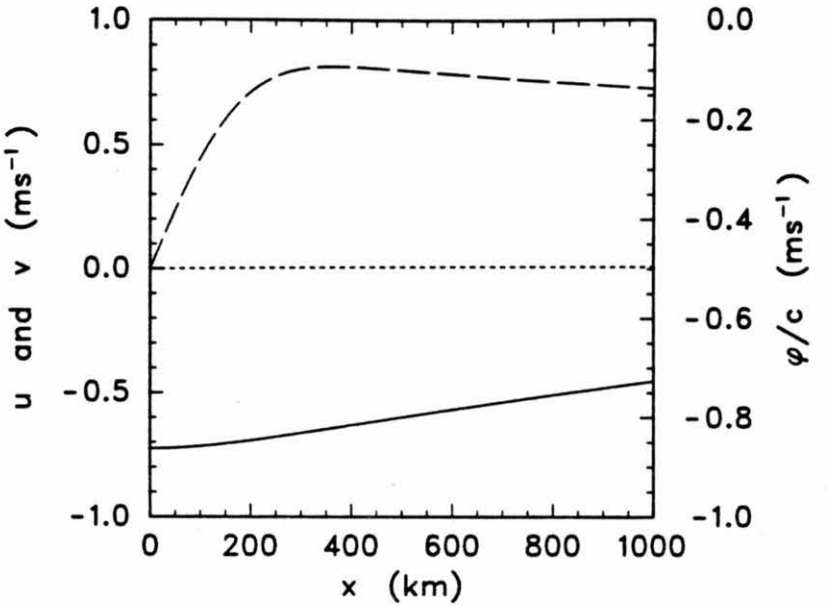

Figure 8. Numerical solution with the balance condition for the case c=250 ms^{-1} with slow forcing.

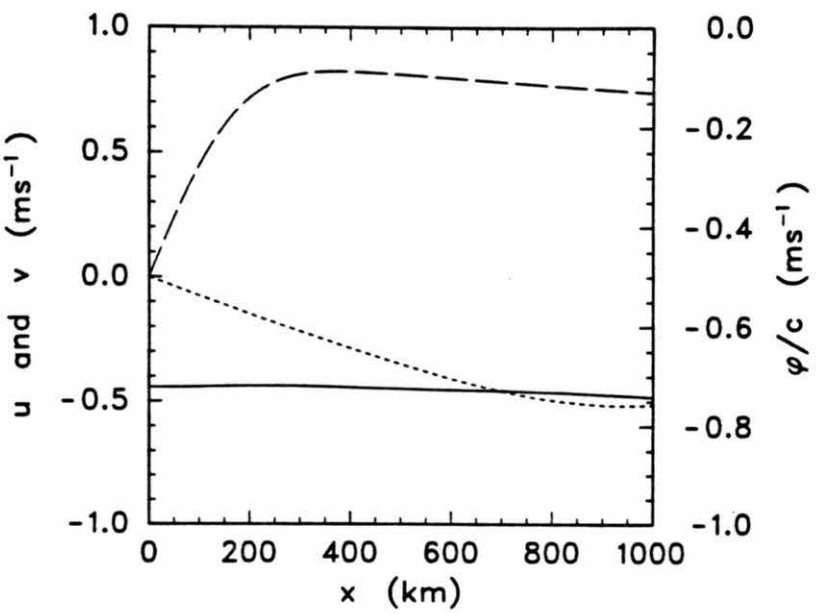

Figure 9. Numerical solution with the balance condition for the case c=250 ms^{-1} with fast forcing.

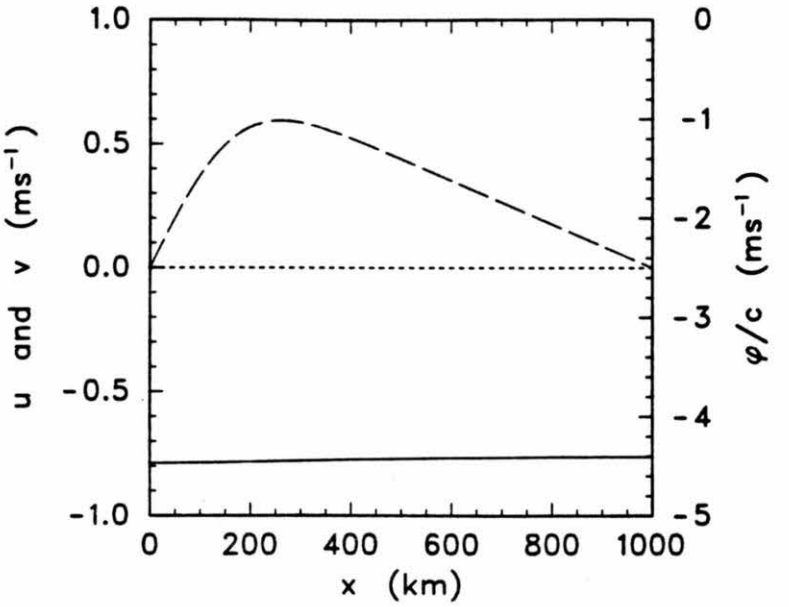

Figure 10. Numerical solution with the wall condition for the case c=250 ms^{-1} with slow forcing.

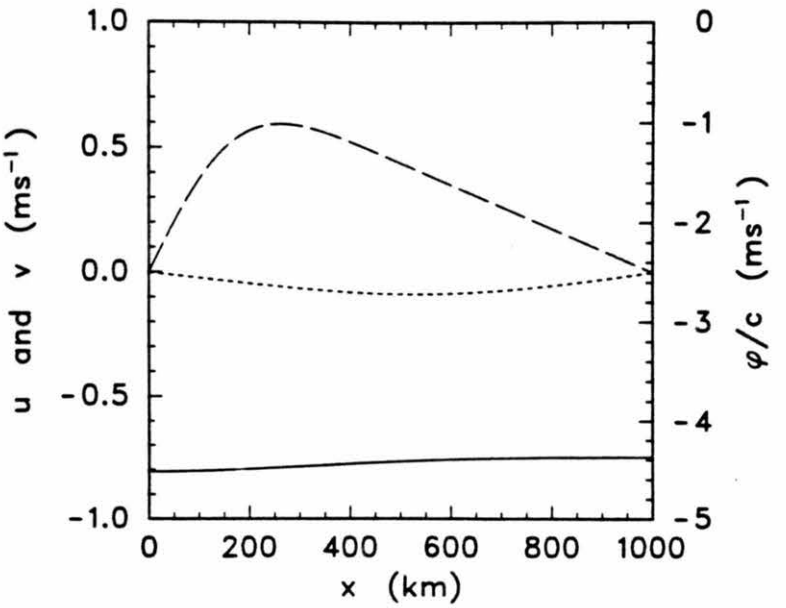

Figure 11. Numerical solution with the wall condition for the case c=250 ms^{-1} with fast forcing.

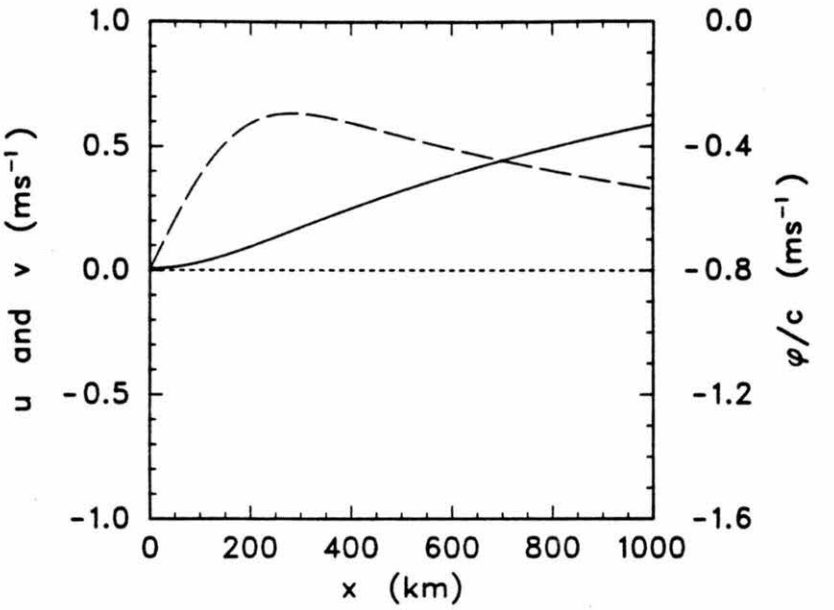

Figure 12. Analytical solution of the linear, y-independent shallow water model for the case c=50 ms^{-1}.

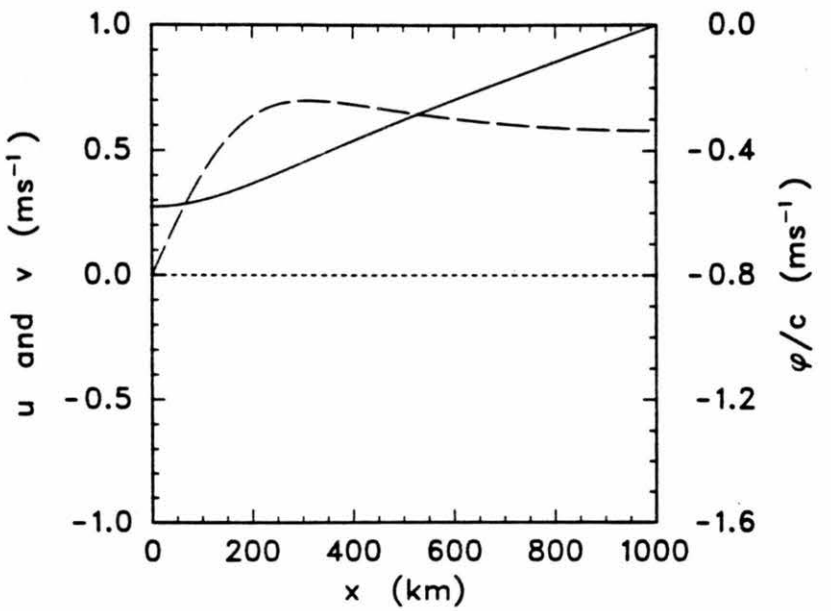

Figure 13. Numerical solution with the homogeneous characteristic condition for the case c=50 ms^{-1}.

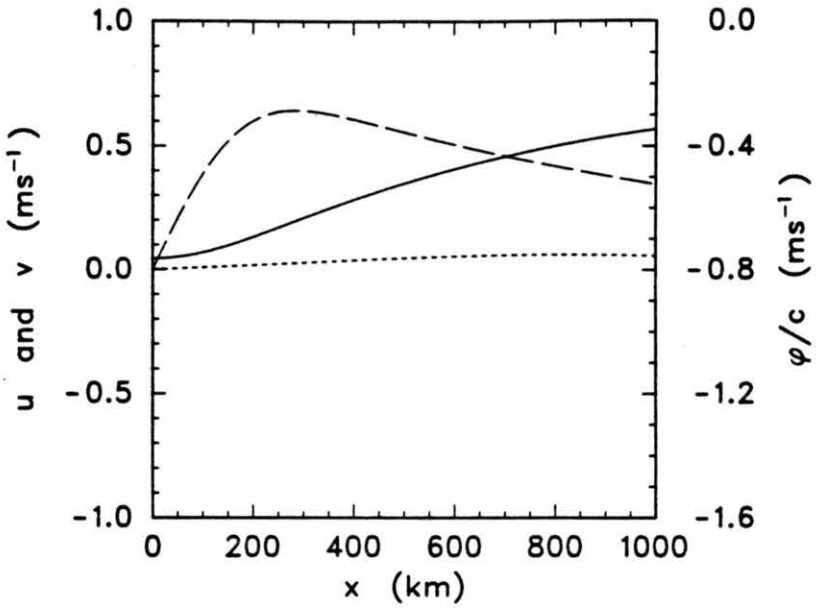

Figure 14. Numerical solution with the balance condition for the case c=50 ms^{-1} with slow forcing.

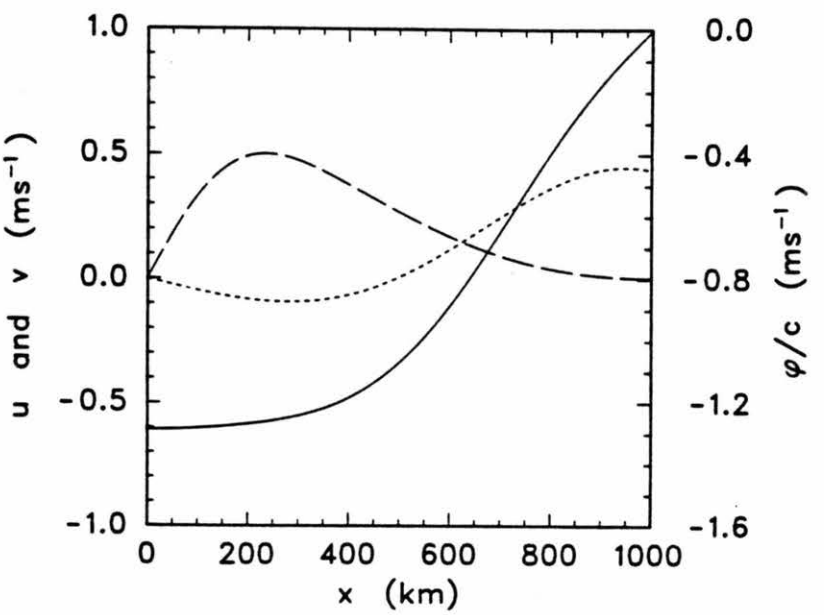

Figure 15. Numerical solution with the balance condition for the case c=50 ms^{-1} with fast forcing.

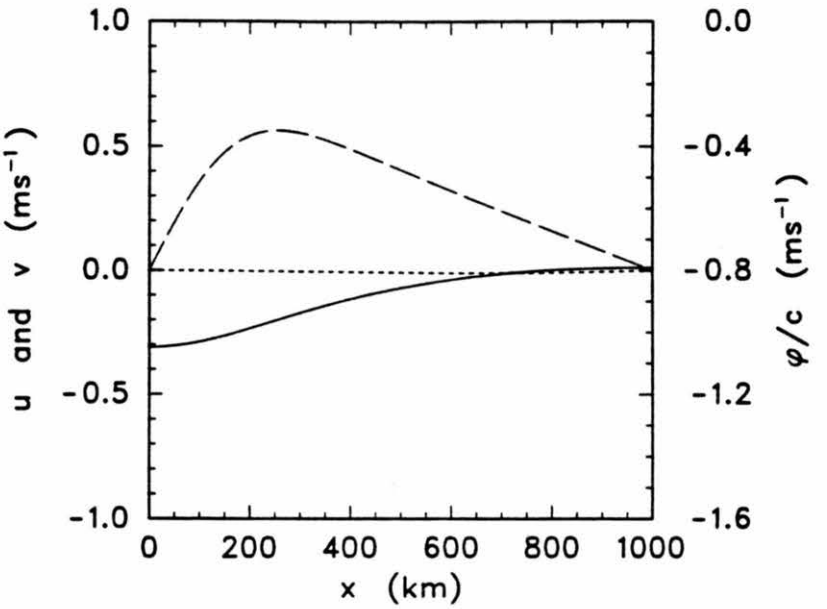

Figure 16. Numerical solution with the wall condition for the case c=50 ms^{-1} with slow forcing.

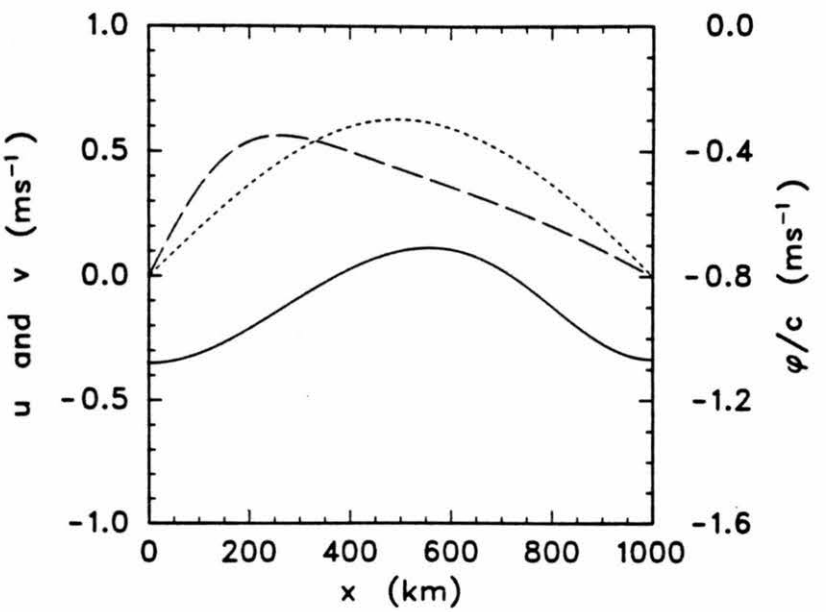

Figure 17. Numerical solution with the wall condition for the case c=50 ms^{-1} with fast forcing.

final state shown in Fig. 13 is reached in both the slow and fast forcing cases; as before this boundary condition has distorted v near the boundary and shifted ϕ by a constant. With the balance condition only a small amount of distortion due to trapped gravity waves is evident in the slow forcing case (Fig. 14), but with fast forcing (Fig. 15) the gravity waves nearly dominate the solution. Similarly poor results are also obtained with the wall condition with slow forcing (Fig. 16) and with fast forcing (Fig. 17).

Figure 18 shows the analytical final state for the case c=10 ms^{-1}, which corresponds roughly to the ninth internal mode of the atmosphere. With the inhomogeneous characteristic condition the numerical solutions at t=96 hours show some evidence of gravity waves in both the slow forcing (Fig. 19) and fast forcing (Fig. 20) cases. This is because c is small enough that waves on the scale of the domain have frequencies close to the Coriolis frequency f and hence are substantially reflected by the characteristic condition. Since there is little balanced flow near the boundary, the solution obtained with the homogeneous characteristic condition, shown in Fig. 21 for the fast forcing case, is very close to that obtained with the inhomogeneous characteristic condition. Finally, the balance and wall conditions, being totally reflecting, produce still worse results, as shown in Figs. 22-25.

The relative accuracies of the various boundary conditions as evidenced by the above results are confirmed in detail in Table 1, which gives the L_2 errors in u, v and ϕ/c for each of the cases presented above. For the characteristic boundary conditions the errors presented are asymptotic errors obtained with the Chebyshev-tau method; for c=10 ms^{-1} the errors decay only slowly due to partial reflection of gravity

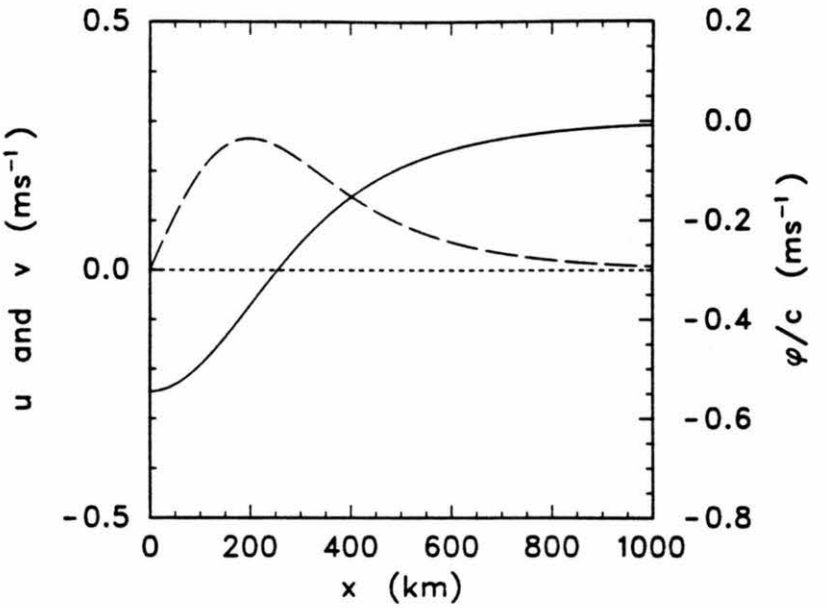

Figure 18. Analytical solution of the linear, y-independent shallow water model for the case c=10 ms^{-1}.

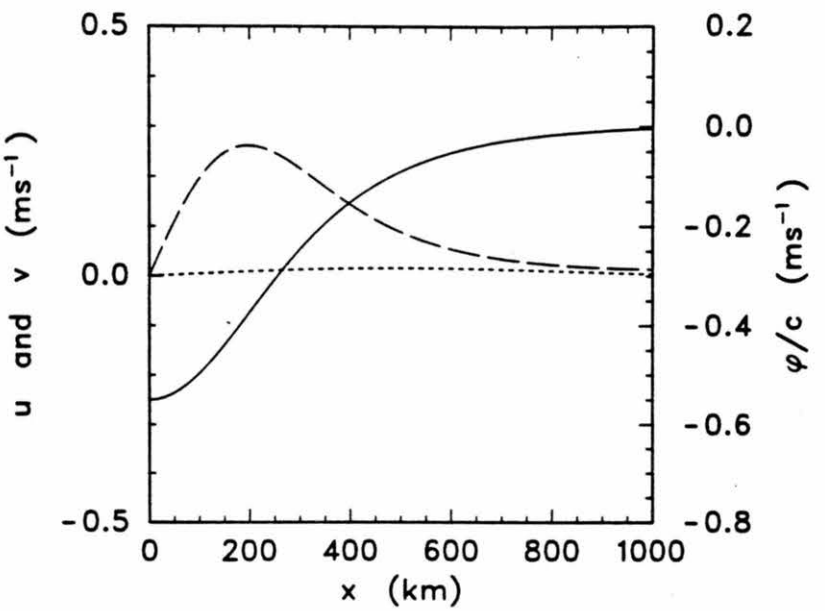

Figure 19. Numerical solution with the inhomogeneous characteristic condition for the case c=10 ms^{-1} with slow forcing.

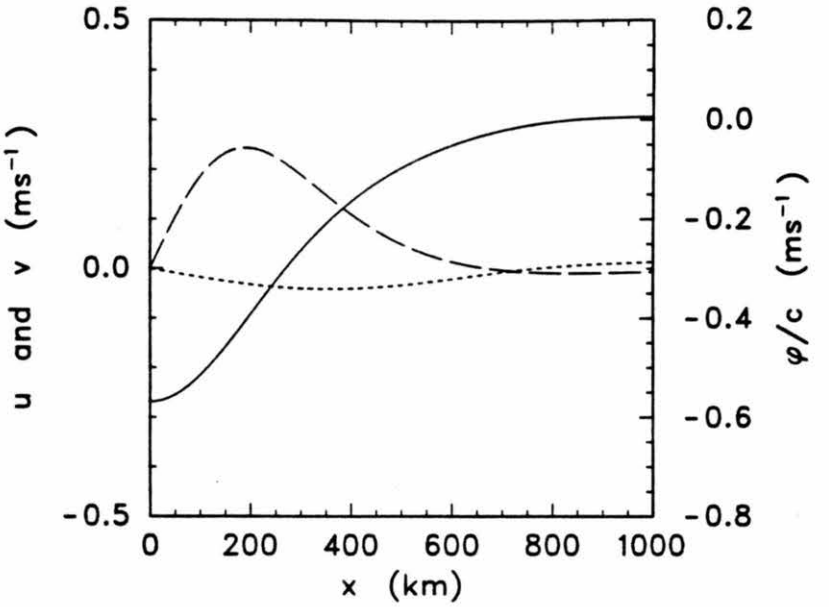

Figure 20. Numerical solution with the inhomogeneous characteristic condition for the case c=10 ms^{-1} with fast forcing.

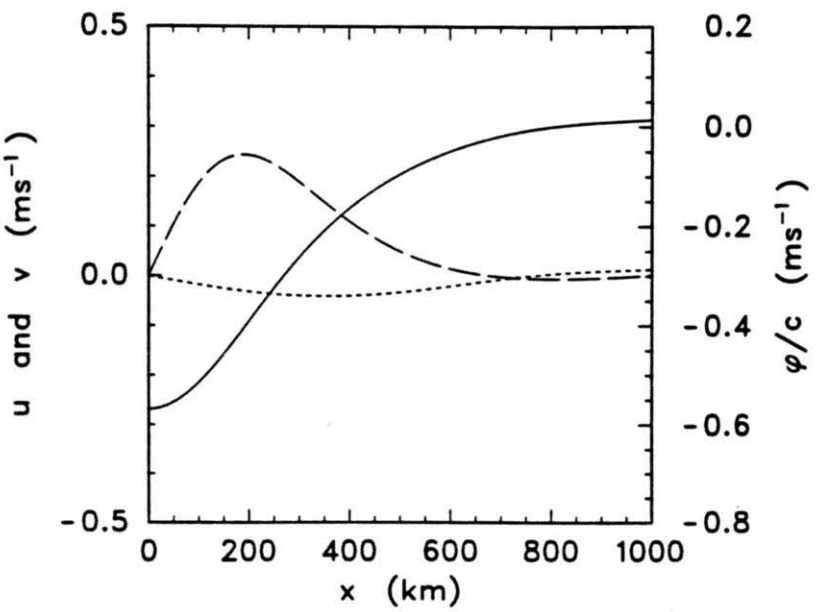

Figure 21. Numerical solution with the homogeneous characteristic condition for the case c=10 ms^{-1} with fast forcing.

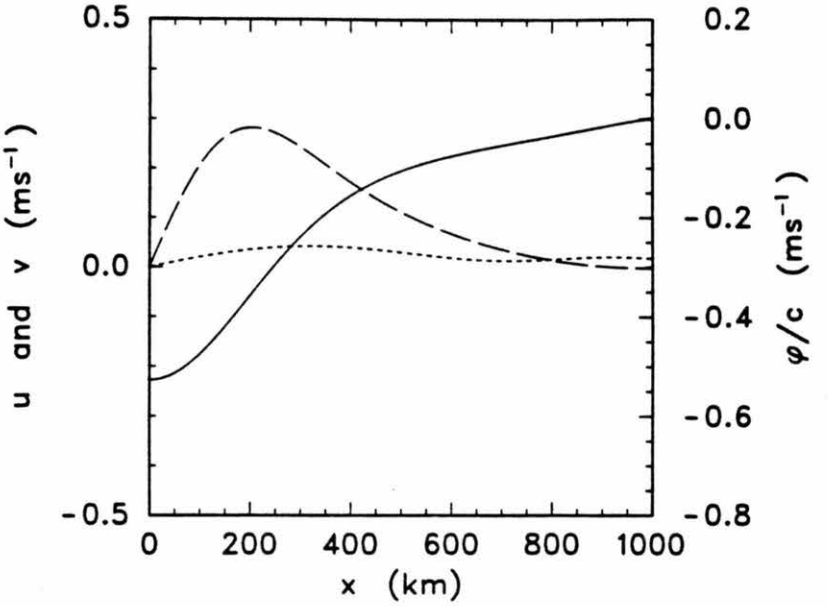

Figure 22. Numerical solution with the balance condition for the case c=10 ms^{-1} with slow forcing.

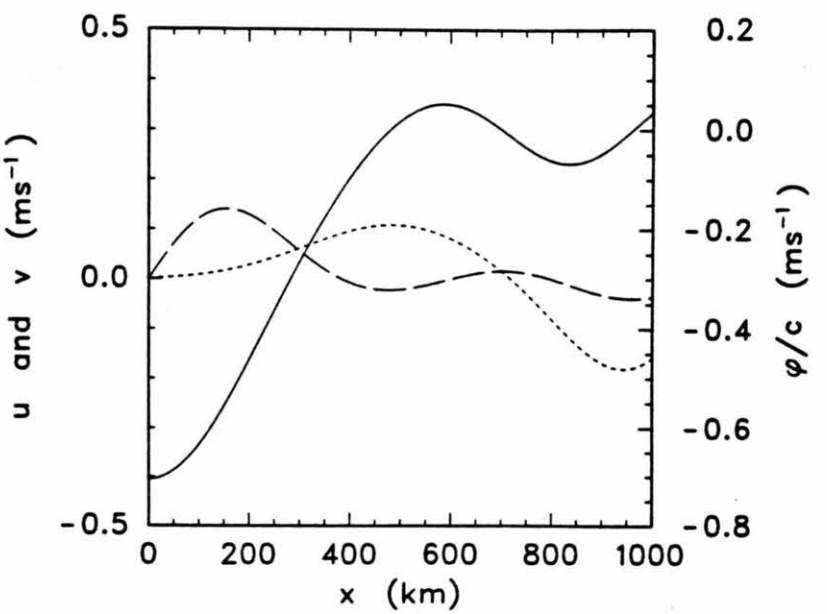

Figure 23. Numerical solution with the balance condition for the case c=10 ms^{-1} with fast forcing.

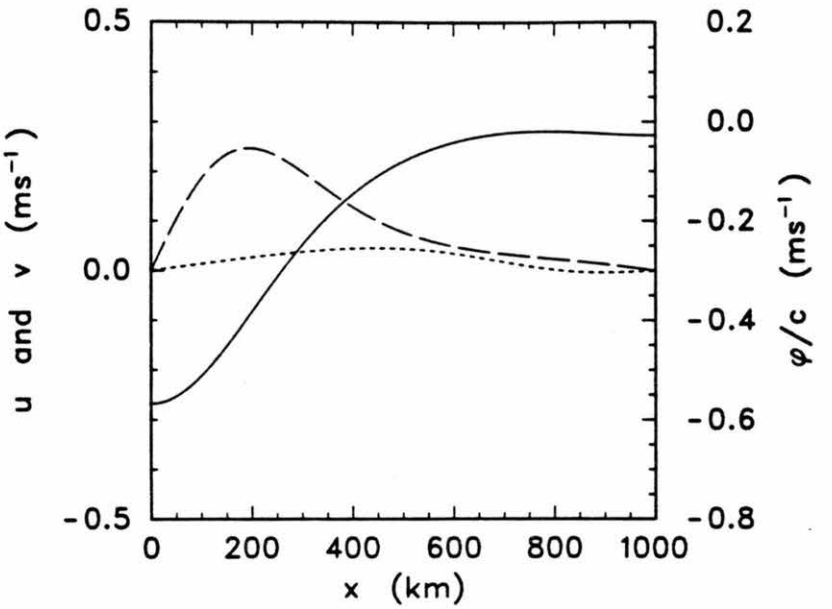

Figure 24. Numerical solution with the wall condition for the case c=10 ms^{-1} with slow forcing.

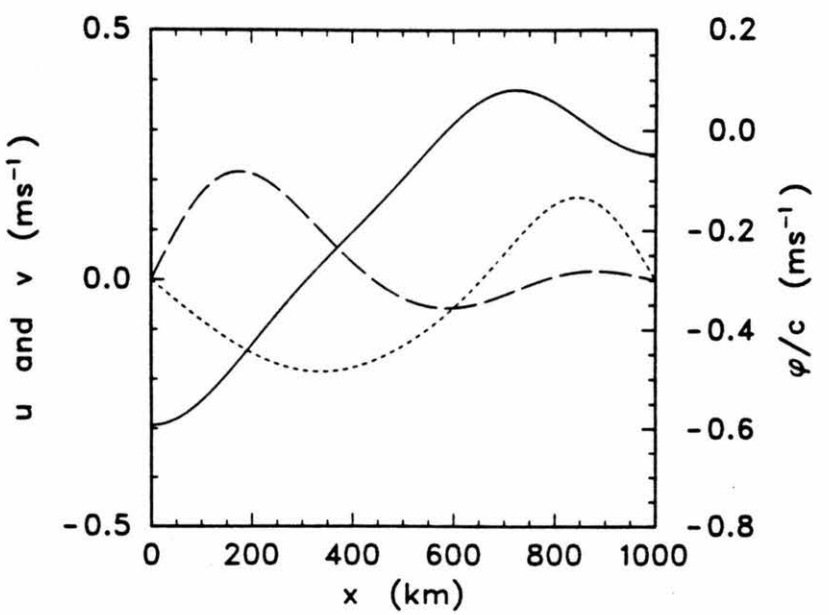

Figure 25. Numerical solution with the wall condition for the case c=10 ms^{-1} with fast forcing.

Table 1. L_2 errors in u, v and ϕ/c for the Chebyshev-tau method with various boundary conditions (Numbers in parentheses are exponents of 10).

c (ms^{-1})	t_o (hours)	Boundary condition at x=b=1000 km	L_2 errors (ms^{-1})		
			u	v	ϕ/c
250	12	Inhomo. char.	2.74(-13)	9.66(-7)	1.23(-8)
		Homo. char.	1.09(-12)	8.25(-2)	7.16(-1)
		Balance	6.17(-3)	3.90(-4)	3.09(-3)
		Wall	7.45(-4)	4.18(-1)	3.63(0)
	3	Inhomo. char.	5.75(-12)	9.66(-7)	1.23(-8)
		Homo. char.	1.29(-11)	8.25(-2)	7.16(-1)
		Balance	1.91(-1)	3.33(-2)	2.62(-1)
		Wall	4.34(-2)	4.16(-1)	3.63(0)
50	12	Inhomo. char.	9.09(-13)	9.65(-7)	5.77(-8)
		Homo. char.	2.25(-12)	1.36(-1)	2.53(-1)
		Balance	3.97(-2)	1.28(-2)	2.13(-2)
		Wall	1.36(-2)	1.78(-1)	3.33(-1)
	3	Inhomo. char.	3.50(-13)	9.65(-7)	5.78(-8)
		Homo. char.	2.40(-13)	1.36(-1)	2.53(-1)
		Balance	4.05(-1)	1.75(-1)	3.20(-1)
		Wall	3.04(-1)	2.46(-1)	4.25(-1)
10	12	Inhomo. char.	1.38(-3)	3.61(-3)	2.09(-3)
		Homo. char.	1.37(-3)	3.23(-3)	4.07(-3)
		Balance	2.26(-2)	1.73(-2)	1.31(-2)
		Wall	2.19(-2)	1.88(-2)	1.53(-2)
	3	Inhomo. char.	1.43(-2)	5.05(-3)	5.05(-3)
		Homo. char.	1.42(-2)	4.55(-3)	3.56(-3)
		Balance	1.07(-1)	7.75(-2)	7.34(-2)
		Wall	1.16(-1)	7.48(-2)	7.55(-2)

waves, so errors at the arbitrary time t=192 hours are shown. For the balance and wall conditions the errors are averaged over a given period (1, 5 and 25 hours for c=250, 50 and 10 ms^{-1}, respectively), starting at the time of the corresponding figures, in order to smooth out the effects of trapped gravity waves. From this Table we conclude the following. First, the inhomogeneous characteristic condition gives the best results in each case, usually by many orders of magnitude. Second, with little balanced flow near the boundary the two characteristic conditions give comparable errors which decay slowly with time due to partial relection of gravity waves. Third, the balance condition is preferable to both the wall and homogeneous characteristic conditions when the forcing is slow and there is significant balanced flow near the boundary. Finally, with fast forcng the balance and wall conditions give comparably poor results.

For the results presented above the Chebyshev-tau and Chebyshev-collocation solutions are the same on the scale of the graphs. Indeed, Table 1 shows that the overall accuracy of the method is limited by the accuracy of the boundary condition, not the discretization method, for all but the inhomogeneous characteristic condition. For that condition, however, there are significant differences between the tau and collocation solutions. Table 2 shows the L_2 errors in u, v and ϕ/c at t=96 hours obtained using the inhomogeneous characteristic condition for different values of the spectral truncation N; these results are for the case c=50 ms^{-1} with fast forcing. For the tau method (the first column for each of u, v and ϕ/c) u is essentially zero, indicating that all gravity waves have propagated out of the domain, and both v and ϕ/c

Table 2. L_2 errors in u', v' and ϕ'/c at t=96 hours, for the case c=50 ms^{-1} with fast forcing, as functions of the spectral truncation N. The columns labeled col. (phys.) and col. (spec.) are for the collocation method with the boundary conditions applied in physical space (the usual method) and spectral space, respectively.

N	L_2 error in u (ms^{-1})			L_2 error in v (ms^{-1})			L_2 error in ϕ/c (ms^{-1})		
	tau	col. (phys.)	col. (spec.)	tau	col. (phys.)	col. (spec.)	tau	col. (phys.)	col. (spec.)
4	5.85(-13)	1.38(-3)	2.47(-12)	1.82(-2)	5.72(-2)	5.38(-2)	5.80(-3)	2.68(-2)	2.64(-2)
8	4.31(-13)	2.13(-6)	3.64(-12)	9.33(-4)	2.19(-3)	1.67(-3)	1.52(-4)	1.47(-4)	1.46(-4)
12	4.43(-13)	6.51(-6)	5.25(-12)	5.12(-5)	9.39(-5)	5.79(-5)	3.82(-6)	6.72(-6)	3.34(-6)
16	3.50(-13)	3.65(-6)	4.68(-12)	9.65(-7)	1.18(-6)	8.94(-7)	5.78(-8)	8.06(-6)	6.62(-8)
20	1.09(-12)	4.72(-6)	1.30(-11)	1.23(-8)	5.99(-8)	1.72(-8)	8.52(-10)	3.76(-6)	7.00(-10)
24	1.09(-12)	1.71(-6)	1.33(-11)	2.56(-10)	4.74(-8)	2.98(-10)	9.68(-12)	3.26(-6)	1.32(-10)

converge exponentially with N as expected. However, in the collocation method (the second column) u is small but nonzero and ϕ/c does not converge exponentially with N. Since v does converge fairly quickly, it is likely that this lessened accuracy of the collocation method is related to the boundary condition, which involves u and ϕ/c and is applied in physical space. Indeed, if the same condition is applied in spectral space for the collocation method (by transforming u and ϕ to spectral space, applying the boundary condition exactly as in the tau method and transforming back), the accuracy obtained (the third column) is nearly as good as in the tau method. This result is not unexpected, since for linear problems such as the one studied here the tau and collocation approximations differ only by the projection of the initial conditions and forcing and the application of the boundary conditions (Gottlieb and Orszag, 1977, p. 15). Nevertheless, the relative inaccuracy of the collocation method with boundary conditions applied in physical space as usual is surprising and merits further study.

To test the nonlinear versions of the one-dimensional shallow water model we use the case c=50 ms^{-1} with fast forcing. With Φ_0=250 m^2s^{-2} as above the problem is essentially linear, so the linear form (3.22) of the characteristic condition still works well and the inflow condition (3.33) is not needed in practice. In this case the tau and collocation solutions are similar to the linear solutions presented above, both with the advective and rotational forms of the equations. When the amplitude of the forcing is increased to Φ_0=4000 m^2s^{-2}, however, the problem is indeed nonlinear, and the nonlinear form (3.32) of the characteristic condition produces significantly less reflection of gravity waves (as evidenced by oscillations in u) than the linear form (3.22).

Furthermore, the inflow condition (3.33) is in fact necessary; without it, the v field develops large oscillations which are clearly not physically meaningful. Thus for the numerical results presented below (computed for the case Φ_o=4000 m^2s^{-2}) we use the nonlinear form of the characteristic condition and apply the inflow condition at x=b.

Figure 26 shows the analytical final state of the linear model, for the purpose of comparison. The nonlinear Chebyshev-tau solution at t=36 hours is shown in Fig. 27; the tau solutions obtained from the advective and rotational forms are identical on the scale of this figure. The main effect of the nonlinear terms is to steepen the slope of v near x=0, shifting the peak in v from about x=275 km to about x=150 km and reducing ϕ at x=0 slightly. The oscillations present in the v field are due to the inexact specification of the boundary value of v (the values used are from (3.59) which is exact for the linear solution only). Since in the tau method the inflow condition determines the last spectral coefficient $\hat{v}_N$, the error introduced at the boundary causes some high wavenumber oscillations throughout the domain. In contrast, the Chebyshev-collocation solution in Fig. 28 (computed from the advective form) has less high wavenumber oscillation in v, but shows some evidence of gravity waves in u and ϕ. The collocation solution computed from the rotational form (Fig. 29) is similar but has slightly less evidence of gravity waves.

In general, models which include nonlinear advective processes (such as the shallow water model) have the potential for forming shocks or near-discontinuities, in much the same way that the slope of v near x=0 increased in the example above. This poses a problem for most numerical methods, since eventually the gradient may become too sharp to

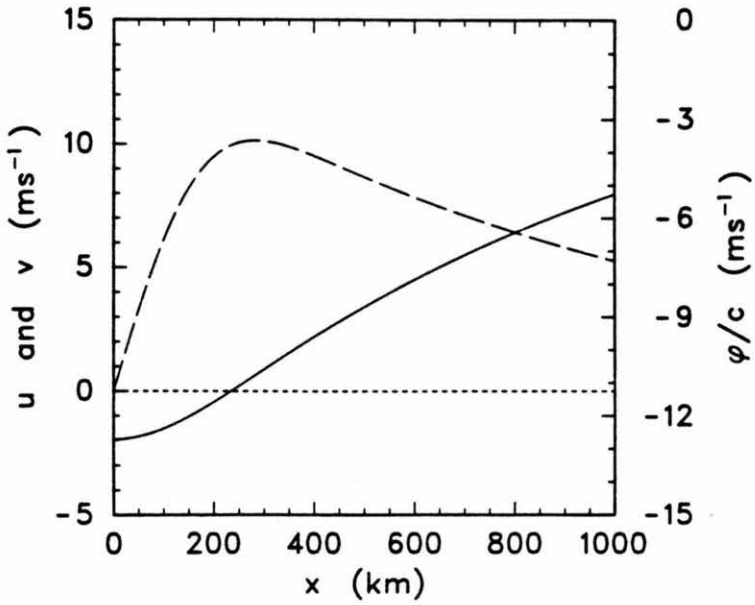

Figure 26. Analytical solution of the linear, y-independent shallow water model for the case c=50 ms^{-1} with Φ_o=4000 m^2s^{-2} .

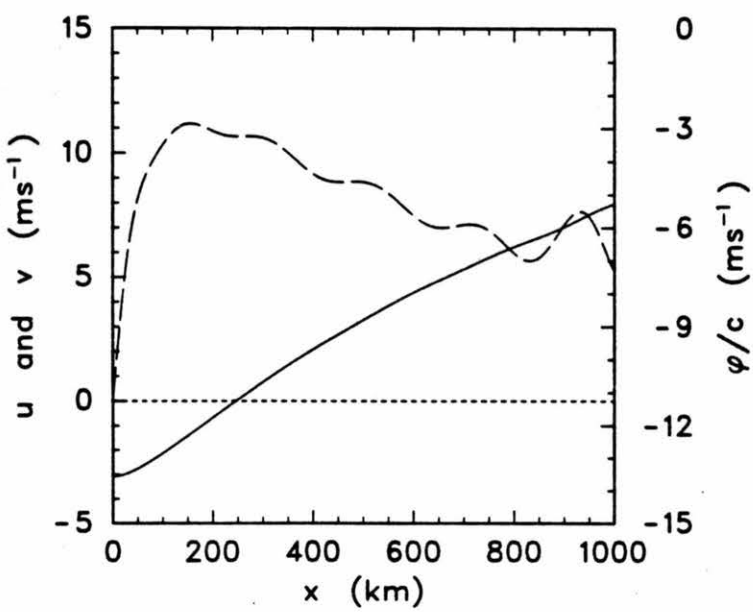

Figure 27. Chebyshev-tau solution of the nonlinear model.

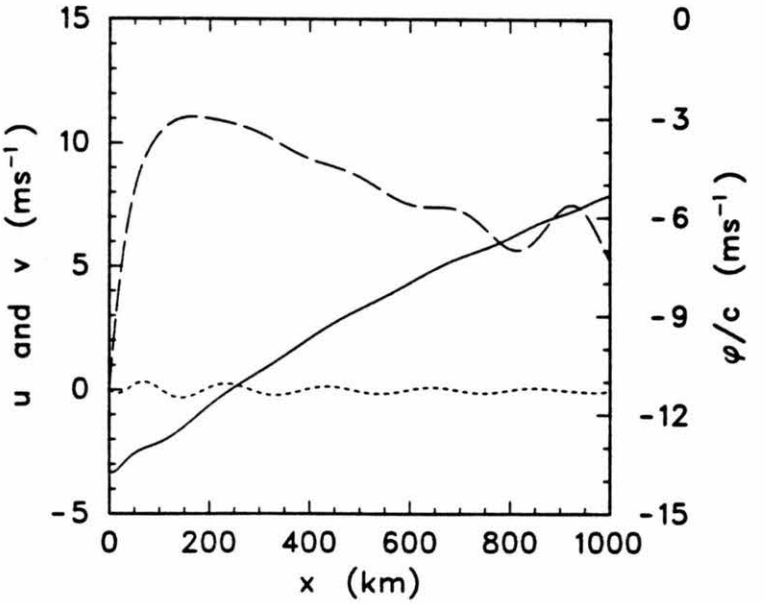

Figure 28. Chebyshev-collocation solution of the nonlinear model in advective form.

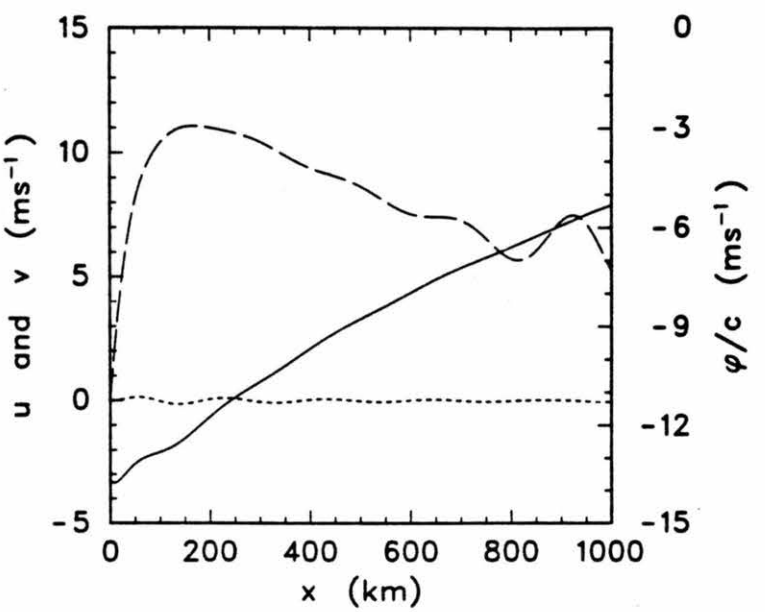

Figure 29. Chebyshev-collocation solution of the nonlinear model in rotational form.

be resolved, regardless of the discretization scheme. In spectral models this lack of resolution results in high wavenumber oscillations (e.g., Schubert et al., 1984). Fox and Orszag (1973) claim that in pseudospectral (collocation) models these oscillations may lead to instability unless the equations are formulated in a conservative or rotational form. No evidence of such instability was detected in the one-dimensional model considered here, and even with the spectral truncation reduced to N=8 very little oscillation developed. In cases where such oscillations do develop they may be reduced by including suitable friction terms or filtering, which may also help in reducing oscillations and spurious gravity waves introduced by incorrect specification of boundary values. Since the inclusion of friction terms can strongly influence the efficiency of Chebyshev methods, this topic will be addressed again in the next chapter.

To test the Chebyshev spectral versions of the two-dimensional shallow water model we use a two-dimensional analogue of the test case used above. Specifically, the fields u, v and ϕ are zero initially, the wind field forcing is zero (F=G=0), and the mass field is forced by a separable geopotential sink Q, similar to (3.54), with space dependence given by

$$\Phi(x,y) = \Phi_0 \exp\left[-\left(\frac{x-x_c}{x_0}\right)^2 - \left(\frac{y-y_c}{y_0}\right)^2\right] \qquad (3.62)$$

and time dependence given by (3.56). For the results presented below the model domain is [0,3000 km] x [0,3000 km], the forcing is centered at (x_c,y_c) = (1000 km, 1000 km) with e-folding width $x_0=y_0$=200 km and

amplitude $\Phi_0=2500\ m^2s^{-2}$, and the forcing time scale t_0 is 3 hours. As before, $f=5x10^{-5}s^{-1}$, corresponding to the latitude 20°N, and we choose $c=50\ ms^{-1}$ which corresponds roughly to the first internal mode of the atmosphere. The spectral truncation N=24 is used in both x and y.

The nonlinear numerical solutions at t=6 hours, computed using the homogeneous characteristic condition and the wall condition, are shown in Figs. 30a and 30b, respectively. In these and subsequent figures, ϕ/c is represented by contour lines (with contour interval $0.5\ ms^{-1}$ and dotted lines for negative values) and the wind field by vectors at discrete points (scaled so that a vector from one point to the next would have magnitude $4\ ms^{-1}$). We see that the gravity wave front generated by the forcing has just started to reach the boundaries, with the wall condition distorting the solution slightly. Three hours later the solution with the characteristic condition (Fig. 31a) shows the wave passing through the boundary, while the wall condition (Fig. 31b) has reflected it. By t=12 hours there is some distortion in the solution with the characteristic condition, as shown in Fig. 32a. Some of this may be due to partial reflection of gravity waves; more likely, most of it is due to applying the characteristic condition in the homogeneous form where there is significant balanced flow, e.g. on the x-axis near x=1000 km. However, this distortion is minimal compared to that due to reflection of gravity waves by the wall condition (Fig. 32b). At t=24 hours the gravity waves have essentially left the domain in the solution with the characteristic condition (Fig. 33a), while they almost dominate the solution with the wall condition (Fig. 33b).

The solutions with the characteristic condition presented above were computed by the tau method using the rotational form (3.2) of the

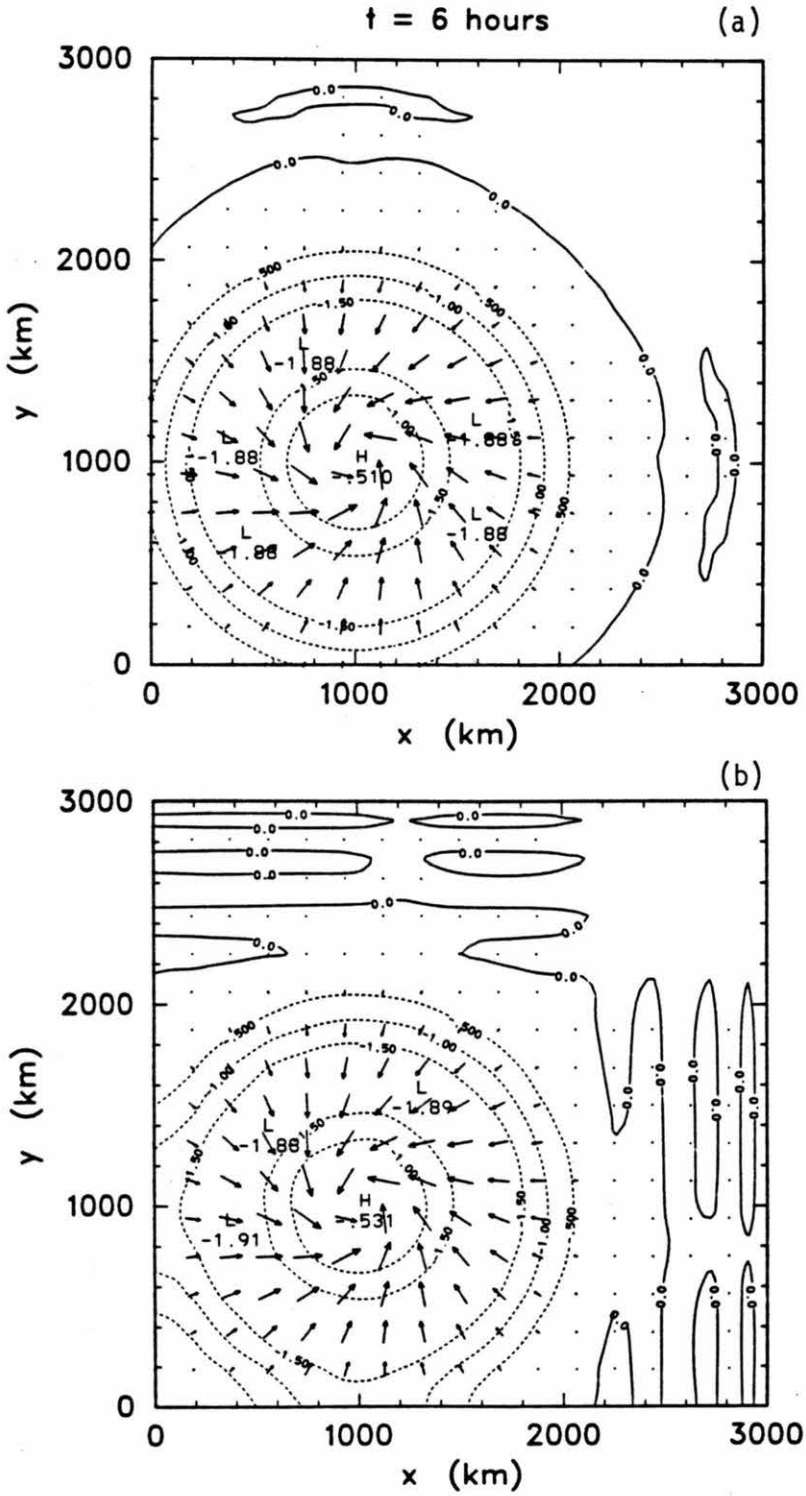

Figure 30. Chebyshev-tau solution of the two-dimensional shallow water model at t=6 hours using (a) the homogeneous characteristic condition and (b) the wall condition.

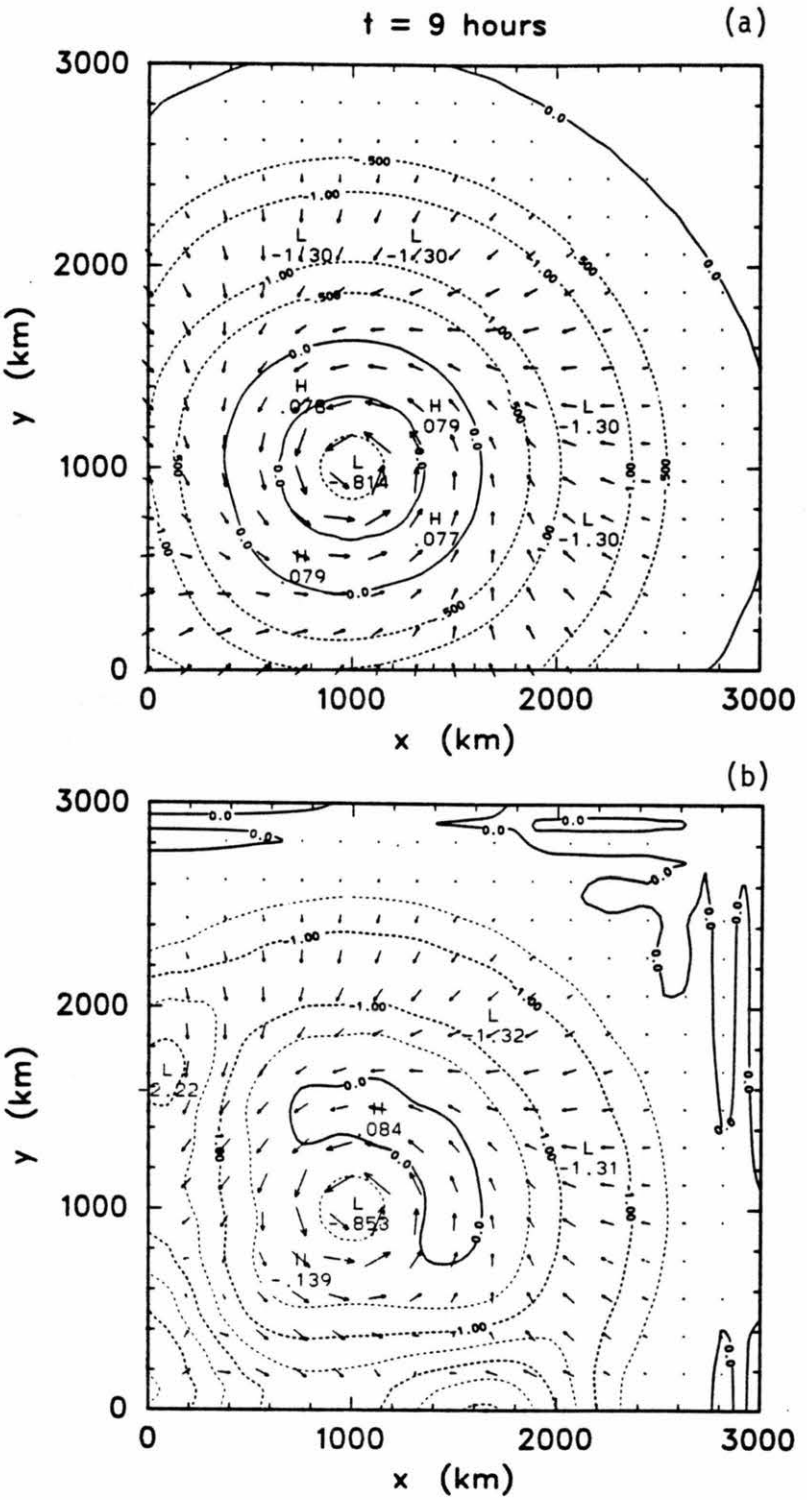

Figure 31. Chebyshev-tau solution of the two-dimensional shallow water model at t=9 hours using (a) the homogeneous characteristic condition and (b) the wall condition.

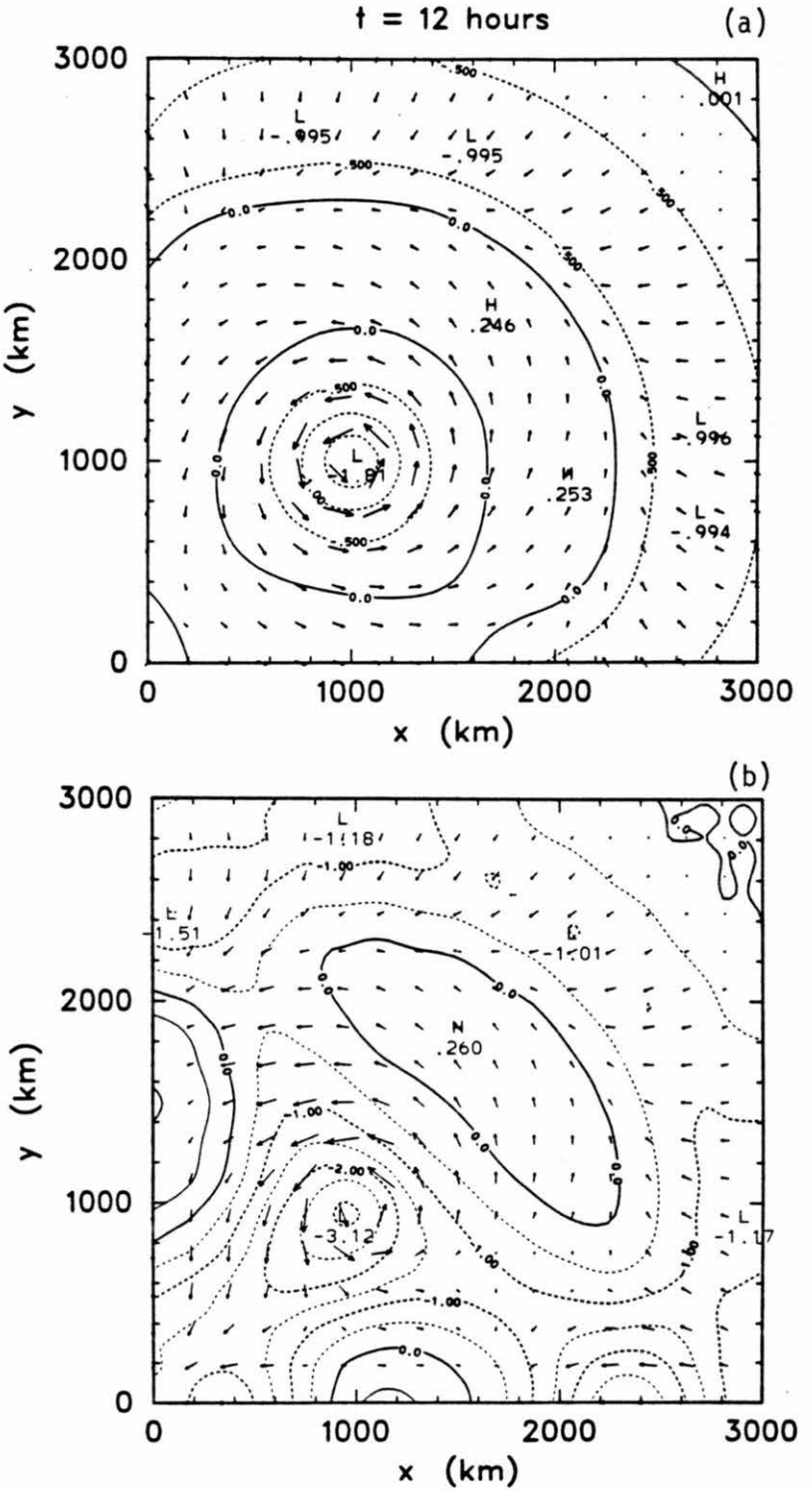

Figure 32. Chebyshev-tau solution of the two-dimensional shallow water model at t=12 hours using (a) the homogeneous characteristic condition and (b) the wall condition.

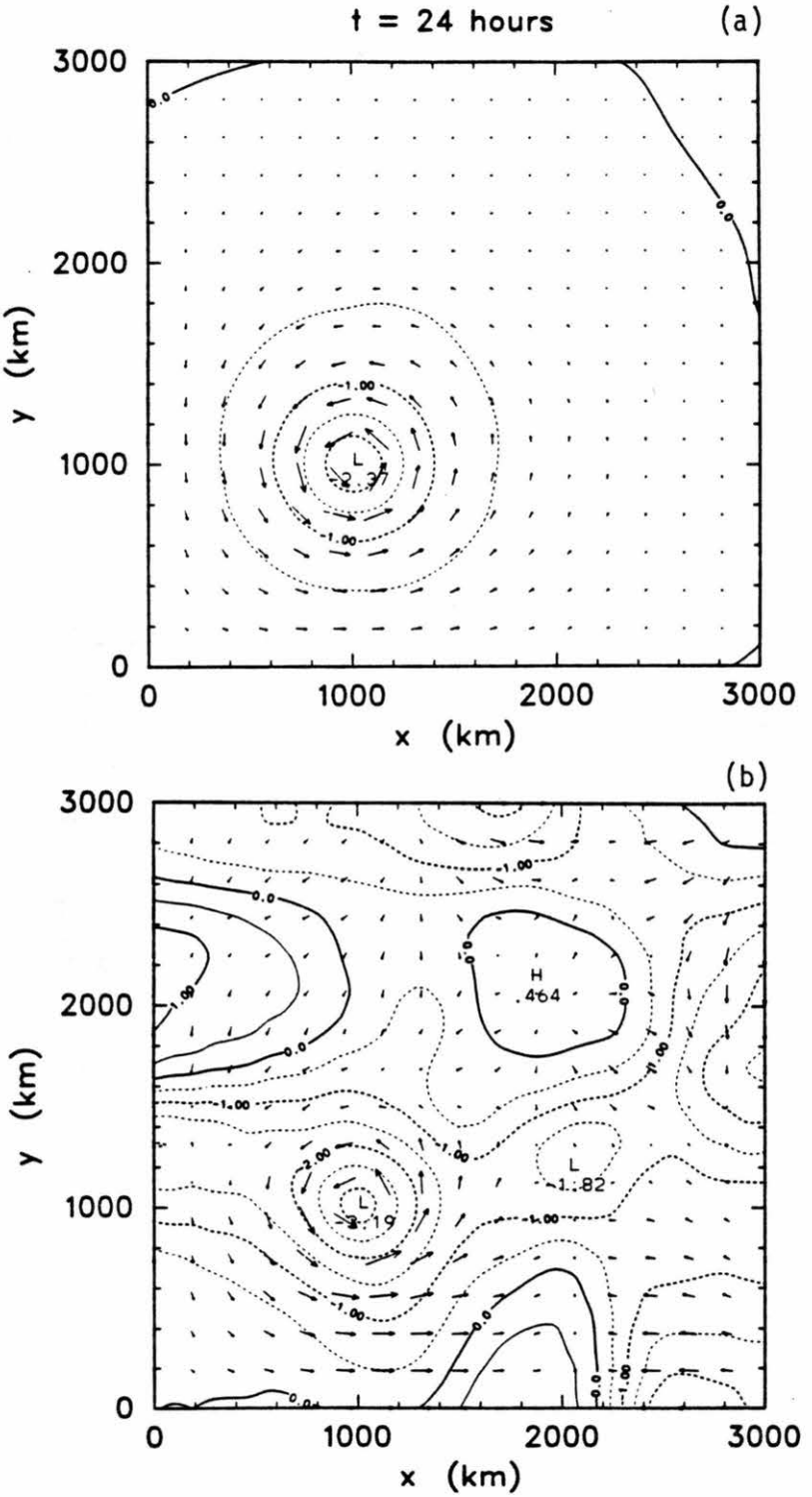

Figure 33. Chebyshev-tau solution of the two-dimensional shallow water model at t=24 hours using (a) the homogeneous characteristic condition and (b) the wall condition.

equations; the tau solution using the advective form (3.1) is very similar, and hence is not shown. However, since the nonlinear characteristic condition (3.32) and the inflow condition (3.33) are difficult to apply in two dimensions with the tau discretization, only the linear form (3.30) of the characteristic condition was applied. Corresponding solutions at t=24 hours computed by the collocation method from the advective and rotational forms are shown in Figs. 34a and 34b, respectively. Although these results were computed using the boundary conditions (3.32) and (3.33) [with $(u_{||})_B$ specified as zero], which are appropriate for the nonlinear problem, and also involve aliasing, they differ little from the tau results shown in Fig. 33a. The collocation solution from the rotational form, however, does show a slight "squaring off" of the vortex not seen in the other methods. As in the one-dimensional case, no evidence of instability was seen for the collocation method based on the advective form of the equations.

One significant difference between the tau and collocation methods for this problem is the computer time they require. As mentioned previously, the tau method requires more work per time step than the collocation method since the transforms involved are both larger and two-dimensional. Table 3 shows the amount of computer time required to evaluate all terms in the model equations using each of the various discretization methods and equation forms with the spectral truncation N=24 in both x and y. These estimates are based on timing tests performed on a CRAY-1 computer, using code written to take maximum advantage of the vector processing on that machine. They suggest that the collocation method may be twice as fast as the tau method. However, the overall efficiency of the model depends also on the time

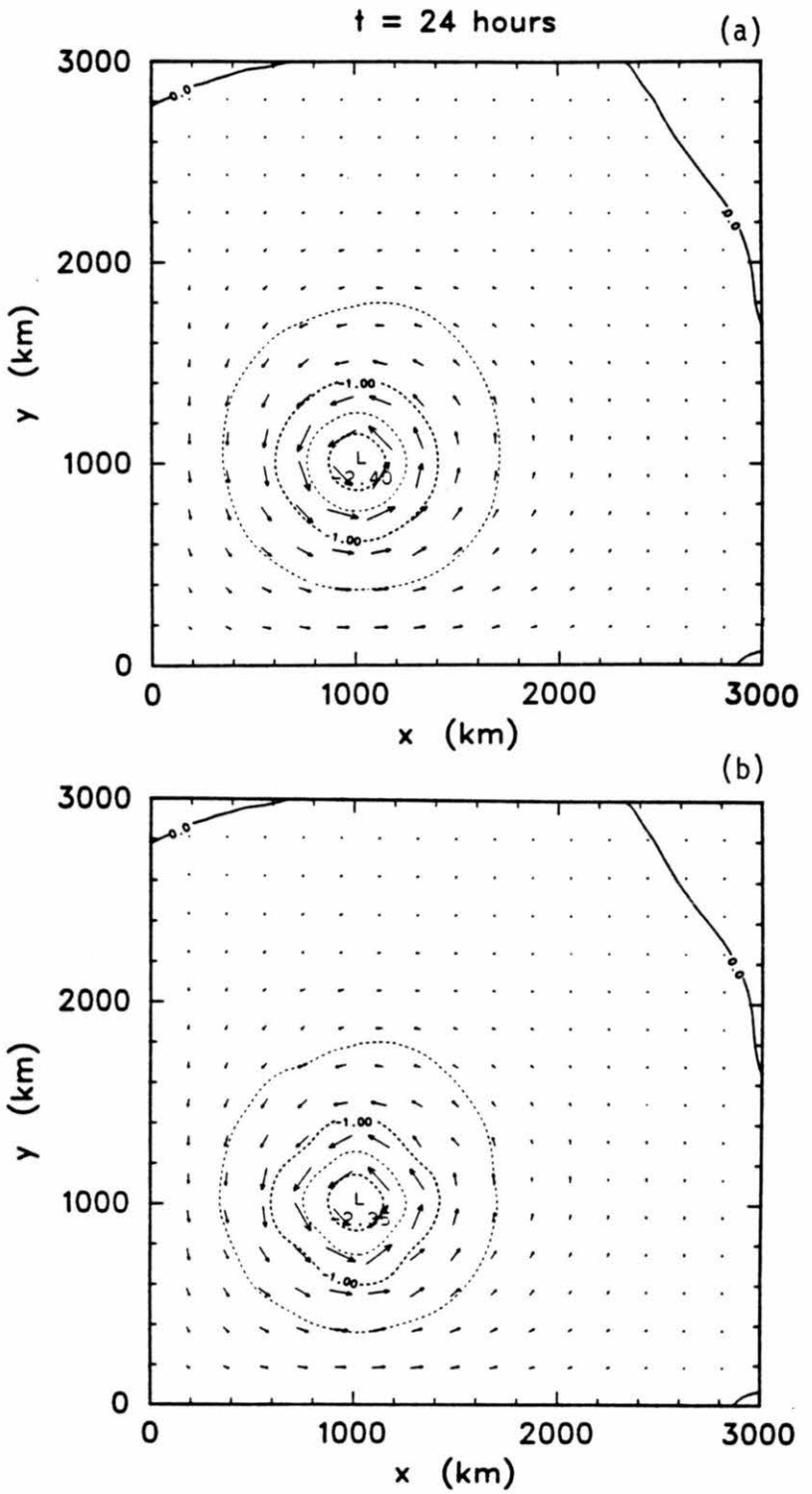

Figure 34. Chebyshev-collocation solution of the two-dimensional shallow water model at t=24 hours using (a) the advective form and (b) the rotational form of the governing equations.

differencing scheme used and the related considerations of accuracy and stability. These topics are discussed in detail in the next chapter.

Table 3. Computer time (milliseconds) required to evaluate all terms in the shallow water model.

Equation Form	Space Discretization	
	tau	collocation
linear	1	3
advective	12	4
rotational	9	4

CHAPTER 4

TIME DIFFERENCING AND EFFICIENCY

Discretizing the governing equations of a model in space using a spectral method results in a set of ordinary differential equations in time which may be written in the form

$$\frac{d\underset{\sim}{u}}{dt} = \underset{\sim}{F}(\underset{\sim}{u},t) \ . \tag{4.1}$$

Here the vector $\underset{\sim}{u}(t)$ consists of the spectral coefficients (Galerkin and tau projections) or the values at collocation points (collocation projection) of the model variables. Often there are diagnostic relations (i.e. equations not involving time derivatives) in addition to (4.1), such as boundary conditions, which must be satisfied by u for all t. If the basis functions of the spectral method are the normal modes of the linear part of the model then (4.1) reduces to a set of forced oscillation equations, similar to (3.17), which are coupled only through the nonlinear terms; the linear part of the model can then be solved analytically (e.g., DeMaria and Schubert, 1984; Schubert and DeMaria, 1984). However, such normal mode spectral models are usually feasible only with reflecting or periodic boundary conditions.

In more general situations, such as in the Chebyshev models developed above, the model variables are coupled and (4.1) can be solved only approximately (this is also true for the nonlinear terms in normal mode models). Typically one uses a finite difference discretization in time. That is, $\underset{\sim}{u}(t)$ is represented by values $\underset{\sim}{u}^{(k)}$ at discrete time

levels t_k (k=0,1,2,...) and (4.1) is approximated using finite differences. This approximate form is used to compute the solution at a time level t_{k+1} from information at time t_k (and possibly other previous levels), the model being initialized at $t=t_o$ from specified initial conditions. The choice of time differencing schemes affects the efficiency and accuracy of a spectral model and greatly affects the ease of programming.

In this chapter we discuss time differencing for spectral methods, especially those based on Chebyshev polynomial expansions. Section 4.1 deals with explicit time differencing schemes, which are the easiest to implement. Two modifications have been proposed in the literature to improve the performance of explicit schemes for spectral methods; these are discussed briefly in section 4.2. In section 4.3 we describe implicit schemes for tau and collocation models; these schemes are rather difficult to implement but may be quite efficient in some cases.

4.1 Explicit Schemes

The time-discretized form of (4.1) is called an <u>explicit</u> scheme when it can be solved explicitly for $\underset{\sim}{u}^{(k+1)}$ in terms of values at previous time levels, e.g. $\underset{\sim}{u}^{(k)}$, $\underset{\sim}{u}^{(k-1)}$, etc. Typical explicit schemes include the Euler (or forward) scheme

$$\frac{\underset{\sim}{u}^{(k+1)} - \underset{\sim}{u}^{(k)}}{\Delta t} = \underset{\sim}{F}^{(k)} , \tag{4.2}$$

the modified Euler (or second-order Runge-Kutta) scheme

$$\left.\begin{aligned} \frac{\underset{\sim}{u}^{(k+\frac{1}{2})} - \underset{\sim}{u}^{(k)}}{\frac{1}{2}\Delta t} &= \underset{\sim}{F}^{(k)} \\ \frac{\underset{\sim}{u}^{(k+1)} - \underset{\sim}{u}^{(k)}}{\Delta t} &= \underset{\sim}{F}^{(k+\frac{1}{2})} \end{aligned}\right\} , \tag{4.3}$$

and the second-order Adams-Bashforth scheme

$$\frac{\underset{\sim}{u}^{(k+1)} - \underset{\sim}{u}^{(k)}}{\Delta t} = \tfrac{3}{2}\,\underset{\sim}{F}^{(k)} - \tfrac{1}{2}\,\underset{\sim}{F}^{(k-1)} , \tag{4.4}$$

where $t_k = k\Delta t$ with Δt a fixed positive number and $\underset{\sim}{F}^{(k)} = \underset{\sim}{F}(\underset{\sim}{u}^{(k)}, t_k)$. These and other explicit schemes have been extensively discussed and analyzed, e.g. Kurihara, 1965; Lilly, 1965; Young, 1968; Mesinger and Arakawa, 1976; Stoer and Bulirsch, 1980.

With explicit time differencing, spectral models are quite easy to program. Since the operations involved in the right-hand side $\underset{\sim}{F}$ of (4.1), such as transforms and derivatives, are performed on known values of $\underset{\sim}{u}$, they need be programmed only once as "canned" or "library" routines, which are then simply called as needed. The resulting spectral codes are often simpler than corresponding finite difference codes. In fact, it is often possible to simply write the spectral code directly from the continuous form of the equations, without ever writing down the discrete form of the equations. Explicit time differencing is definitely desirable when it is suitably efficient.

The choice between different explicit schemes is a compromise between considerations of accuracy, work, storage and stability. The Euler scheme (4.2) is the simplest explicit scheme; in it the right-hand side $\underset{\sim}{F}$ is evaluated once per time step and storage is required for $\underset{\sim}{u}$ and $\underset{\sim}{F}$ at one time level. However, the Euler scheme is only first-order

accurate in time, i.e. the error at any fixed time t decreases like Δt as $\Delta t \to 0$. Higher accuracy can be achieved in several ways. The modified Euler scheme (4.3) achieves second-order accuracy, i.e., the error decreases like $(\Delta t)^2$ as $\Delta t \to 0$, by evaluating $\underset{\sim}{F}$ twice per time step. Since essentially all of the computer time is spent in evaluating $\underset{\sim}{F}$, this scheme requires twice as much work per time step as the Euler scheme. It also requires additional storage for $\underset{\sim}{u}$ at the intermediate level $t_{k+\frac{1}{2}}$; however, storage requirements are generally inconsequential in spectral models since the number of model variables needed is relatively small due to the high accuracy of the spectral discretization. The Adams-Bashforth scheme (4.4) is also second order and requires the same storage as the modified Euler scheme (4.3), but only involves one evaluation of $\underset{\sim}{F}$, and thus the same amount of work as the Euler scheme (4.2), per time step. However, since $\underset{\sim}{u}^{(k+1)}$ depends on both $\underset{\sim}{u}^{(k)}$ and $\underset{\sim}{u}^{(k-1)}$, this scheme has a computational mode, i.e. a component of the numerical solution which has no physical significance.

A key consideration in the choice of a time differencing scheme is stability. For problems in which the true (continuous) solution does not grow in time without bound, the appropriate type of stability to consider is absolute stability. A time differencing scheme (or, more roperly, the overall numerical model), is said to be <u>absolutely stable</u> for a fixed time step Δt if the numerical solution does not grow in time without bound. In general, explicit schemes are absolutely stable only for small enough Δt, so their absolute stability is said to be <u>conditional</u>. Therefore, with explicit schemes the size of the time step (and thus the overall efficiency of the method) is dictated by both accuracy and stability considerations.

Finite difference models with explicit time differencing generally have stability conditions of the form

$$\Delta t = 0 \left(\frac{\Delta x}{c}\right) , \tag{4.5}$$

where Δx is the (spatial) mesh size and c is the maximum speed at which information can propagate in the model. For sufficiently simple problems such conditions can be obtained easily by the von Neumann method (Haltiner and Williams, 1980, sec. 5.5), which essentially considers only a single (spatial) Fourier mode of the solution and ignores boundary conditions. In contrast, with a Chebyshev discretization in space a more complicated matrix stability analysis is needed. However, since the resolution of a truncated Chebyshev series of degree N is $O(N^{-2})$ near the boundaries, as shown by (2.14) and (2.15), one can argue heuristically from (4.5) that Chebyshev spectral models with explicit time differencing may have stability conditions of the form

$$\Delta t = 0 \left(\frac{L}{cN^2}\right) , \tag{4.6}$$

where the length L measures the domain size. This form has been confirmed in some special cases by detailed analyses. For example, with the modified Euler scheme (4.3) the linear advection model discussed in section 2.4 has the stability condition $\Delta t \leq \beta^*/N^2$, with $\beta^* \approx 3.4$ for the Chebyshev-tau method and $\beta^* \approx 17$ for the Chebyshev-collocation method (Fulton and Taylor, 1984).

It has been argued (e.g., Gottlieb and Orszag, 1977, sec. 9) that the stability condition (4.6) is "severe". Indeed, from (4.5) a finite

difference model with N equally spaced gridpoints in one direction requires only $\Delta t = O(N^{-1})$ for stability while a Chebyshev spectral model with N modes requires $\Delta t = O(N^{-2})$. However, this comparison ignores the difference between exponential and algebraic convergence, which makes it possible to choose N much smaller for the spectral method than for the finite difference method. A more pertinent comparison is between the time steps allowed in the two methods when N is chosen to give a certain accuracy.

Suppose, therefore, that a problem is to be solved numerically so that the error at a specified time is at most 10^{-r}, with r a given number. Noting that the finite difference and spectral methods give errors $O(N^{-p})$ (where p is the order of the method) and $O(10^{-N/N_o})$ (where N_o is a constant), respectively, we can estimate the required spatial resolution N, and, from (4.5) and (4.6), the corresponding time step Δt needed for stability as shown in Table 4. Note that the entries in this Table give the dependence on r for large r, e.g. N=O(r) for Chebyshev spectral methods. When high enough accuracy is desired (large enough r), the time step $\Delta t=O(10^{-r/2})$ required by (4.5) for stability in finite difference methods is in fact <u>smaller</u> than the time step $\Delta t=O(r^{-2})$ required by (4.6) for Chebyshev spectral methods. Thus (4.6) is <u>less</u> "severe" than (4.5) when interpreted in terms of the resolution N needed for accuracy.

Furthermore, one must also take into account the accuracy of the time differencing scheme. For example, second-order schemes result in errors proportional to $(\Delta t)^2$, so to achieve the accuracy 10^{-r} one must choose $\Delta t=O(10^{-r/2})$, independent of the space discretization (except with first-order space differencing, for which $\Delta t=O(10^{-r})$ is required

Table 4. Estimates of how the required resolution (N and Δt) and work (number of operations) depend on the desired accuracy 10^{-r} for different space discretizations. Second-order time differencing is assumed, and time steps which are unstable or inaccurate for large r are noted.

Space discretization	N for accuracy 10^{-r}	Δt for stability	Δt for accuracy	work per time step	total work
first-order finite difference	10^{r}	10^{-r}	$10^{-r/2}$ (unstable)	10^{r}	10^{2r}
second-order finite difference	$10^{r/2}$	$10^{-r/2}$	$10^{-r/2}$	$10^{r/2}$	10^{r}
Chebyshev spectral (slow transforms)	r	r^{-2} (inaccurate)	$10^{-r/2}$	r^{2}	$r^{2}10^{r/2}$
Chebyshev spectral (fast transforms)	r	r^{-2} (inaccurate)	$10^{-r/2}$	r log r	(r log r)$10^{r/2}$

for stability). Comparing the time steps required for stability and accuracy in Chebyshev spectral methods as shown in Table 4, we conclude that when high enough accuracy is desired the time step is limited by accuracy rather than stability. In practice, "high enough" accuracy may be very modest. For example, Fig. 35 shows the time steps required for accuracy and for stability in the linear advection model studied in section 2.4 with the modified Euler scheme (4.3). Here Δt for accuracy was chosen so that the L_2 error at t=1.0 for the test problem (2.45) was within 10% of the error due to the space discretization alone, and Δt for stability was taken from Fulton and Taylor (1984). With the collocation discretization the time step for this problem is limited by accuracy, not stability, for all N; with the tau discretization it is limited by accuracy for $N \gtrsim 16$, which from Fig. 3 corresponds to an accuracy of about one part in one hundred. Thus, the stability condition (4.6) for Chebyshev spectral methods is not only not "severe"; in practical problems it may be altogether inconsequential since the time step may be limited by accuracy rather than stability.

To compare the efficiency of finite difference and Chebyshev spectral methods we note that finite difference methods require O(N) operations per time step while spectral methods require $O(N^2)$ operations (with "slow" transforms or interaction coefficients) or O(N log N) operations (with fast transforms) per time step. Using the previous estimates of N and Δt we can then estimate the number of operations per time step and the total operations required to compute the solution at a fixed time with error at most 10^{-r}, as shown in the last two columns of Table 4. Since $r^2 10^{r/2}$ does not increase with r as fast as 10^r does, we conclude that the Chebyshev spectral method -- even with explicit time

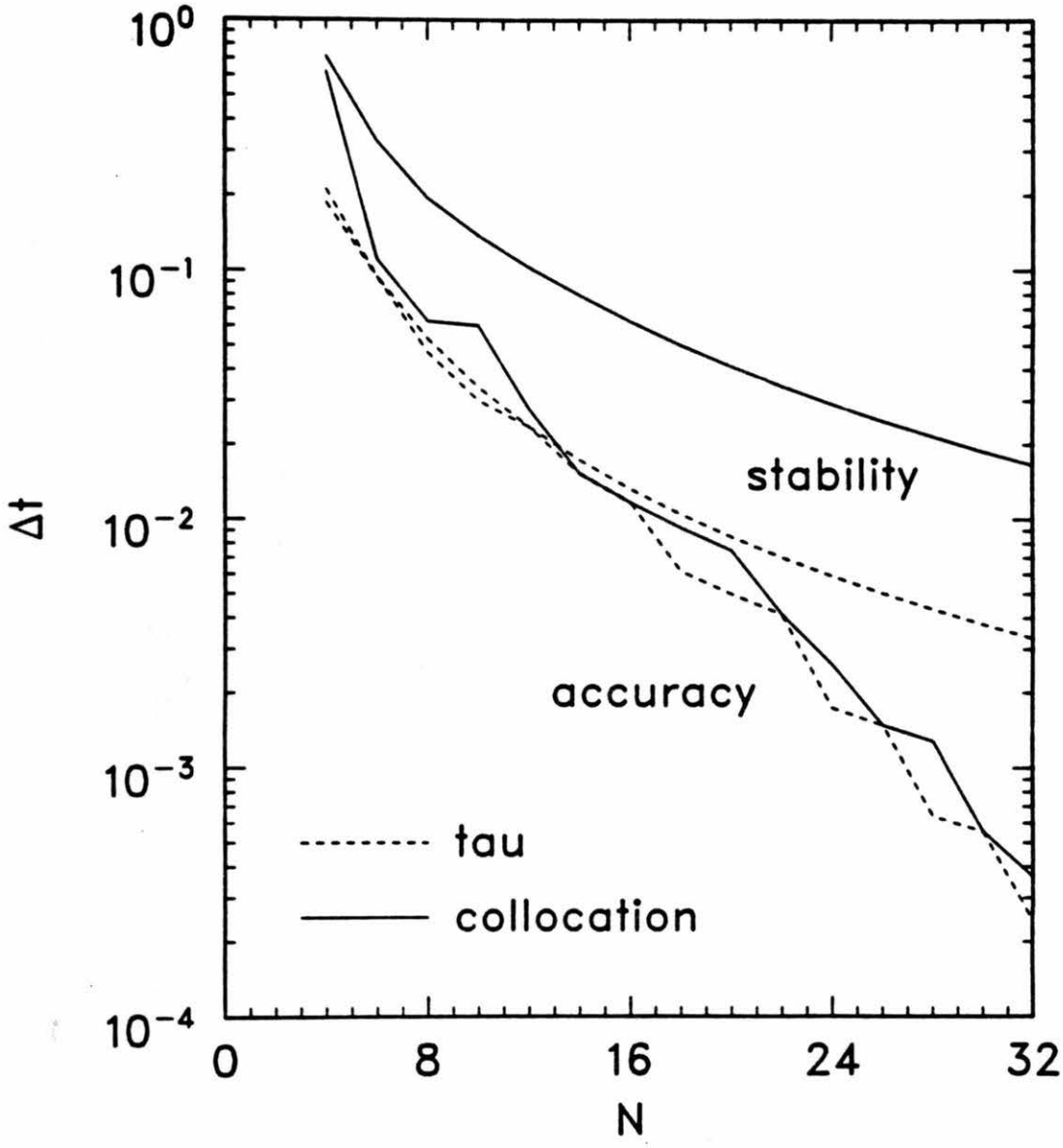

Figure 35. Time steps required for stability and accuracy in terms of the spectral truncation N for the linear advection model.

differencing and "slow" transforms -- is inevitably more efficient than the finite difference methods, when the accuracy desired is high enough. This asympotic result is quite general, and basically reflects the exponential convergence of the spectral discretization.

The question "at what level of accuracy do Chebyshev spectral methods become more efficient than finite difference methods" does not have a general, definitive answer. In practice, efficiency depends not only on the problem to be solved, the character of the solution (e.g., smoothness) and the particular space and time discretizations chosen, but also on the computer system (e.g., vector or nonvector architecture), the speed of any library routines used (e.g., FFT routines) and the skill of the programmer. However, to obtain a rough idea of whether Chebyshev spectral methods can compete with finite difference methods when modest accuracy is desired, we again consider the linear advection equation with the test case (2.45). This problem was solved repeatedly with the upstream difference, centered difference and Chebyshev collocation space discretizations and the modified Euler time discretization, using different resolutions N (with Δt chosen for accuracy) to obtain the solution at t=1.0. The resulting error in the numerical solution is shown in Fig. 36 as a function of the computer time used in obtaining it on a CRAY-1 computer (not including the time required to initialize the model). For this particular problem the Chebyshev collocation method is more efficient than the upstream difference method for essentially all accuracies, and more efficient than the centered difference method when the accuracy desired is more than one part in about ten thousand. However, it should be noted that the latter crossover point occurs when $N \approx 28$ for the Chebyshev

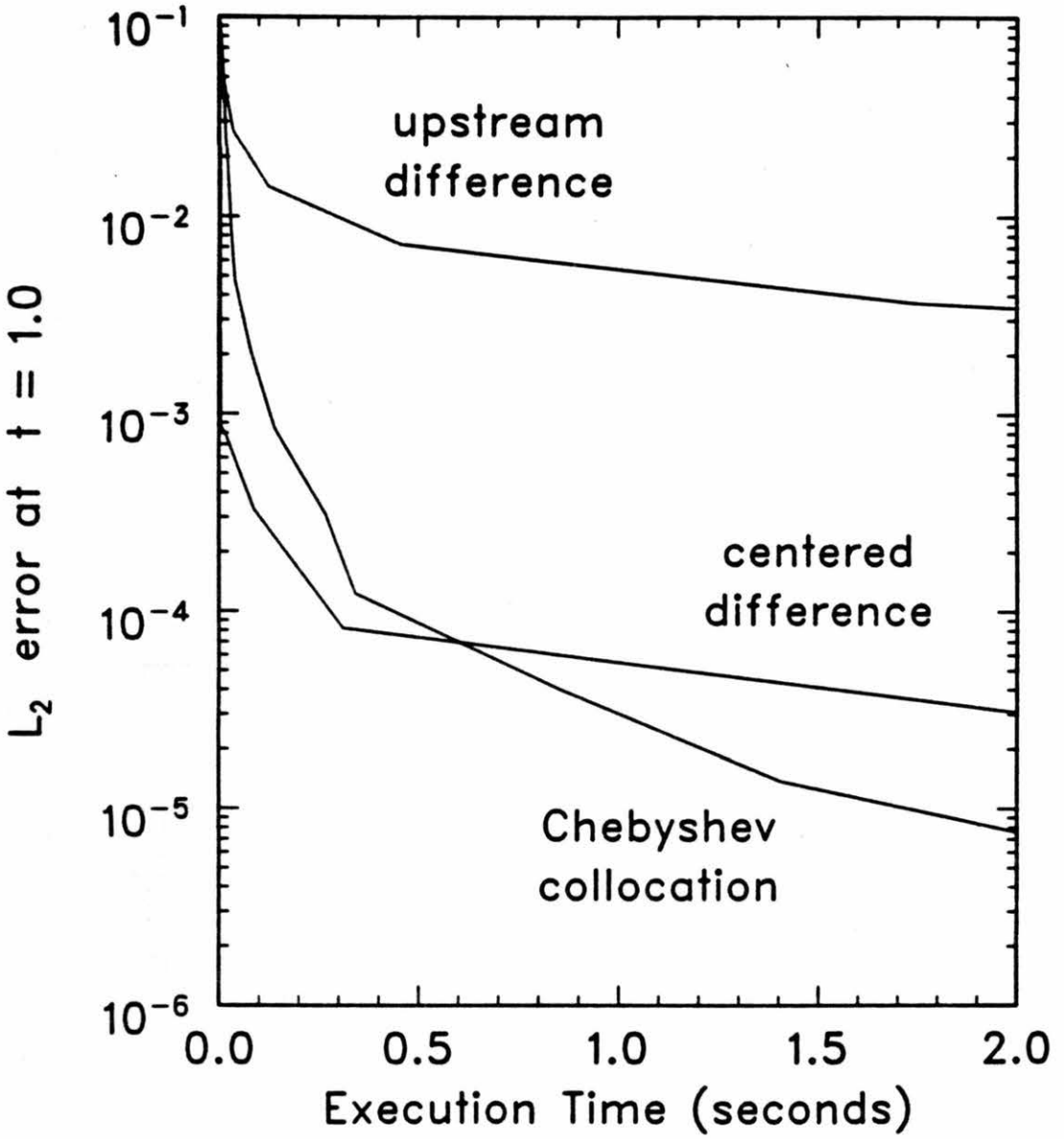

Figure 36. Accuracy of the numerical solution (L_2 error at t=1.0) as a function of the computer time required to obtain it using three space discretizations.

collocation method and $N \approx 1200$ for the centered difference method. Furthermore, for these results "slow" transforms were used (so that N could be chosen freely); the use of fast transforms would speed up the collocation method somewhat. Finally, since the time step used in the collocation method is strongly limited by accuracy, the efficiency could presumably be increased significantly by using a more accurate (e.g., fourth-order) time differencing scheme.

One final question about efficiency concerns the calculation of derivatives in the Chebyshev collocation method. This calculation as normally performed requires two Chebyshev transforms plus the derivative operation in spectral space. Furthermore, in order to compute the transforms using the FFT algorithm and take full advantage of symmetry one must do additional pre- and post- processing (Cooley et al., 1970). Thus it has been suggested (Hussaini et al., 1983) that it may be more efficient to simply generate the matrix which represents the entire collocation derivative operation and do a matrix multiply. This hypothesis was tested with careful implementations of both procedures on a CRAY-1 computer, using an assembly-language implementation of the FFT algorithm of Temperton (1983a, b, c) and making full use of vectorization. For N=8, 16, 32 and 64 the transform procedure for calculating the derivative was 1.4, 2.5, 5 and 10 times faster, respectively, than the matrix procedure.

4.2 Modified Explicit Schemes

In hopes of improving the performance of conventional explicit time differencing schemes while retaining their simplicity, several simple modifications have been introduced specifically for use with spectral

methods. In this section we briefly discuss two such modifications which appear promising but are not useful in practice.

As discussed above, the stability condition (4.6) for Chebyshev spectral methods is neither "severe" nor necessarily the condition which limits the time step in practice. Nevertheless, Gottlieb and Turkel (1980) introduced a modified explicit scheme which they claimed allows time steps to be "chosen by accuracy requirements alone". For the linear advection equation this scheme depends on replacing the derivative relation (2.24) by the "filtered" version

$$\Delta t\, \hat{u}_n^{(1)} = \frac{2\Delta t}{c_n} \sum_{\substack{m=n+1 \\ m+n \text{ odd}}}^{N} m f(m^2 \alpha \Delta t) \hat{u}_m \,. \qquad (4.7)$$

Here Δt is the time step to be used in the explicit scheme, α is a constant filter parameter and f is a filter function satisfying $f(0)=1$ and $f(z) \to 0$ as $z \to \infty$. Gottlieb and Turkel argue that by choosing α and f suitably the modified Euler scheme (4.3) may be made unconditionally algebraically stable. Algebraic stability (Gottlieb and Orszag, 1977, sec. 5) is a less stringent requirement than absolute stability; nevertheless, the time step needed for both kinds of stability is $O(N^{-2})$ for the unfiltered discretization, so one might hope that the filter would also relax the condition (4.6) for absolute stability.

A detailed analysis (Fulton and Taylor, 1984) shows that this is not the case. In fact, small amounts of filtering do not change the stability properties significantly while large amounts of filtering render the scheme absolutely unstable for any size time step. In practice, the growth of the solution with time can be made quite small

by using a large amount of filtering, but the resulting solutions are inaccurate to the point of being useless. This is not surprising, since the filtered derivative (4.7) essentially changes the space discretization. Therefore, the Gottlieb-Turkel scheme for Chebyshev spectral methods is not recommended.

A different modification for the Adams-Bashforth scheme was proposed by Gazdag (1976). The central idea was to utilize the values of the right-hand side $\underset{\sim}{F}$ of (4.1) more effectively, since computing these values accounts for almost all of the computational effort in spectral methods. Gazdag proposed the "partially corrected" Adams-Bashforth scheme

$$\frac{\tilde{\underset{\sim}{u}}^{(k+1)} - \underset{\sim}{u}^{(k)}}{\Delta t} = \tfrac{3}{2}\,\underset{\sim}{F}^{(k)} - \tfrac{1}{2}\,\tilde{\underset{\sim}{F}}^{(k-1)} , \tag{4.8a}$$

$$\frac{\underset{\sim}{u}^{(k+1)} - \underset{\sim}{u}^{(k)}}{\Delta t} = \tfrac{1}{2}\,\tilde{\underset{\sim}{F}}^{(k)} + \tfrac{1}{2}\,\tilde{\underset{\sim}{F}}^{(k+1)} . \tag{4.8b}$$

Here the Adams-Bashforth predictor step (4.8a) is used to produce a first approximation $\tilde{\underset{\sim}{u}}^{(k+1)}$ to $\underset{\sim}{u}$ at t_{k+1}, which is then improved in the trapezoidal "partial" corrector step (4.8b). The term "partial" is used since the first approximations $\tilde{\underset{\sim}{u}}$ are used in computing all values of $\underset{\sim}{F}$, rather than just for $\underset{\sim}{F}^{(k+1)}$ as in a "full" predictor-corrector scheme. Thus this scheme requires only one evaluation of $\underset{\sim}{F}$ per time step.

As discussed previously, the Adams-Bashforth scheme (4.4) admits two modes in the numerical solution. For the simple oscillation equation $du/dt = i\omega u$ (ω real) the physical mode is in fact unconditionally <u>unstable</u> while the computational mode damps with time. Nevertheless, the scheme is often useful in practice since the growth

rate is small for small Δt and may be overcome by any dissipative processes in the problem. Gazdag (1976) showed that with the scheme (4.8) the physical mode is stable and the associated error is reduced somewhat. However, he neglected to mention the computational mode. In fact, the scheme (4.8) has <u>two</u> computational modes, since $\underset{\sim}{u}^{(k)}$ depends on $\underset{\sim}{\tilde{u}}^{(k)}$ and $\underset{\sim}{\tilde{u}}^{(k-1)}$ in addition to $\underset{\sim}{u}^{(k)}$. One of these computational modes is unstable for the oscillation equation when $\omega\Delta t \gtrsim 0.65$. Thus small time steps are required even though the physical mode is stable, so the method is of little use in practice.

4.3 Implicit Schemes

The time-discretized form of (4.1) is called an <u>implicit scheme</u> when it cannot be solved directly for $\underset{\sim}{u}^{(k+1)}$. A typical implicit scheme is the trapezoidal (Crank-Nicolson) scheme

$$\frac{\underset{\sim}{u}^{(k+1)} - \underset{\sim}{u}^{(k)}}{\Delta t} = \tfrac{1}{2}\,\underset{\sim}{F}^{(k)} + \tfrac{1}{2}\,\underset{\sim}{F}^{(k+1)} \,, \tag{4.9}$$

which is second-order accurate. Implicit schemes are in general unconditionally stable, so that time steps can be chosen by accuracy requirements alone. However, they are considerably more difficult to implement for Chebyshev spectral methods, since the resulting matrix equations are essentially full due to the global nature of the spectral approximation.

One might ask why implicit schemes should be considered at all, if they are difficult to implement. Indeed, the time steps needed for accuracy with implicit and explicit schemes of the same order are about the same, so if explicit schemes are limited by accuracy and not

stability they would be preferable, since they are much simpler to implement. However, there are cases in which time steps for explicit schemes are limited by stability; these occur when the stability condition is related to a physical process which is represented in the model but which is relatively unimportant for the particular problem being studied. In such a situation the equations are said to be stiff. For example, the stability condition for the shallow water model (3.1) is based on the speed $c=\phi^{\frac{1}{2}}$ at which gravity waves can propagate; however, with slow enough forcing such waves contribute very little to the actual solution. Similarly, in Chebyshev spectral models the inclusion of a "friction" term proportional to the Laplacian of a model variable leads to a stability condition of the form $\Delta t=O(N^{-4})$; this is unduly restrictive when the specific form of friction assumed is merely a somewhat arbitrary representation of general dissipative processes.

There are two basic approaches in the situation described above. The first is to simply remove the terms responsible for the stiffness from the equations. However, this is not always possible to do. For example, one can approximate the shallow water model by a balanced model which allows no gravity waves, but such a model also neglects nonlinear advection terms which may be of importance. The second approach is to use an implicit time differencing scheme. Generally, only the terms which contribute to the stiffness are treated implicitly, with the time step chosen as needed for the accuracy and stability of the remaining terms. In order for this approach to be worth the effort, the time step used must be several times larger than that permitted with a fully explicit scheme, and thus the terms treated implicitly will in general

not be treated accurately. Possible ways of implementing implicit schemes in Chebyshev spectral models are discussed below.

4.3.1 The Chebyshev-tau method. With Chebyshev-tau space discretization, the equations resulting from implicit time differencing can sometimes be solved directly. For example, using the trapezoidal implicit scheme (4.9) to discretize the Chebyshev-tau version (2.38) of the linear advection model in time results in

$$\hat{u}_{n,k+1} + \frac{c\Delta t}{2}\,\hat{u}^{(1)}_{n,k+1} = \hat{F}_{n,k+1} \qquad (n=0,\ldots,N-1)\ , \tag{4.10a}$$

$$\sum_{n=0}^{N} (-1)^n\,\hat{u}_{n,k+1} = g_{k+1}\ , \tag{4.10b}$$

where

$$\hat{F}_{n,k+1} = \hat{u}_{n,k} - \frac{c\Delta t}{2}\,\hat{u}^{(1)}_{n,k} + \frac{\Delta t}{2}\,(\hat{f}_{n,k} + \hat{f}_{n,k+1}) \tag{4.11}$$

and the subscript k denotes values at $t_k = k\Delta t$. In (4.10) the right-hand side can be computed directly at time t_k and hence is regarded as known; the left-hand side, coupled with the Chebyshev derivative relation (2.24), represents a matrix times the vector of the coefficients $\hat{u}_{0,k+1},\ldots,\hat{u}_{N,k+1}$ which are sought. This matrix is upper triangular, except for the last row which comes from the boundary condition (4.10b), and thus if $\hat{u}_{N,k+1}$ is known the remaining coefficients can be obtained by back substitution. Specifically, writing the recurrence relation (2.27) for the derivative as

$$c_{n-1}\,\hat{u}^{(1)}_{n-1,k+1} = \hat{u}^{(1)}_{n+1,k+1} + 2n\,\hat{u}_{n,k+1} \quad (n=1,\ldots,N-1)\,, \qquad (4.12)$$

one can start with the values $\hat{u}_{N,k+1}$ and $\hat{u}^{(1)}_{N+1,k+1} = \hat{u}^{(1)}_{N,k+1} = 0$ and solve (4.12) for $\hat{u}^{(1)}_{N-1,k+1}$, then (4.10a) for $\hat{u}_{N-1,k+1}$, then (4.12) for $\hat{u}^{(1)}_{N-2,k+1}$, then (4.10a) for $\hat{u}_{N-2,k+1}$, etc., to compute $\hat{u}_{o,k+1},\ldots,\hat{u}_{N,k+1}$.

To generate the required starting value $\hat{u}_{N,k+1}$, one can eliminate $\hat{u}_{o,k+1},\ldots,\hat{u}_{N-1,k+1}$ from (4.10b) using (4.10a). This amount to using Gaussian elimination to decompose the linear system represented by (4.10). Another approach (which may generalize more readily to more complicated problems) is to write

$$\hat{u}_{n,k+1} = \hat{v}_{n,k+1} + \alpha\,\hat{w}_n \quad (n=0,\ldots,N)\,, \qquad (4.13)$$

where α is a constant to be determined and $\hat{u}_{n,k+1}$ and $\hat{w}_n$ satisfy

$$\left.\begin{aligned} \hat{v}_{n,k+1} + \frac{c\Delta t}{2}\,\hat{v}^{(1)}_{n,k+1} &= \hat{F}_{n,k+1} \quad (n=0,\ldots,N-1) \\ \hat{v}_{N,k+1} &= 0 \end{aligned}\right\} \qquad (4.14)$$

and

$$\left.\begin{aligned} \hat{w}_n + \frac{c\Delta t}{2}\,\hat{w}^{(1)}_n &= 0 \quad (n=0,\ldots,N-1) \\ \hat{w}_N &= 1 \end{aligned}\right\}\,. \qquad (4.15)$$

Substituting (4.13) into (4.10a) and using (4.14) and (4.15) is easy to show that (4.10a) is satisfied independent of α. Both (4.14) and (4.15) can be solved by the back substitution procedure outlined above (note that $\hat{w}_o,\ldots,\hat{w}_N$ need be computed only once), and then α can be determined

by requiring (4.13) to satisfy the boundary condition (4.10b). Note that this procedure may be somewhat sensitive to roundoff errors, however, due to possible cancellation in (4.13).

If nonlinear advection terms such as $u\partial u/\partial x$ are to be treated implicitly, it is usually convenient to split the advecting velocity u into a specified component U and a residual u-U, and treat the linear term $U\partial u/\partial x$ implicitly and the nonlinear term $(u-U)\partial u/\partial x$ explicitly. If U is chosen to be a linear function of x, then the term $U\partial u/\partial x$ is a polynomial of the same degree as u and can be handled implicitly as described above, using the relation (2.28) for the operation $x\partial u/\partial x$. Since the time step allowed by stability will depend on u-U, one should choose U so that u-U is small, especially near the boundaries where the resolution of the Chebyshev series is the greatest.

Friction terms of the form $-\nu\partial^2 u/\partial x^2$, where ν is a viscosity coefficient, can also be treated implicitly. However, although the corresponding implicit equations are essentially upper triangular, their solution by the methods outlined above is not recommended since it is definitely sensitive to roundoff error. Instead, they should be converted to a diagonally-dominant tridiagonal form (Gottlieb and Orszag, 1977, sec. 10). Haidvogel (1979) showed that the inclusion of such friction terms can lead to instabilities unless the spectral truncation N is large enough to resolve the resulting boundary layers, and recommended the use of fractional-step time differencing schemes. In two dimensions, the implicit equations resulting from Laplacian friction terms in Chebyshev-tau models can be solved by the method of Haidvogel and Zang (1979).

4.3.2 The Chebyshev-collocation method. With Chebyshev-collocation space discretization, implicit time differencing (of linear terms) leads to a matrix equation of the form

$$L_{sp}\, \underset{\sim}{u} = \underset{\sim}{f}\ , \tag{4.16}$$

where $\underset{\sim}{f}$ represents values which are known at a time level t_k and $\underset{\sim}{u}$ represents the model variables (values at collocation points) at the next level t_{k+1}, much as in the tau method. The difference here is that in addition to the simple spectral derivative relations, the collocation method also involves Chebyshev transforms and hence the matrix L_{sp} is invariably full. Direct solution of (4.16), e.g. by Gaussian elimination, may be practical in some one-dimensional cases. In general, however, indirect (iterative) methods must be used, both for efficiency (particularly since the FFT algorithm cannot be used in direct methods) and to avoid round-off errors.

One such indirect method is the spectral iteration method of Orszag (1980) and McCrory and Orszag (1980). This is basically a defect correction method which uses an approximation L_{ap} to the operator L_{sp} to generate a sequence of approximations $\{\underset{\sim}{u}^{(r)}\}_{r=0}^{\infty}$ which converges to $\underset{\sim}{u}$. The simplest iteration scheme is

$$L_{ap}\, \underset{\sim}{u}^{(r+1)} = L_{ap}\, \underset{\sim}{u}^{(r)} - \alpha(L_{sp}\, \underset{\sim}{u}^{(r)} - \underset{\sim}{f}) \tag{4.17}$$

where α is a constant iteration parameter; more complicated schemes are also possible. The key to the method is choosing L_{ap} so that it both adequately approximates L_{sp} and is easily inverted so that (4.17) can be solved for $\underset{\sim}{u}^{(r+1)}$. Orszag (1980) recommends choosing L_{ap} as a low-order

finite difference operator corresponding to L_{sp}; the resulting sequence $\{\underset{\sim}{u}^{(r)}\}_{r=0}^{\infty}$ then converges fairly quickly to $\underset{\sim}{u}$. However, inverting L_{ap} may be a nontrivial problem, especially since the corresponding finite differences must be formulated on a grid of Chebyshev collocation points, which are not equally spaced.

A more attractive method for solving implicit spectral equations such as (4.16) is the spectral multigrid method introduced by Zang et al. (1982, 1984). This method combines the powerful multigrid concepts developed by Brandt (1977) and others with spectral discretizations. A detailed discussion of this method is outside the scope of this study. However, it should be noted that even this method, in order to be efficient, involves constructing a finite difference approximation L_{ap} to L_{sp}, although it need not be inverted exactly (Brandt et al., 1984).

The extreme complexity of the above methods for implementing implicit time differencing in Chebyshev spectral models should be contrasted with the extreme simplicity of such models with explicit time differencing. Unless the size of the time step is excessively limited by stability (e.g. if the velocity scale which determines the stability condition is very much larger than the velocity scale of the part of the solution of physical interest), implicit time differencing may not be worth either the computational cost or the programming effort.

CHAPTER 5

VERTICAL NORMAL MODE TRANSFORMS

For most meteorological phenomena of interest the vertical structure of the atmosphere cannot be ignored. In nearly all numerical models (even those using spectral discretizations in the horizontal) the vertical dependence has been treated using finite difference methods; occasionally, finite element methods have been used (e.g. Staniforth and Daley, 1977; Béland et al., 1983). Spectral discretizations in the vertical have also been tried, using Legendre polynomials (Machenhauer and Daley, 1972) and Laguerre polynomials (Francis, 1972; Hoskins, 1973) as basis functions, but the results have not been encouraging. The problem seems to be related to the singularity present in the hydrostatic equation when the top of the atmosphere is taken to be where the pressure is zero. Since this singularity is a property of the governing equations in continuous form, improved vertical discretizations will likely be developed only as our understanding of these equations and their solutions increases.

One common method of treating the vertical structure of atmospheric motions is to separate it from the horizontal structure. Although this separation is not always possible, when it is possible it can considerably simplify the problem. Lamb (1932, Arts. 311-312) used this idea in studying long waves in the atmosphere, and gave references to earlier work of a similar nature. Taylor (1936) was perhaps the first to show that a compressible atmosphere may support free oscillations

with several different vertical structures; each of these modes has the horizontal structure of the motions of an incompressible fluid with depth equal to a different value of the separation constant, for which he introduced the term "equivalent depth". Since that time this concept has been applied in the study of atmospheric tides (Siebert, 1961; Chapman and Lindzen, 1970), atmospheric waves (Jacobs and Wiin-Nielsen, 1966; Lindzen, 1967; Wiin-Nielsen, 1971a, b), geostrophic adjustment (Fulton and Schubert, 1980; Silva Dias et al., 1983), normal mode initialization (Daley, 1981; Kasahara and Shigehisa, 1983), and the formulation of lateral boundary conditions (Oliger and Sundström, 1978; Hack and Schubert, 1981), to name only a few of the many applications.

In the standard separation of variables, each of the dependent variables is represented as a horizontally varying part times a vertically varying part. Substitution into the governing equations then yields separate equations for the horizontal and vertical structure which are related by the separation constant. The vertical structure equation, together with appropriate boundary conditions, forms a Sturm-Liouville problem; this must in general be solved numerically, since it involves variable coefficients which are related to the stability of the atmosphere. The resulting eigenvalues are related to the separation constant, and the corresponding eigenfunctions are the vertical normal modes. The whole procedure can be formalized as a vertical normal mode transform (Silva Dias et al., 1983) which makes explicit the connection between the hydrostatic meteorological "primitive" equations and the shallow water equations.

In this chapter we show how the vertical normal mode transform can be implemented in practice, using a Chebyshev spectral method to solve

the vertical structure problem accurately. In section 5.1 we review the formulation of the transform and discuss its properties. The approximate solution of the vertical structure problem and the implementation of the transform are discussed in section 5.2. In section 5.3 we consider the questions of accuracy and aliasing, and then apply the transform to observed sources of heat and vorticity using observed stability profiles.

5.1 Theory

In this section we review the vertical transform and its properties. The discussion is independent of geometrical or dynamical approximations in the horizontal (e.g., f-plane, β-plane, quasi-geostrophy, etc.). We use pressure as the vertical coordinate, since the corresponding weight function (pseudo-density) in the natural vertical inner product is constant, but the problem may be formulated similarly in terms of log pressure (Silva Dias et al., 1983), sigma coordinates (Kasahara and Puri, 1981) or physical height (Oliger and Sundström, 1978).

5.1.1 Governing equations and boundary conditions. Consider the motions of a compressible atmosphere in hydrostatic balance. The horizontal momentum, hydrostatic, continuity and thermodynamic energy equations may be written as

$$\frac{\partial \underset{\sim}{v}}{\partial t} + f \, \underset{\sim}{k} \times \underset{\sim}{v} + \nabla\phi = \underset{\sim}{F} \, , \tag{5.1a}$$

$$\frac{\partial \phi}{\partial p} + \frac{RT}{p} = 0 \, , \tag{5.1b}$$

$$\nabla \cdot \underset{\sim}{v} + \frac{\partial \omega}{\partial p} = 0 \ , \tag{5.1c}$$

$$c_p \frac{\partial T}{\partial t} - \frac{p\sigma}{\kappa} \omega = Q \ , \tag{5.1d}$$

with the following definitions:

p : pressure

t : time

$\underset{\sim}{v}$: horizontal velocity

ω : vertical p-velocity

T : deviation of temperature from $\bar{T}(p)$

ϕ : deviation of geopotential from $\bar{\phi}(p)$

$\underset{\sim}{k}$: vertical unit vector

f : Coriolis parameter

R : gas constant for dry air

c_p : specific heat at constant pressure

κ : $= R/c_p$

σ : static stability $[= p^{-2}(\kappa R\bar{T} - pd R\bar{T}/dp)]$.

We may regard (5.1a) and (5.1d) as being linearized about the motionless hydrostatic basic state $(\bar{T}, \bar{\phi})$, or may retain the nonlinear terms in $\underset{\sim}{F}$ and Q, which also may include friction or specified forcing terms. The atmosphere is taken to be vertically bounded, with the vertical p-velocity required to vanish at the top boundary $p = p_T \geq 0$ and the actual vertical velocity required to vanish at the bottom boundary $p = p_B$. After linearization these boundary conditions are

$$\left.\begin{aligned} \omega &= 0 \qquad \text{at} \quad p = p_T \\ \frac{\partial \phi}{\partial t} - \frac{R\bar{T}}{p} \omega &= 0 \qquad \text{at} \quad p = p_B \end{aligned}\right\} \ . \tag{5.2}$$

Eliminating T and ω between (5.1b)-(5.1d) yields

$$L\left\{\frac{\partial\phi}{\partial t}\right\} + \nabla\cdot\underset{\sim}{v} = L\left\{\frac{\partial\Phi}{\partial t}\right\} \quad . \tag{5.3}$$

Here L is the vertical differential operator

$$L\{\cdot\} = -\frac{\partial}{\partial p}\left[\frac{1}{\sigma}\frac{\partial(\cdot)}{\partial p}\right] \tag{5.4}$$

and the "forced geopotential" Φ, defined by

$$-p\frac{\partial}{\partial p}\left(\frac{\partial\Phi}{\partial t}\right) = \kappa Q \ , \tag{5.5}$$

is the geopotential which would result from Q if the motion were constrained to be nondivergent. Similarly, eliminating ω from the boundary conditions (5.2) yields

$$B_T\left[\frac{\partial\phi}{\partial t} - \frac{\partial\Phi}{\partial t}\right] = B_B\left[\frac{\partial\phi}{\partial t} - \frac{\partial\Phi}{\partial t}\right] = 0 \ , \tag{5.6}$$

where B_T and B_B are the boundary functionals

$$\left.\begin{aligned} B_T[\cdot] &= \left[p\frac{\partial(\cdot)}{\partial p}\right]_{p=p_T} \\ B_B[\cdot] &= \left[p\frac{\partial(\cdot)}{\partial p} + \frac{p^2\sigma}{R\bar{T}}(\cdot)\right]_{p=p_B} \end{aligned}\right\} . \tag{5.7}$$

In obtaining (5.6) we have set $\partial\Phi/\partial t = 0$ at $p = p_B$, thus fixing one of the constants of integration implicit in (5.5).

5.1.2 The vertical transform. The only vertical derivatives in the governing equations (5.1a) and (5.3) appear in the term $L\left\{\frac{\partial\phi}{\partial t} - \frac{\partial\Phi}{\partial t}\right\}$. Following Sneddon (1972), the properties of L are used to design the

vertical transform in such a way that it eliminates this vertical structure. Defining the vertical inner product

$$\langle u,v\rangle = \frac{1}{p_B-p_T}\int_{p_T}^{p_B} u(p)v(p)dp \tag{5.8}$$

for any functions u and v of pressure p, we seek an integral transform of the form

$$\mathcal{T}[u(p)] = \hat{u}_n = \langle u,\Psi_n\rangle \quad , \tag{5.9}$$

where the kernel $\Psi_n(p)$ of the transform is to be chosen so that

$$\mathcal{T}\left[L\left(\frac{\partial\phi}{\partial t} - \frac{\partial\Phi}{\partial t}\right)\right] = \lambda_n\left(\frac{\partial\hat{\phi}_n}{\partial t} - \frac{\partial\hat{\Phi}_n}{\partial t}\right) \tag{5.10}$$

with λ_n a constant. Substituting from (5.4), (5.8) and (5.9) in the left side of (5.10) and integrating by parts twice yields

$$\mathcal{T}\left[L\left(\frac{\partial\phi}{\partial t} - \frac{\partial\Phi}{\partial t}\right)\right] = \frac{1}{p_B-p_T}\int_{p_T}^{p_B}\left(\frac{\partial\phi}{\partial t} - \frac{\partial\Phi}{\partial t}\right) L\{\Psi_n\}\,dp$$

$$+\frac{1}{p_B-p_T}\left[\frac{1}{\sigma}\left\{\left(\frac{\partial\phi}{\partial t} - \frac{\partial\Phi}{\partial t}\right)\frac{d\Psi_n}{dp} - \Psi_n\frac{\partial}{\partial p}\left(\frac{\partial\phi}{\partial t} - \frac{\partial\Phi}{\partial t}\right)\right\}\right]_{p_T}^{p_B} . \tag{5.11}$$

The boundary conditions (5.6) then imply that the desired property (5.10) will hold provided that we choose $\Psi_n(p)$ and λ_n as solutions of the vertical structure problem

$$\left.\begin{aligned} L\{\Psi_n(p)\} &= \lambda_n\Psi_n(p) \\ B_T[\Psi_n] &= B_B[\Psi_n] = 0 \end{aligned}\right\} . \tag{5.12}$$

The theory of Sturm-Liouville eigenvalue problems such as (5.12) is well-known (e.g., Courant and Hilbert, 1953; Stakgold, 1979); we use this theory freely in what follows to establish various properties of the vertical transform. In this discussion $C^{(k)}[p_T,p_B]$ will denote the space of all real-valued functions u of pressure p with $d^{(j)}u/dp^j$ continuous on the interval $[p_T,p_B]$ for j=0,...,k. For concreteness we assume that $\sigma \in C^{(1)}[p_T,p_B]$ with $\sigma(p) > 0$ for $p_T \leq p \leq p_B$, although this assumption may be relaxed somewhat. A natural domain for the operator L is then $D = \{u \in C^{(2)}[p_T,p_B] : B_T[u] = B_B[u] = 0\}$; integrating by parts twice shows $\langle Lu,v\rangle = \langle u,Lv\rangle$ for all u and v in D so L is self-adjoint.

To obtain the inverse vertical transform we use the fact that (5.12) has a countably infinite set of solutions $\{\lambda_n, \Psi_n(p)\}_{n=0}^{\infty}$ with the following properties.

(i) The eigenvalues λ_n are real and satisfy $\lambda_0 < \lambda_1 < \cdots$ with $\lambda_n \to \infty$ as $n \to \infty$;

(ii) The eigenfunctions $\Psi_n(p)$ lie in D and are orthonormal in the inner product (5.8), i.e. $\langle \Psi_m, \Psi_n \rangle = \delta_{mn} = \begin{cases} 1 & m=n \\ 0 & m \neq n \end{cases}$;

(iii) The eigenfunctions $\Psi_n(p)$ form a complete set.

Property (iii) means that any function u of p may be expanded as

$$u(p) = \sum_{n=0}^{\infty} \hat{u}_n \Psi_n(p) , \tag{5.13}$$

with pointwise convergence if $u \in C^{(0)}[p_T,p_B]$ and uniform convergence if $u \in D$. In view of property (ii) the coefficients in this expansion are given by $\hat{u}_n = \langle u, \Psi_n \rangle$. Since this formula is identical to the transform (5.9), (5.13) is the desired inverse transform.

Applying the transform (5.9) to the governing equations (5.1a) and (5.3) and using the property (5.10) results in

$$\frac{\partial \hat{\underset{\sim}{v}}_n}{\partial t} + f \underset{\sim}{k} \times \hat{\underset{\sim}{v}}_n + \nabla \hat{\phi}_n = \hat{\underset{\sim}{F}}_n \ , \tag{5.14a}$$

$$\frac{\partial \hat{\phi}_n}{\partial t} + \frac{1}{\lambda_n} \nabla \cdot \hat{\underset{\sim}{v}}_n = \frac{\partial \hat{\Phi}_n}{\partial t} \ , \tag{5.14b}$$

which is formally equivalent to the divergent barotropic system (i.e., the shallow water equations). The eigenvalue λ_n is often written as $(gh_n)^{-1}$, with g the acceleration due to gravity and h_n the so-called "equivalent depth." As we will show below, each λ_n is positive so we can define real "phase speeds" c_n by $c_n = (gh_n)^{\frac{1}{2}} = \lambda_n^{-\frac{1}{2}}$; each c_n is the (horizontal) phase speed of the single vertical mode n which has vertical structure $\Psi_n(p)$ in the stratified model. Since the solution of the stratified problem has been reduced to the superposition of solutions of barotropic problems corresponding to the various vertical modes, we refer to (5.9), (5.13) as the vertical normal mode transform pair.

5.1.3 Properties of the transform. The energetics of the stratified model (5.1) and the transformed model (5.14) are related by the Parseval relation

$$\langle u,v \rangle = \sum_{n=0}^{\infty} \hat{u}_n \hat{v}_n \ , \tag{5.15}$$

which may be obtained formally by expanding u(p) and v(p) and using the orthonormality of the functions Ψ_n. Taking the dot product of $\underset{\sim}{v}$ with (5.1a) and integrating with respect to p yields the kinetic energy

equation

$$\frac{\partial}{\partial t}\left(\tfrac{1}{2}\langle \underset{\sim}{v},\underset{\sim}{v}\rangle\right) + \langle \underset{\sim}{v},\nabla\phi\rangle = \langle \underset{\sim}{v},\underset{\sim}{F}\rangle \quad , \tag{5.16}$$

where for any two vectors $\underset{\sim}{a}$ and $\underset{\sim}{b}$ we interpret $\langle \underset{\sim}{a},\underset{\sim}{b}\rangle$ as $\langle \underset{\sim}{a}\cdot\underset{\sim}{b},1\rangle$. Then using (5.15) we can write (5.16) as

$$\sum_{n=0}^{\infty}\left[\frac{\partial}{\partial t}\left(\tfrac{1}{2}\,\hat{\underset{\sim}{v}}_n\cdot\hat{\underset{\sim}{v}}_n\right) + \hat{\underset{\sim}{v}}_n\cdot\nabla\hat{\phi}_n\right] = \sum_{n=0}^{\infty}\hat{\underset{\sim}{v}}_n\cdot\hat{\underset{\sim}{F}}_n \ . \tag{5.17}$$

Since (5.17) holds for each n individually, as shown by taking the dot product of (5.14a) with $\hat{\underset{\sim}{v}}_n$, we can identify $\tfrac{1}{2}\hat{\underset{\sim}{v}}_n\cdot\hat{\underset{\sim}{v}}_n$, $\hat{\underset{\sim}{v}}_n\cdot\nabla\hat{\phi}_n$, and $\hat{\underset{\sim}{v}}_n\cdot\hat{\underset{\sim}{F}}_n$ as the contributions from vertical mode n to the kinetic energy, conversion of kinetic to available potential energy, and generation of kinetic energy, respectively.

Similarly, multiplying (5.3) by ϕ, integrating and applying (5.15) yields the available potential energy equation

$$\sum_{n=0}^{\infty}\left[\frac{\partial}{\partial t}\left(\tfrac{1}{2}\,\frac{\hat{\phi}_n^{\,2}}{c_n^{\,2}}\right) + \hat{\phi}_n\,\nabla\cdot\hat{\underset{\sim}{v}}_n\right] = \sum_{n=0}^{\infty}\frac{\hat{\phi}_n}{c_n^{\,2}}\,\frac{\partial\hat{\phi}_n}{\partial t} \ . \tag{5.18}$$

Here the available potential energy is

$$\sum_{n=0}^{\infty}\tfrac{1}{2}\,\frac{\hat{\phi}_n^{\,2}}{c_n^{\,2}} = \tfrac{1}{2}\langle L\phi,\phi\rangle$$

$$= \frac{1}{2(p_B-p_T)}\left[\int_{p_T}^{p_B}\frac{1}{\sigma}\left(\frac{\partial\phi}{\partial p}\right)^2 dp + \left(\frac{p}{R\bar{T}}\,\phi^2\right)_{p=p_B}\right] , \tag{5.19}$$

with the last equality valid only if Q=0 at the top and bottom boundaries. Since (5.18) holds for each n individually, as shown by

multiplying (5.14b) by $\hat{\phi}_n$, we can identify $\hat{\phi}_n^2/c_n^2$, $\hat{\phi}_n \nabla\cdot\hat{\underset{\sim}{v}}_n$, and $\frac{\hat{\phi}_n}{c_n^2}\frac{\partial\hat{\Phi}_n}{\partial t}$ as the contributions from vertical mode n to the available potential energy, conversion from available potential to kinetic energy, and generation of available potential energy, respectively.

The vertical structure problem (5.12) has an interesting variational formulation which is closely related to (5.19). To obtain it we define for any u and v in $C^{(1)}[p_T,p_B]$ the quantity

$$\langle u,v\rangle_E = \frac{1}{p_B-p_T}\left[\int_{p_T}^{p_B} \frac{u'(p)v'(p)}{\sigma(p)}\,dp + \left(\frac{p}{R\bar{T}}uv\right)_{p=p_B}\right], \qquad (5.20)$$

where primes denote differentiation with respect to p. Since this quantity is symmetric, linear in each argument and satisfies $\langle u,u\rangle_E > 0$ unless u=0, (5.20) defines an inner product on $C^{(1)}[p_T,p_B]$. We refer to $\langle\ ,\ \rangle_E$ as the <u>energy inner product</u> since $\langle\phi,\phi\rangle_E$ is the available potential energy; it is related to the vertical inner product $\langle\ ,\ \rangle$ by $\langle u,v\rangle_E = \langle \mathcal{L}u,v\rangle$ when u and v are in D. The fact that $\langle u,v\rangle_E = \langle \mathcal{L}u,v\rangle$ when u and v are in D shows that $\mathcal{L}$ is positive definite. In particular, $0 < \langle\Psi_n,\Psi_n\rangle_E = \lambda_n$ for all n, establishing the claim made in the previous section.

The variational problem associated with the vertical structure problem consists of minimizing the functional $J[\Psi] = \langle\Psi,\Psi\rangle_E$ over all Ψ in $C^{(1)}[p_T,p_B]$ subject to the constraint $K[\Psi] = \langle\Psi,\Psi\rangle = 1$. This is equivalent to minimizing the functional $I[\Psi] = J[\Psi] - \lambda K[\Psi]$, where λ is a Lagrange multiplier for the constraint. This functional may be written as

$$I[\Psi] = \frac{1}{p_B - p_T} \int_{p_T}^{p_B} G(p,\Psi,\Psi')dp \ , \tag{5.21}$$

where

$$G(p,\Psi,\Psi') = \frac{(\Psi')^2}{\sigma} + \left(\frac{\alpha p \Psi^2}{R\bar{T}}\right)' - \lambda \Psi^2 \tag{5.22}$$

with $\alpha = (p-p_T)/(p_B-p_T)$. Setting the variation of (5.21) equal to zero (with no boundary conditions applied) leads to the Euler-Lagrange equations

$$\left.\begin{aligned} &\frac{\partial G}{\partial \Psi} - \left(\frac{\partial G}{\partial \Psi'}\right)' = 0 \qquad (p_T < p < p_B) \\ &\frac{\partial G}{\partial \Psi'} = 0 \quad \text{at} \quad p=p_T \ \text{and} \ p=p_B \end{aligned}\right\} \ . \tag{5.23}$$

Substituting (5.22) into (5.23) then yields the vertical structure problem (5.12). The eigenmodes $\Psi_n(p)$ thus give at least stationary values of $J[\Psi]$ subject to the constraint; a precise formulation of the variational problem is

$$\lambda_n = J[\Psi_n] =$$
$$\min\{J[\Psi]: \Psi \in C^{(1)}[p_T,p_B],\ \langle\Psi,\Psi\rangle = 1,\ \langle\Psi,\Psi_m\rangle = 0 \ (m=0,\ldots,n-1)\} \ . \tag{5.24}$$

Physically this says that for motions of the form $\underset{\sim}{v} = \hat{\underset{\sim}{v}}\,\Psi(p)$, $\phi = \hat{\phi}\,\Psi(p)$ with fixed horizontal and time dependence $\hat{\underset{\sim}{v}}$, $\hat{\phi}$, the available potential energy is minimized subject to fixed kinetic energy when $\Psi = \Psi_o$; for Ψ restricted so it has no projection onto the modes Ψ_o, ..., Ψ_{n-1} the minimum is obtained when $\Psi = \Psi_n$.

5.2 Implementation

For a few special stability profiles (e.g., σ = constant or $p^2\sigma$ = constant) the vertical structure problem (5.12) may be solved analytically in closed form. In most other cases (e.g., $\sigma(p)$ obtained from observations), approximate solutions must be sought. In this section we consider the solution of the vertical structure problem and the subsequent implementation of the vertical transform by a Chebyshev spectral method. Since the boundary conditions are linear and homogeneous, it is convenient to build them into the basis functions and use a Galerkin projection. The resulting method is equivalent to the Rayleigh-Ritz method for this problem; since the latter is a powerful general method closely related to the variational formulation (e.g. Ciarlet et al., 1968; Pierce and Varga, 1972), we introduce the approximation from the Rayleigh-Ritz point of view.

5.2.1 Solution of the vertical structure problem. The Rayleigh-Ritz method for (5.12) proceeds from the variational formulation (5.24). Recognizing that in practice we cannot minimize $J[\Psi]$ over all Ψ in $C^{(1)}[p_T,p_B]$, we choose a finite-dimensional subspace S_N of $C^{(1)}[p_T,p_B]$ and minimize $J[\Psi]$ over it instead . (The elements of S_N need not satisfy the upper and lower boundary conditions, but better results generally are obtained if they do.) Thus the Rayleigh-Ritz method defines approximate eigenvalues $\tilde{\lambda}_n$ and eigenfunctions $\tilde{\Psi}_n(p)$ by

$$\tilde{\lambda}_n = J[\tilde{\Psi}_n] = \min\{J[\Psi]: \Psi\epsilon S_N,\ \langle\Psi,\Psi\rangle = 1,\ \langle\Psi,\tilde{\Psi}_m\rangle = 0\ (m=0,\ldots,n-1)\}\ . \quad (5.25)$$

This variational problem leads to

$$\langle\tilde{\Psi}_n,\Psi\rangle_E = \tilde{\lambda}_n\langle\tilde{\Psi}_n,\Psi\rangle \quad (\text{all } \Psi \text{ in } S_N)\ , \quad (5.26)$$

which is identical to the Galerkin equation for (5.12) if the elements of S_N satisfy the boundary conditions.

To solve for $\tilde{\lambda}_n$ and $\tilde{\Psi}_n$ we fix a basis $\{\chi_0(p), \ldots, \chi_N(p)\}$ for S_N. This introduces a one-to-one correspondence between functions $u(p)$ in S_N and (N+1) component vectors $\underset{\sim}{u} = [u_0,\ldots,u_N]^T$ of their coordinates with respect to this basis. In particular, each $\tilde{\Psi}_n(p)$ corresponds to a vector $\underset{\sim}{\psi}_n = [\psi_{0,n},\ldots,\psi_{N,n}]^T$ with

$$\tilde{\Psi}_n(p) = \sum_{j=0}^{N} \psi_{j,n}\, \chi_j(p) \ . \tag{5.27}$$

Noting that we need only consider $\Psi = \chi_i$ $(i=0,\ldots,N)$ in (5.26) and substituting from (5.27) we obtain

$$\sum_{j=0}^{N} \langle \chi_i,\chi_j\rangle_E\, \psi_{j,n} = \tilde{\lambda}_n \sum_{j=0}^{N} \langle \chi_i,\chi_j\rangle\, \psi_{j,n} \quad (i=0,\ldots,N) \ , \tag{5.28}$$

which may be written in matrix form as

$$\underset{\approx}{A}\, \underset{\sim}{\psi}_n = \tilde{\lambda}_n\, \underset{\approx}{B}\, \underset{\sim}{\psi}_n \ . \tag{5.29}$$

Here $\underset{\approx}{A}$ and $\underset{\approx}{B}$ are matrices of order N+1 with entries $A_{ij} = \langle \chi_i,\chi_j\rangle_E$ and $B_{ij} = \langle \chi_i,\chi_j\rangle$; this connection with the inner products guarantees that both matrices are real, symmetric and positive definite. Therefore, the generalized eigenvalue problem (5.29) has solutions $\{\tilde{\lambda}_n,\underset{\sim}{\psi}_n\}_{n=0}^{N}$ with the following properties.

(i) The eigenvalues $\tilde{\lambda}_n$ are real, with $0<\tilde{\lambda}_0<\tilde{\lambda}_1<\ldots<\tilde{\lambda}_N$.

(ii) The eigenvectors $\underset{\sim}{\psi}_n$ are orthonormal in the sense $\underset{\sim}{\psi}_m^T\, \underset{\approx}{B}\underset{\sim}{\psi}_n = \delta_{mn}$.

(iii) The eigenvectors $\underset{\sim}{\psi}_n$ form a complete set.

In view of property (i) we can define the approximate phase speeds $\tilde{c}_n = \tilde{\lambda}_n^{-\frac{1}{2}}$. As shown in the next section, property (ii) implies that $\langle \tilde{\Psi}_m, \tilde{\Psi}_n \rangle = \delta_{mn}$, and property (iii) implies that the functions $\Psi_n(p)$ span S_N. Thus the numerical solution obtained by the Rayleigh-Ritz method preserves much of the character of the analytical solution of (5.12).

5.2.2 Application of the vertical transform. Having obtained the approximate vertical structure functions $\tilde{\Psi}_n(p)$ in terms of the basis functions $\chi_j(p)$, the application of the vertical transform is now straightforward, amounting to simply a change of basis. For any function $u(p)$ in S_N we have the two representations

$$u(p) = \sum_{j=0}^{N} u_j \chi_j(p) = \sum_{n=0}^{N} \hat{u}_n \tilde{\Psi}_n(p) . \tag{5.30}$$

The coefficients $\underset{\sim}{u} = [u_0,\ldots,u_N]^T$ and $\hat{\underset{\sim}{u}} = [\hat{u}_0,\ldots,\hat{u}_N]^T$ in these representations are related by

$$\hat{\underset{\sim}{u}} = \underset{\approx}{T}\, \underset{\sim}{u} , \quad \underset{\sim}{u} = \underset{\approx}{T}^{-1} \hat{\underset{\sim}{u}} , \tag{5.31}$$

where $\underset{\approx}{T}^{-1}$ is the matrix whose columns are the vectors $\underset{\sim}{\psi}_n$ and $\underset{\approx}{T} = (\underset{\approx}{B}\, \underset{\approx}{T}^{-1})^T$. Thus (5.31) is a numerical representation of the transform pair (5.9), (5.13). Similarly, the inner products of any functions u and v in S_N may be expressed as

$$\langle u,v \rangle = \underset{\sim}{v}^T \underset{\approx}{B}\, \underset{\sim}{u} = \hat{\underset{\sim}{v}}^T \hat{\underset{\sim}{u}} = \sum_{n=0}^{N} \hat{u}_n \hat{v}_n \tag{5.32}$$

and

$$\langle u,v\rangle_E = \underset{\sim}{v}^T \underset{\approx}{A}\, \underset{\sim}{u} = \hat{\underset{\sim}{v}}^T \underset{\approx}{E}\, \hat{\underset{\sim}{u}} = \sum_{n=0}^{N} \tilde{\lambda}_n \hat{u}_n \hat{v}_n \,, \tag{5.33}$$

where $\underset{\approx}{E} = (\underset{\approx}{T}^{-1})^T \underset{\approx}{A}\, \underset{\approx}{T}^{-1} = \text{diag}\,[\tilde{\lambda}_0,\ldots,\tilde{\lambda}_N]$.

5.2.3 Basis functions. Many different types of functions may be used as basis functions for the Rayleigh-Ritz method. If the vertical transform is used within a numerical model which employs a series expansion (i.e., finite element or spectral) method in the vertical, the basis functions of the numerical model are the natural choice for use in computing the vertical transform (Daley, 1979; Béland et al., 1983). In other applications the choice of basis functions may depend on considerations of accuracy, efficiency, storage required and ease of programming.

Piecewise polynomials (splines) have become popular for use in the Rayleigh-Ritz method (Wendroff, 1965; Birkhoff et al., 1966; Johnson, 1969; Prenter, 1975). Typically, one chooses S_N as a space of piecewise cubic functions over a partition of the interval $[p_T,p_B]$, with a basis of B-splines (deBoor, 1978) which satisfy the boundary conditions; "jump" conditions arising from known discontinuities in $\sigma(p)$ may also be built into such a basis. The approximation of an arbitrary function $f(p)$ by an element g in S_N then involves solving a well-conditioned banded linear system; if f is sufficiently smooth, this approximation generally has accuracy $O(N^{-4})$. Since the matrices $\underset{\approx}{A}$ and $\underset{\approx}{B}$ are banded, the eigenvalue problem (5.29) may be solved efficiently, e.g. by the algorithm of Peters and Wilkinson (1969); the resulting approximate eigenvalues and eigenfunctions have accuracy $O(N^{-6})$ and $O(N^{-3})$, respectively (Ciarlet et al., 1968). Greater accuracy may be obtained

by using higher-order splines, at the cost of increased program complexity.

Still greater accuracy can be obtained by choosing S_N instead as the subspace of all polynomials of degree at most N+2 which satisfy the upper and lower boundary conditions. An analytic function f(p) may be approximated by an element g of this subspace with exponential accuracy; i.e., the error in the approximation is asymptotically $O(e^{-N/N_o})$ with N_o constant. Similarly, if the true eigenfunctions $\Psi_n(p)$ are analytic then the resulting approximate eigenvalues and eigenfunctions also have exponential accuracy (Ciarlet et al., 1968). There is a trade-off here between accuracy and efficiency, since the matrices involved are full. However, the high accuracy implies that N may be chosen relatively small, so the computer time and storage required are in general inconsequential. In view of the high accuracy and the ease of programming with polynomials, we use this polynomial subspace for all results reported here.

To ensure that the matrices $\underset{\approx}{A}$ and $\underset{\approx}{B}$ are well-conditioned we construct a basis for the polynomial subspace S_N from the Chebyshev polynomials (2.12) as follows. Mapping the interval $p_T \leq p \leq p_B$ onto $-1 \leq s \leq 1$ by $s = 2(p_B-p)/(p_B-p_T)-1$, we define

$$\chi_j(p) = T_{j+2}(s) - a_j\, T_o(s) - b_j\, T_1(s) \quad (0 \leq j \leq N) \,. \tag{5.34}$$

The constants a_j and b_j are chosen so that each χ_j satisfies the boundary conditions $B_T[\chi_j] = B_B[\chi_j] = 0$, resulting in

$$\left.\begin{aligned} a_j &= (-1)^j + b_j \left\{1 + \frac{2}{p_B - p_T}\left[1 + (-1)^j\right]\left(\frac{\bar{RT}}{p\sigma}\right)_{p=p_B}\right\} \\ b_j &= (j+2)^2 \end{aligned}\right\} . \qquad (5.35)$$

With this basis the method is a Chebyshev-Galerkin method (Gottlieb and Orszag, 1977). To compute the elements of the matrices $\underset{\approx}{A}$ and $\underset{\approx}{B}$ we use a least-squares Chebyshev polynomial fit to $[p^2\sigma(p)]^{-1}$ and compute the resulting integrals exactly by Gauss-Legendre quadrature. The eigenvalue problem (5.29) is then solved by the EISPACK routine RSG, which converts it to a standard symmetric eigenvalue problem via the Cholesky decomposition of $\underset{\approx}{B}$ and solves that problem by the QR algorithm.

Any continuous function f(p) can be approximated by an element g of S_N by a least-squares fit in some appropriate norm. If the norm comes from an inner product then the resulting approximation

$$g(p) = \sum_{j=0}^{N} g_j \chi_j(p) \qquad (5.36)$$

to f can be computed from the linear system

$$\sum_{j=0}^{N} (\chi_i, \chi_j) g_j = (f, \chi_i) \qquad (i=0,\ldots,N) , \qquad (5.37)$$

where (,) denotes the inner product chosen. For the results presented here we use the Chebyshev inner product (2.16) with x replaced by s, since the resulting fit is essentially uniform, i.e. it nearly minimizes the maximum pointwise error $|f(p)-g(p)|$ (Rivlin, 1969). The linear system (5.37) is solved using the Cholesky decomposition, using Gauss-Chebyshev quadrature to evaluate the inner product (2.16).

5.3 Results

In this section we present solutions of the vertical structure problem obtained by the method of the previous section and apply the vertical transform to observed tropical forcing profiles.

5.3.1 Solutions and accuracy. The accuracy of the Rayleigh-Ritz method may be illustrated by comparing the numerical solutions $\tilde{c}_n$, $\tilde{\Psi}_n$ to the true solutions c_n, Ψ_n for a case which can be solved analytically. Here we consider the case $p^2\sigma = R\Gamma$ = constant, for which (5.12) may be solved easily in log pressure coordinates (e.g. Fulton and Schubert, 1980). Figure 37 shows the relative error $|\tilde{c}_n - c_n|/c_n$ in the phase speeds as a function of the truncation N for various vertical modes n; Fig. 38 shows the corresponding error $\tilde{\Psi}_n - \Psi_n$ in the vertical structure functions measured in the vertical norm $\|\cdot\| = \langle \cdot, \cdot \rangle^{\frac{1}{2}}$. The values p_B=1010 mb, p_T=100 mb, Γ=23.79 K and $\bar{T}(p_B)$=29.38°C have been assumed. The exponential convergence of the method is clearly evident; for example, increasing N by 2 gives an order of magnitude improvement in $\tilde{c}_0$, and increasing N by 3 gives an order of magnitude improvement in $\tilde{\Psi}_0$. Machine accuracy for $\tilde{c}_0$ is reached near N=24 and roundoff error affects the solutions somewhat for larger N. The dashed curves indicate that for modes n=0,...,N/2 the eigenvalues and eigenfunctions have relative errors at most about 0.5-1.0% and 10-20%, respectively. From this point on, only numerical solutions will be considered (N=32 unless otherwise specified) and hence the tildes on $\tilde{c}_n$ and $\tilde{\Psi}_n$ will be dropped.

A constant Γ atmosphere is only a first approximation to reality. In the tropics Γ typically varies from about 40 K in the lower troposphere (~800 mb), with lower values near the surface, to about 10 K in the upper troposphere (~250 mb), with much higher values in the

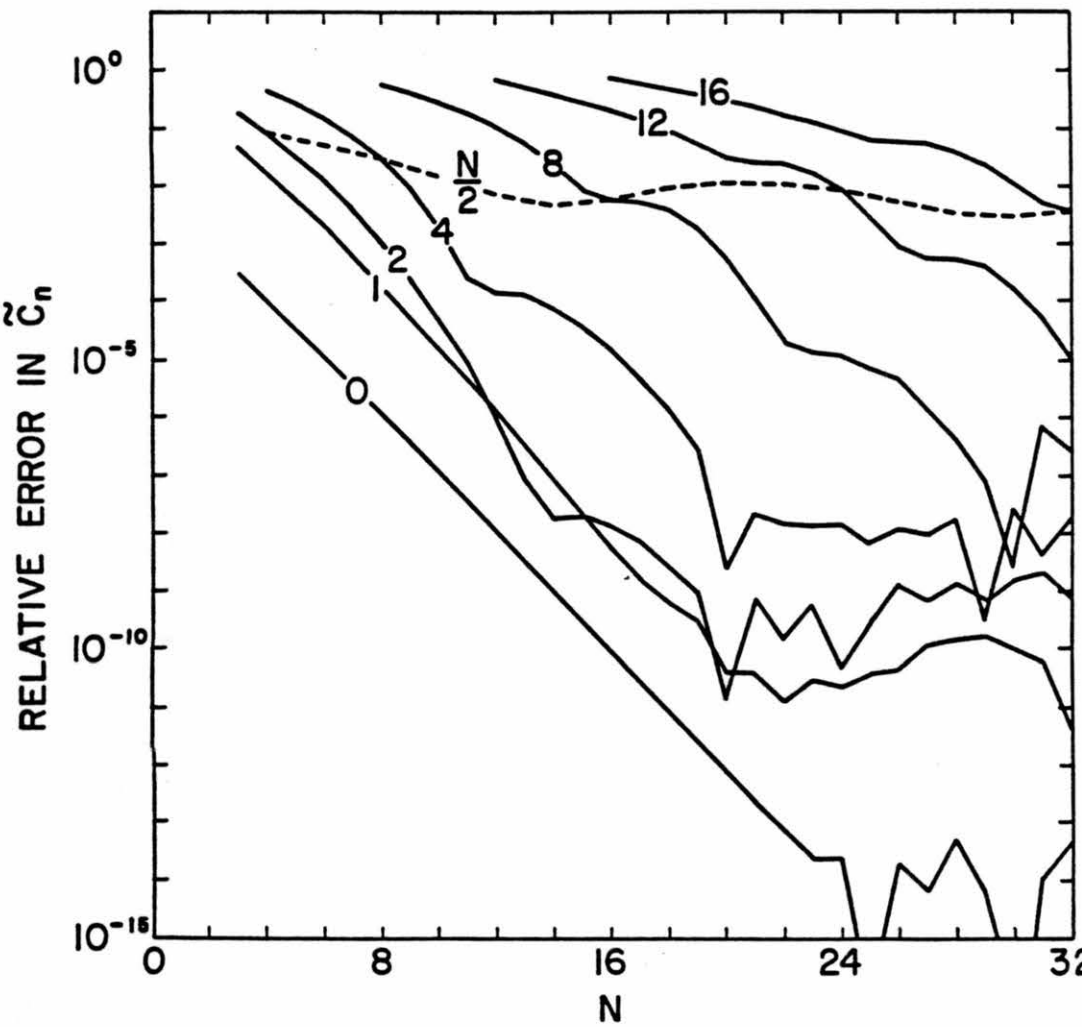

Figure 37. Relative error $|\tilde{c}_n - c_n|/c_n$ in the phase speeds as a function of the truncation N for various modes n as labeled.

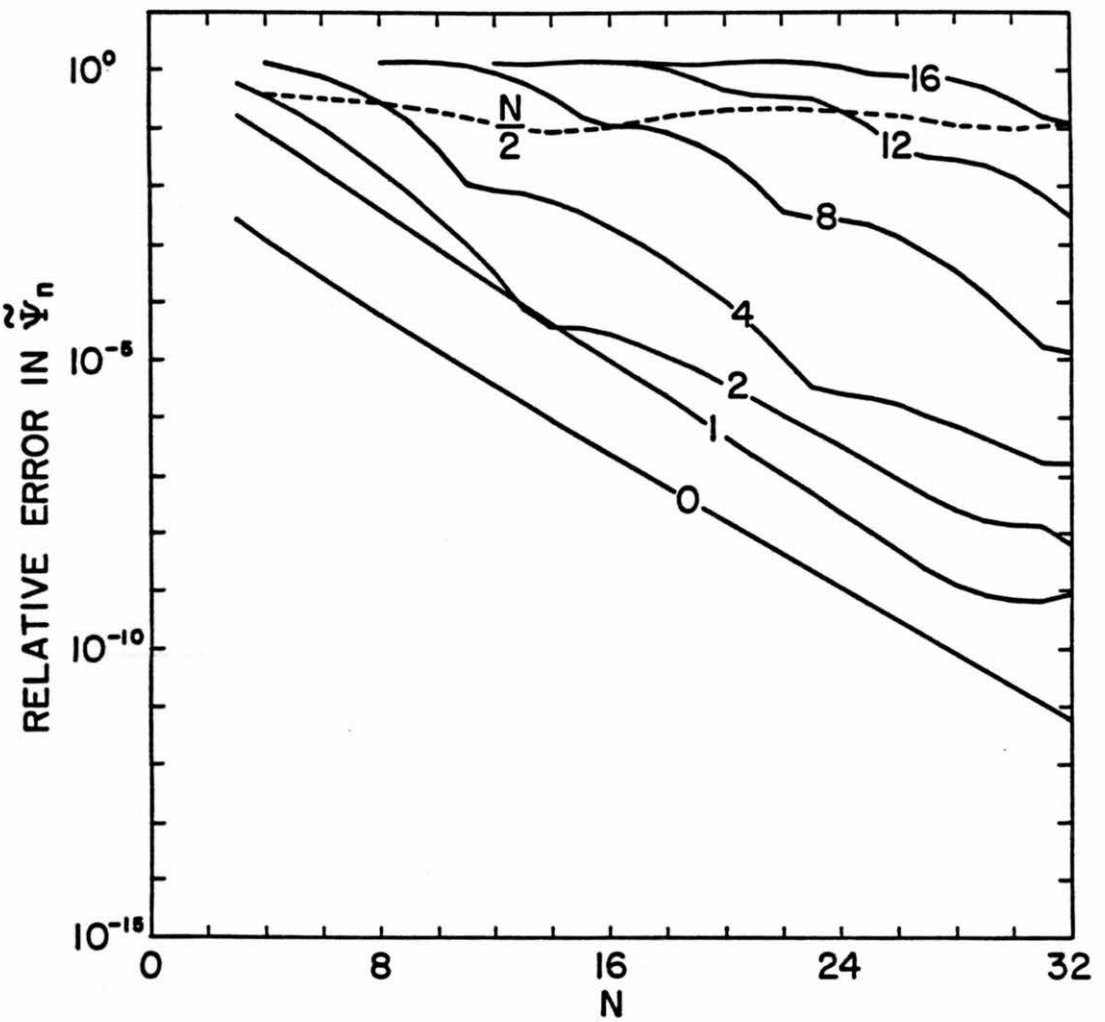

Figure 38. Vertical norm of the error in the vertical structure functions, $\| \tilde{\Psi}_n - \Psi_n \|$, as a function of the truncation N for various vertical modes n as labeled.

stratosphere. Figure 39 shows the first four vertical structure functions for the GATE temperature sounding of Table 8; phase speeds for the higher modes appear in Table 9. Comparison with solutions for much larger N indicates that the convergence of c_n and Ψ_n for this basic state is exponential but slower than for the constant Γ case considered above. The mode n=0 is referred to as the external mode since it has no zeros (nodes) internal to the atmosphere; the modes n=1,2,... are referred to as internal modes, with mode n having n zeros internal to the atmosphere.

5.3.2 Sampling and aliasing. Measuring an atmospheric variable such as wind or geopotential amounts to sampling a continuous function of pressure at discrete levels, which inherently limits the amount of vertical structure which can be resolved by the data. To examine the effects of this sampling we evaluated the vertical structure functions $\Psi_m(p)$ at various discrete levels and then projected this "data" back onto the vertical modes. The results of these calculations are presented in Tables 5-7, which give the energy per mode (square of the spectral coefficient) as a percentage of the input energy 1.

For Table 5, 12 standard levels (denoted by (s) in Table 8) from the surface p_B=1010 mb to the top p_T=50 mb were used. These levels do not give enough resolution in the upper troposphere and stratosphere to adequately represent Ψ_m for $m \gtrsim 4$. This leads to significant aliasing; i.e., Ψ_m for larger m projects a significant amount of energy onto the lower modes, especially the first internal mode. This aliasing is reduced somewhat by placing the top at p_T=100 mb as in Table 6, since this eliminates the stratosphere where the vertical structure functions are highly oscillatory. Still better results are obtained by sampling

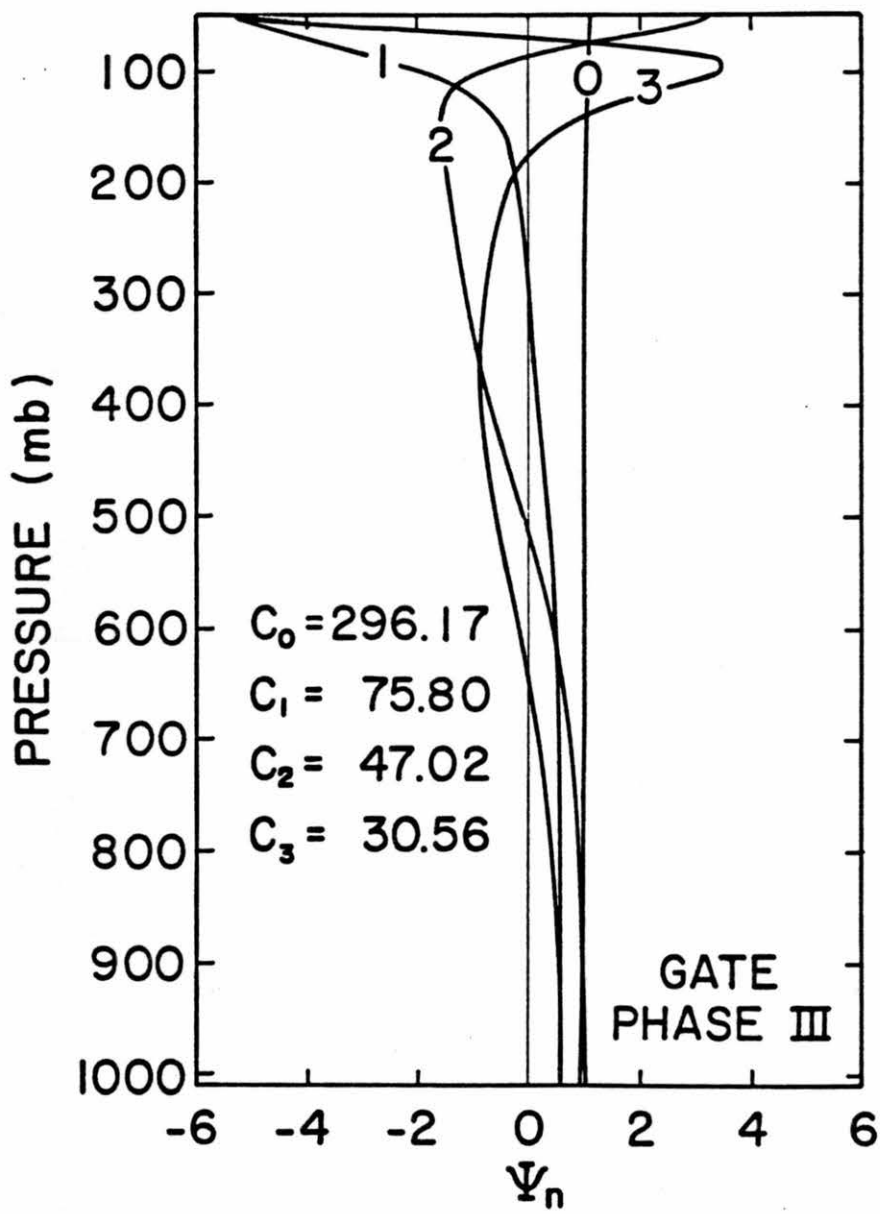

Figure 39. First four vertical structure functions for the GATE temperature sounding of Table 8. Corresponding phase speeds (ms^{-1}) are listed at the lower left.

Table 5. Percent energy in mode n for reconstruction of Ψ_m from values at 12 standard levels with p_T=50 mb.

n	c_n (ms^{-1})	m=0	m=1	m=2	m=3	m=4	m=5	m=6	m=7	m=8	m=9	m=10
0	296.17	100	0	0	0	1	4	6	4	3	0	0
1	75.80	0	105	0	8	19	59	64	51	27	23	31
2	47.02	0	0	105	2	4	11	8	5	9	19	23
3	30.56	0	0	0	100	0	0	0	1	15	34	29
4	22.92	0	0	0	4	54	15	5	0	2	1	0
5	18.88	0	0	0	8	16	19	10	1	0	4	15
6	15.58	0	0	0	1	2	8	44	8	7	1	0
7	13.55	0	0	0	1	0	0	7	29	10	0	4
8	11.66	0	0	0	1	1	1	1	9	42	2	0
9	10.31	0	0	0	0	0	0	0	0	8	30	11
10	9.21	0	0	0	1	1	0	1	1	1	19	16

Table 6. Percent energy in mode n for reconstruction of Ψ_m from values at 11 standard levels with p_T=100 mb.

n	c_n (ms^{-1})	m=0	m=1	m=2	m=3	m=4	m=5	m=6	m=7	m=8	m=9	m=10
0	286.87	100	0	0	0	0	0	1	6	0	6	19
1	51.61	0	100	0	0	0	2	3	4	17	10	6
2	28.85	0	0	106	0	1	5	8	15	35	27	16
3	20.58	0	0	0	107	1	1	3	14	0	13	29
4	15.23	0	0	0	0	100	1	0	0	10	0	6
5	12.34	0	0	0	0	0	91	0	0	1	1	3
6	10.22	0	0	0	0	0	2	65	1	20	0	1
7	8.74	0	0	0	0	1	2	7	18	1	13	28
8	7.64	0	0	0	0	0	4	5	2	12	2	1
9	6.80	0	0	0	0	0	1	2	4	3	36	0
10	6.12	0	0	0	0	0	0	0	3	0	1	13

Table 7. Percent energy in mode n for reconstruction of Ψ_m from values at 12 levels equally spaced in log(p) with p_T=50 mb.

n	c_n (ms^{-1})	m=0	m=1	m=2	m=3	m=4	m=5	m=6	m=7	m=8	m=9	m=10
0	296.17	100	0	0	0	0	0	0	0	0	0	0
1	75.80	0	100	0	0	0	0	0	0	1	1	3
2	47.02	0	0	100	0	0	0	0	0	0	1	1
3	30.56	0	0	0	100	0	0	0	0	1	3	6
4	22.92	0	0	0	0	99	0	0	1	1	5	4
5	18.88	0	0	0	0	0	99	0	1	6	9	17
6	15.58	0	0	0	0	0	0	101	2	5	16	5
7	13.55	0	0	0	0	0	0	0	109	5	1	4
8	11.66	0	0	0	0	0	0	0	0	66	1	10
9	10.31	0	0	0	0	0	0	0	2	12	19	6
10	9.21	0	0	0	0	0	0	0	2	13	14	39

at levels equally spaced in log pressure as in Table 7. This spacing is suggested by the fact that the zeros of the vertical structure functions have this spacing when Γ is constant; it reduces aliasing significantly. These results indicate that without a careful choice of sampling levels, aliasing may give misleading information about the vertical modes present in observational data. Since the various modes differ significantly in their dynamics due to their different phase speeds (and, hence, different Rossby radii), this effect may influence any conclusions drawn from the data.

5.3.3 Application to tropical data. Vertical transforms of global data have been computed by Kasahara and Puri (1981) using the normal modes of a numerical model. Here we use the method described in section 5.2 to transform observed tropical forcing profiles. The data for this application was provided by M. Yanai and is given in Table 8. It consists of two data sets: Marshall Islands and GATE. In addition to a mean temperature profile, each data set consists of time mean profiles of apparent heat source

$$Q = Q_1 \equiv c_p \left[\frac{\partial \bar{T}}{\partial t} + \overline{\underset{\sim}{v} \cdot \nabla T} + \bar{\omega} \left(\frac{\partial \bar{T}}{\partial p} - \frac{R\bar{T}}{pc_p} \right) \right] \tag{5.38}$$

and apparent vorticity source

$$\underset{\sim}{k} \cdot \nabla \times \underset{\sim}{F} = Z \equiv \frac{\partial \bar{\zeta}}{\partial t} + \nabla \cdot \left[(\bar{\zeta} + \bar{f}) \underset{\sim}{\bar{v}} \right] + \underset{\sim}{k} \cdot \nabla \times \left(\bar{\omega} \frac{\partial \underset{\sim}{\bar{v}}}{\partial p} \right) , \tag{5.39}$$

where $\tilde{\zeta} = k \cdot \nabla \times \underset{\sim}{\tilde{v}}$ and the overbar now denotes a horizontal average. The mean Marshall Islands profiles result from averaging 383 analysis times and have been used in the studies of Yanai et al. (1973), Yanai et al.

Table 8. Physical space profiles of $\bar{T}$ (°C), Q_1 (°C/day) and Z ($10^{-11}s^{-2}$) as functions of p (mb) (s denotes the standard levels used in section 5.3.2).

	MARSHALL ISLANDS MEAN			GATE MEAN			GATE DISTURBED		GATE UNDISTURBED	
p	$\bar{T}$	Q_1	Z	$\bar{T}$	Q_1	Z	Q_1	Z	Q_1	Z
50(s)	-60.63	0.00	0.00	-62.22	0.00	0.00	0.00	0.00	0.00	0.00
100(s)	-73.42	1.46	8.98	-75.46	0.12	-0.45	0.08	-2.62	0.15	0.79
150(s)	-68.51	2.65	9.12	-69.07	-0.53	0.40	-0.67	3.61	-0.44	-1.44
200(s)	-55.42	2.54	6.74	-56.00	-0.77	4.10	-0.02	11.35	-1.26	-0.07
250(s)	-43.37	2.85	4.10	-43.76	0.40	3.20	1.81	8.27	-0.55	0.27
300(s)	-33.22	4.29	2.51	-33.33	1.84	-1.19	3.90	-4.02	0.46	0.43
350	-24.82	5.38	1.92	-24.85	2.79	-6.72	5.26	-14.19	1.15	-2.42
400	-17.66	6.01	2.04	-17.89	2.98	-7.68	5.44	-13.87	1.34	-4.11
450	-11.73	6.39	3.14	-12.08	3.09	-3.77	5.26	-7.49	1.64	-1.62
500(s)	-6.71	6.42	4.09	-7.34	3.54	0.44	5.48	-2.86	2.24	2.34
550	-2.25	6.17	2.70	-3.28	4.04	1.96	5.92	-1.82	2.78	4.13
600	1.68	5.60	0.68	0.39	4.18	1.48	6.05	-1.60	2.93	3.25
650	5.40	4.73	0.81	3.98	3.94	0.61	5.65	-1.15	2.80	1.63
700(s)	8.78	4.07	3.56	7.55	3.68	0.72	5.20	0.04	2.66	1.11
750	11.75	3.73	5.03	10.78	3.59	2.25	4.94	3.49	2.69	1.55
800	14.41	3.33	3.44	13.54	3.61	3.33	4.75	5.26	2.84	2.22
850(s)	16.90	2.66	1.20	15.96	3.37	1.39	4.25	2.95	2.78	0.48
900	19.69	1.80	-1.81	18.42	2.55	-3.99	3.17	-2.50	2.14	-4.85
950	22.75	0.93	-5.24	21.28	1.17	-9.02	1.35	-8.89	1.05	-9.09
1000(s)	26.08	0.12	-6.94	24.60	0.08	-10.32	-0.03	-12.10	0.16	-9.29
1010(s)	26.78	0.00	-7.00	25.30	0.00	-10.36	0.00	-12.20	0.00	-9.30

(1976) and Chu et al. (1981). The mean GATE profiles result from averaging 145 analysis times and are a by-product of the study of Sui and Yanai (1984)[1]. In addition, the GATE data has been partitioned into disturbed (53 analysis times) and undisturbed (92 analysis times) situations based on satellite-derived upper level cloudiness.

The profiles of Q_1 and Z for the Marshall Islands and GATE are displayed in Fig. 40. From the point of view of Q_1 the GATE region is less active in the mean than the Marshall Islands region. In fact, the Marshall Islands mean Q_1 closely resembles the GATE disturbed Q_1. In contrast, from the point of view of Z, the GATE region seems quite active. An interesting overall difference between the Q_1 and Z profiles is the more complicated vertical structures associated with Z. This difference is important in determining which vertical modes are excited by the two apparent sources.

The spectral space representations (with N=32 and p_T=50 mb) of the apparent heat and vorticity sources are given in Table 9. Similar results (not shown) for different truncations N (e.g. N=8, 16) and different model tops (e.g. p_T=25, 100mb) show differences with Table 9 which are rather small as long as one views the spectral representation in terms of the phase speed c rather than the mode index n. Perhaps the most striking feature of Table 9 is the difference in the width of the spectra for Q_1 and Z, with Q_1 being projected primarily onto the narrow range $30<c<300$ ms^{-1} and Z onto the broad range $7<c<300$ ms^{-1}.

---

[1]The data used by Sui and Yanai (1984) is in turn based on the upper-air objective wind analysis of K. Ooyama and J. H. Chu (see Esbensen et al., 1982, for a brief description) and the objective thermodynamic analysis of Esbensen and Ooyama (1983).

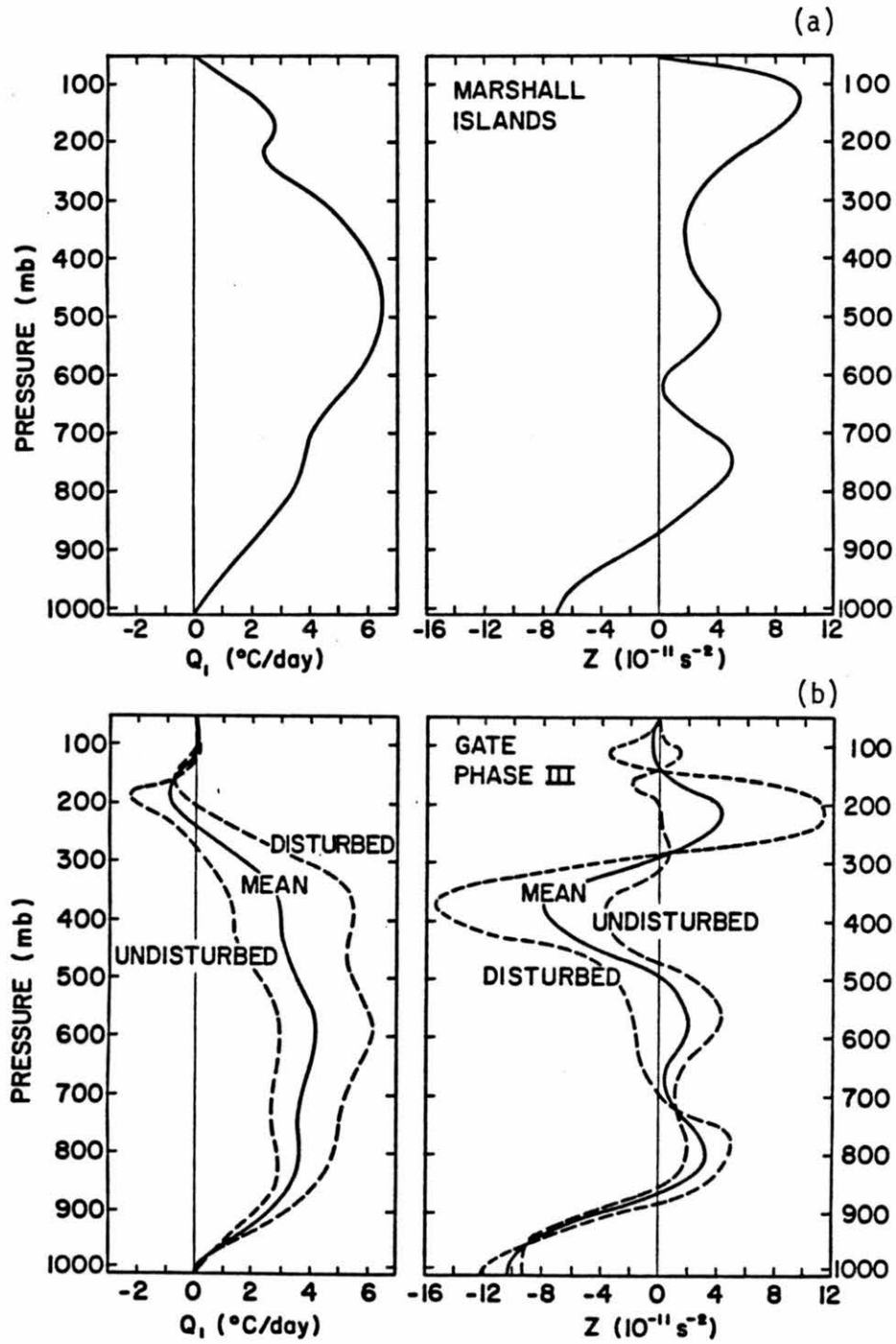

Figure 40. Vertical profiles of the apparent heat source Q_1 and the apparent vorticity source Z for the Marshall Islands (a) and for GATE (b).

Table 9. Spectral space profiles of c_n (ms^{-1}), $\partial\hat{\Phi}_n/\partial t$ ($m^2 s^{-2}$ day^{-1}) and $\hat{Z}_n$ (10^{-11} s^{-2}) as functions of the vertical mode index n.

	MARSHALL ISLANDS MEAN			GATE MEAN			GATE DISTURBED		GATE UNDISTURBED	
n	c_n	$\lvert\partial\hat{\Phi}_n/\partial t\rvert$	Z_n	c_n	$\lvert\partial\hat{\Phi}_n/\partial t\rvert$	Z_n	$\lvert\partial\hat{\Phi}_n/\partial t\rvert$	Z_n	$\lvert\partial\hat{\Phi}_n/\partial t\rvert$	Z_n
0	296.66	967	2.617	296.17	614	1.002	948	1.758	391	0.566
1	77.22	562	1.046	75.80	199	0.451	376	0.722	81	0.294
2	46.66	541	2.208	47.02	311	0.478	514	0.579	175	0.419
3	31.07	55	0.553	30.56	95	0.098	116	0.747	81	0.277
4	23.36	31	0.138	22.92	43	0.117	18	2.353	59	1.171
5	18.91	11	1.096	18.88	1	0.899	9	0.108	8	1.479
6	15.72	11	1.089	15.58	9	2.293	23	3.576	1	1.555
7	13.53	9	0.606	13.55	22	2.076	37	3.354	12	1.340
8	11.67	2	0.298	11.66	13	0.484	13	0.036	13	0.784
9	10.31	1	0.517	10.31	3	0.445	10	1.318	2	0.058
10	9.20	1	0.931	9.21	7	0.059	10	0.462	5	0.172
11	8.14	1	1.205	8.14	3	1.492	5	2.802	2	0.737
12	7.22	4	0.898	7.22	6	1.486	5	1.790	6	1.310
13	6.40	2	0.567	6.41	1	0.634	1	0.312	1	0.816
14	5.72	0	0.133	5.73	2	0.606	3	0.888	1	0.443
15	5.16	1	0.024	5.16	2	0.498	2	0.769	2	0.341
16	4.68	0	0.086	4.68	0	0.309	0	0.243	0	0.346
17	4.27	1	0.175	4.27	1	0.155	2	0.326	1	0.056
18	3.92	0	0.199	3.92	0	0.111	0	0.103	0	0.113
19	3.61	0	0.172	3.62	0	0.064	0	0.135	0	0.024
20	3.34	1	0.197	3.33	0	0.055	0	0.187	0	0.021

With the data at hand the generation of kinetic and available potential energy cannot be determined, as they involve products of forcing terms with perturbation fields which are not known. Nevertheless, we can compute the quantity $(\hat{\Phi}_t/c)^2$ which is shown in Fig. 41 as a function of the phase speed c. If the time scale of the heating is short enough for it to be regarded as impulsive, then the curves in Fig. 41 give the relative distribution of initial available potential energy for the given Q_1 profiles. The sharp spectral peak then gives some justification for studies such as those of Gill (1980) and Silva Dias et al. (1983) which use equatorial β-plane shallow water models with $c \approx 50\ ms^{-1}$. This discussion complements that of Geisler and Stevens (1982) which considered the projection of an idealized heating profile onto the normal modes of an atmosphere with constant static stability.

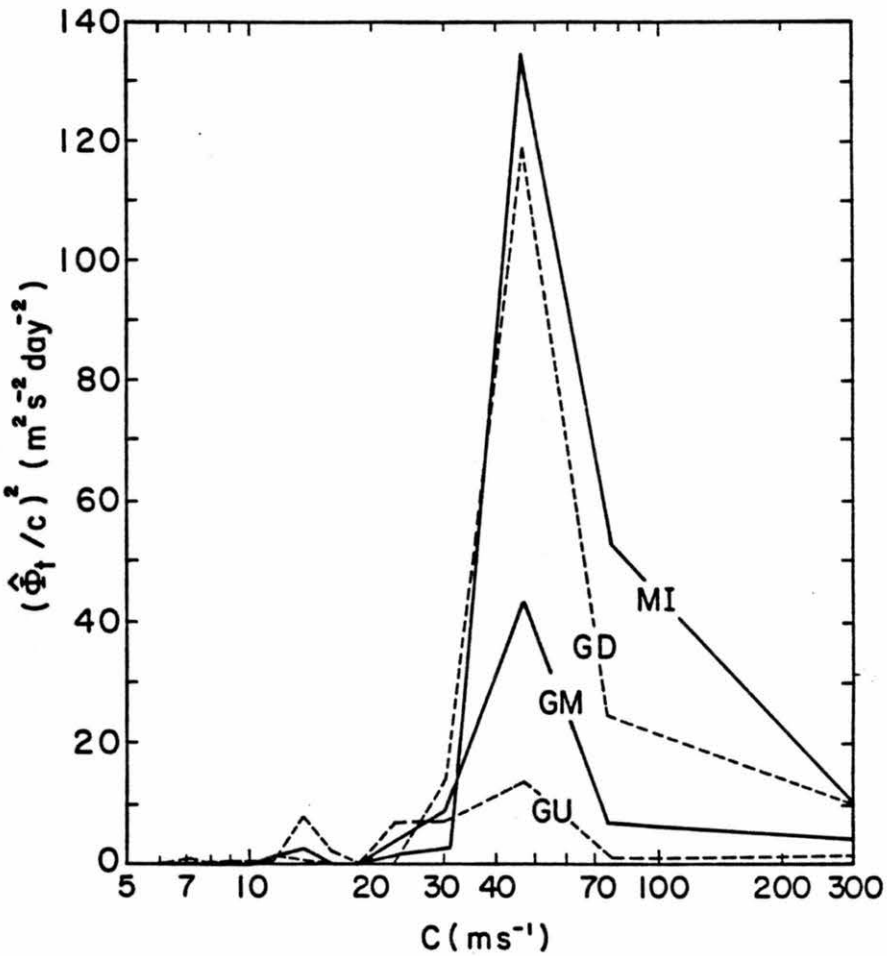

Figure 41. Plots of $(\hat{\Phi}_t/c)^2$ as a function of c for the Marshall Islands (MI), GATE mean (GM), GATE disturbed (GD) and GATE undisturbed (GU) apparent heat sources.

CHAPTER 6

SUMMARY AND CONCLUSIONS

Spectral methods are techniques for obtaining highly accurate solutions of problems involving differential equations. Such techniques are widely used in global atmospheric modeling. In this study we have investigated the usefulness of spectral methods in limited area modeling. The appropriate techniques, based on Chebyshev polynomial expansions, were reviewed and illustrated by applying them to the simple linear advection equation. The nonlinear shallow water model was then used as a more realistic prototype; Chebyshev spectral methods for this model were developed and tested using a variety of boundary conditions, equation forms and projections. Time differencing schemes for such methods were discussed with particular emphasis on the question of overall efficiency.

The principal conclusion of this study is that spectral methods are indeed practical for limited area models. Compared to finite difference methods, spectral methods offer:

(i) higher accuracy with far fewer degrees of freedom (and thus much less computer storage),

(ii) greater efficiency (less work for the same accuracy) when the accuracy desired is high enough,

(iii) ease of programming (when explicit time differencing is used).

In regard to point (iii), it has often been claimed that implicit time differencing is needed since the stability condition for Chebyshev spectral methods with explicit time differencing is "severe". We have shown that this condition is less severe than the corresponding condition for finite difference methods; in addition, time steps may in fact be limited by accuracy rather than stability, in which case simple explicit time differencing is practical and efficient. In view of the above considerations, spectral methods should be considered as a practical alternative to finite difference methods for limited area modeling, especially when accurate solutions are desired.

Comparing the Chebyshev-tau and Chebyshev-collocation methods, we have found that each has its own advantages. The tau method treats at least some boundary conditions more accurately and allows quadratic nonlinear terms to be evaluated without aliasing. Furthermore, in cases where implicit time differencing is necessary for efficiency, the tau method may be preferable since there is some hope of solving the tau equations directly, without using complicated iterative schemes. On the other hand, the collocation method is likely to be faster (at least twice as fast for the two-dimensional shallow water model) and is often easier to implement, especially for problems with complicated nonlinearities or nonlinear boundary conditions. Both methods can be formulated using either the advective or the rotational form of the equations. With the tau discretization both forms give similar solutions, but the rotational form is preferred in two dimensions since it requires less work. With the collocation discretization the advective form seems to produce better results in two dimensions.

In this study Chebyshev spectral methods have been used to discretize models in the horizontal, and have not been used to discretize an atmospheric model in the vertical. Rather, a Chebyshev-Galerkin method was used in solving a simpler but related problem, namely the vertical structure problem associated with vertical normal mode transforms. The results of transforming observed tropical forcing profiles show that the forcing of the mass field occurs primarily for vertical modes with phase speeds in the range 30-300 ms^{-1}, while significant forcing of the wind field occurs for phase speeds as low as 7-8 ms^{-1}. Sensitivity studies indicate that spectral space profiles in terms of the phase speed c are relatively independent of the truncation N and the assumed top pressure p_T used, but that significant aliasing onto the first few modes can occur if the physical space profile is not sampled at optimum levels.

While this study sheds some light on how to apply spectral methods to limited area models, many questions remain. The application of boundary conditions in the tau and collocation methods should be examined in detail to determine why the collocation method is less accurate in the one-dimensional shallow water model, and to see whether this is a special case or a problem with the method in general. A variety of explicit time differencing schemes should be compared in detail for accuracy and efficiency, to see if there is a "best" scheme for Chebyshev spectral models; in particular, fourth order schemes should be considered. The representation of dissipative processes in Chebyshev models should also be investigated. Most of these topics can be addressed using the models developed for this study; however, more realistic test cases should be considered, including some in which the

solutions are not particularly smooth. Finally, the use of Chebyshev spectral techniques for the vertical discretization in atmospheric models should be investigated.

As a final remark, we note that the spectral techniques considered in this study are so accurate that they may be too accurate to be of much use in some limited area models. As stated previously, one of the fundamental problems in limited area modeling is to minimize the impact of computationally imposed boundaries. The numerical examples presented here suggest that errors due to inexact specification of boundary conditions and boundary values may be much larger than spectral discretization errors. In more complicated models, especially those intended for operational use in forecasting, additional sources of error are present, such as the specification of initial fields and the representation of small-scale physical processes such as cumulus precipitation. Chebyshev spectral methods probably allow such problems to be solved much more accurately than they can be specified at present. Spectral methods may effectively eliminate discretization errors from limited area models; much more work is needed to reduce the other sources of error.

REFERENCES

Abramowitz, M., and I. Stegun, 1964: Handbook of Mathematical Functions. Dover edition, 1965, Dover, New York, 1046 pp.

Atkinson, K. A., 1978: An Introduction to Numerical Analysis. Wiley, New York, 587 pp.

Bayliss, A., and E. Turkel, 1980: Radiation boundary conditions for wave-like equations. Comm. Pure Appl. Math., 23, 707-725.

Béland, M., J. Côté and A. Staniforth, 1983: The accuracy of a finite-element vertical discretization scheme for primitive equation models: comparison with a finite-difference scheme. Mon. Wea. Rev., 111, 2298-2318.

Bennett, A. F., 1976: Open boundary conditions for dispersive waves. J. Atmos. Sci., 33, 176-182.

Birkhoff, G., C. de Boor, B. Swartz and B. Wendroff, 1966: Rayleigh-Ritz approximation by piecewise cubic polynomials. SIAM J. Numer. Anal., 3, 188-203.

Bourke, W., B. McAvaney, K. Puri and R. Thurling, 1977: Global modeling of atmospheric flow by spectral methods. In Methods in Computational Physics, 17, Academic Press, New York, 267-324.

Boyd, J. P., 1978: The choice of spectral functions on a sphere for boundary and eigenvalue problems: A comparison of Chebyshev, Fourier and associated Legendre expansions. Mon. Wea. Rev., 106, 1184-1191.

Brandt, A., 1977: Multi-level adaptive solutions to boundary-value problems. Math. Comp., 31, 333-390.

Brandt, A., S. R. Fulton and G. D. Taylor, 1984: Improved spectral multigrid methods for periodic elliptic problems. J. Comp. Phys., in press.

Brigham, E. O., 1974: The Fast Fourier Transform. Prentice-Hall, Englewood Cliffs, NJ, 252 pp.

Chapman, S., and R. S. Lindzen, 1970: Atmospheric Tides. Gordon and Breach, New York, 200 pp.

Chu, J.-H., M. Yanai and C.-H. Sui, 1981: Effects of cumulus convection on the vorticity field in the tropics. Part I: The large-scale budget. J. Meteor. Soc. Japan, 59, 535-546.

Ciarlet, P. G., M. H. Schultz and R. S. Varga, 1968: Numerical methods of high-order accuracy for nonlinear boundary value problems, III. Eigenvalue problems. Numer. Math., 12, 120-133.

Cooley, J. W., P. A. W. Lewis and P. D. Welch, 1970: The Fast Fourier Transform algorithm: programming considerations in the calculation of sine, cosine and Laplace transforms. J. Sound Vib., 12, 315-337.

Courant, R., and D. Hilbert, 1953: Methods of Mathematical Physics, volume 1. Wiley-Interscience, New York, 561 pp.

Courant, R., and D. Hilbert, 1962: Methods of Mathematical Physics, volume 2. Wiley-Interscience, New York, 830 pp.

Cullen, M. J. P., 1974: Integration of the primitive equations on a sphere using the finite element method. Quart. J. Roy. Meteorol. Soc., 100, 555-562.

Daley, R., 1979: The application of non-linear normal mode initialization to an operational forecast model. Atmosphere-Ocean, 17, 97-124.

Daley, R., 1981: Normal mode initialization. Rev. Geophys. Space Phys., 19, 450-468.

de Boor, C., 1978: A Practical Guide to Splines. Springer-Verlag, New York, 392 pp.

DeMaria, M., and W. H. Schubert, 1984: Experiments with a spectral tropical cyclone model. J. Atmos. Sci., 41, 901-924.

Eliasen, E., B. Machenhauer and E. Rasmussen, 1970: On a numerical method for integration of the hydrodynamical equations with a spectral representation of the horizontal fields. Report No. 2, Institut for Teoretisk Meteorologi, Kobenhavns Universitet, 35 pp.

Elvius, T., and A. Sundström, 1973: Computationally efficient schemes and boundary conditions for a fine-mesh barotropic model based on the shallow-water equations. Tellus, 25, 132-156.

Engquist, B., and A. Majda, 1977: Absorbing boundary conditions for the numerical simulation of waves. Math. Comp., 31, 629-651.

Esbensen, S. K., E. I. Tollerud and J.-H. Chu, 1982: Cloud-cluster-scale circulations and the vorticity budget of synoptic-scale waves over the eastern Atlantic intertropical convergence zone. Mon. Wea. Rev., 110, 1677-1692.

Esbensen, S. K., and K. V. Ooyama, 1983: An objective anlaysis of temperature and relative humidity data over the B and A/B ship arrays during Phase III of GATE. Available from S.K. Esbensen, Department of Atmospheric Sciences, Oregon State University, Corvallis, OR, 97331, 87 pp.

Fox, D. G., and S. A. Orszag, 1973: Pseudospectral approximation to two-dimensional turbulence. J. Comp. Phys., 11, 612-619.

Fox, L., and I. B. Parker, 1968: Chebyshev Polynomials in Numerical Analysis. Oxford University Press, London, 205 pp.

Francis, P. E., 1972: The possible use of Laguerre polynomials for representing the vertical structure of numerical models of the atmosphere. Quart. J. Roy. Meteorol. Soc., 98, 662-667.

Fulton, S. R., and W. H. Schubert, 1980: Geostrophic adjustment in a stratified atmosphere. Atmos. Sci. Paper No. 326, Department of Atmospheric Science, Colorado State University, Fort Collins, CO, 80523, 97 pp.

Fulton, S. R., and G. D. Taylor, 1984: On the Gottlieb-Turkel time filter for Chebyshev spectral methods. J. Comp. Phys., 55, 302-312.

Galerkin, B. G., 1915: Rods and Plates. Series occurring in various questions concerning the elastic equilibrium of rods and plates. Vestnik Inzhenerov, 19, 897-908 (translation 63-18924, Clearinghouse, Fed. Sci. Tech. Info., Springfield, VA).

Gazdag, J., 1976: Time-differencing schemes and transform methods. J. Comp. Phys., 20, 196-207.

Geisler, J. E., and D. E. Stevens, 1982: On the vertical structure of damped steady circulation in the tropics. Quart. J. Roy. Meteorol. Soc., 108, 87-93.

Gill, A. E., 1980: Some simple solutions for heat-induced tropical circulation. Quart. J. Roy. Meteor. Soc., 106, 447-462.

Gottlieb, D., and S. A. Orszag, 1977: Numerical Analysis of Spectral Methods. NSF-CBMS Monograph No. 26, NTIS No. AD-A056 922, Soc. Ind. and Appl. Math., Philadelphia, 172 pp.

Gottlieb, D., and E. Turkel, 1980: On time discretizations for spectral methods. Stud. Appl. Math., 63, 67-86.

Hack, J. J., and W. H. Schubert, 1981: Lateral boundary conditions for tropical cyclone models. Mon. Wea. Rev., 109, 1404-1420.

Haidvogel, D. B., 1979: Resolution of downstream boundary layers in the Chebyshev approximation to viscous flow problems. J. Comp. Phys., 33, 313-324.

Haidvogel, D. B., and T. Zang, 1979: The accurate solution of Poisson's equation by expansion in Chebyshev polynomials. J. Comp. Phys., 30, 167-180.

Haidvogel, D. B., A. R. Robinson and E. E. Schulman, 1980: The accuracy, efficiency, and stability of three numerical models with application to open ocean problems. J. Comp. Phys., 34, 1-53.

Haltiner, G. J., and R. T. Williams, 1980: Numerical Prediction and Dynamic Meteorology, second edition. John Wiley and Sons, New York, 477 pp.

Hoskins, B. J., 1973: Comments on "The possible use of Laguerre polynomials for representing the vertical structure of numerical models of the atmosphere" by P. E. Francis. Quart. J. Roy Meteorol. Soc., 99, 571-572.

Hussaini, M. Y., C. L. Streett and T. A. Zang, 1983: Spectral methods for partial differential equations. ICASE Report No. 83-46, Institute for Computer Applications in Science and Engineering, NASA Langley Research Center, Hampton, VA 23665, 62 pp.

Israeli, M., and S. A. Orszag, 1981: Approximation of radiation boundary conditions. J. Comp. Phys., 41, 115-135.

Jacobs, S. J., and A. Wiin-Nielsen, 1966: On the stability of a barotropic basic flow in a stratified atmosphere. J. Atmos. Sci., 23, 682-687.

Johnson, O. G., 1969: Error bounds for Sturm-Liouville eigenvalue approximations by several piecewise cubic Rayleigh-Ritz methods. SIAM J. Numer. Anal., 6, 317-333.

Kasahara, A., and K. Puri, 1981: Spectral representation of three-dimensional global data by expansion in normal mode functions. Mon. Wea. Rev., 109, 37-51.

Kasahara, A., and Y. Shigehisa, 1983: Orthogonal vertical normal modes of a vertically staggered discretized atmospheric model. Mon. Wea. Rev., 111, 1724-1735.

Kurihara, Y., 1965: On the use of implicit and iterative methods for the time integration of the wave equation. Mon. Wea. Rev., 93, 33-46.

Lamb, H., 1932: Hydrodynamics, sixth ed. Dover ed. (1945), New York, 732 pp.

Lanczos, C., 1938: Trigonometric interpolation of empirical and analytical functions. J. Math. Phys., 7, 123-199.

Lanczos, C., 1956: Appied Analysis. Prentice-Hall, Englewood Cliffs, NJ.

Lanczos, C., 1973: Legendre versus Chebyshev polynomials. In Topics in Numerical Analysis, J. J. Miller, ed., Academic Press, New York, 191-201.

Lilly, D. K., 1965: On the computational stability of numerical solutions of time-dependent non-linear geophysical fluid dynamics problems. Mon. Wea. Rev., 93, 11-26.

Lindzen, R. S., 1967: Planetary waves on beta-planes. Mon. Wea. Rev., 95, 441-451.

Machenhauer, B., 1979: The Spectral Method. In Numerical Methods Used in Atmospheric Models, vol. 2, GARP Publication Series No. 17, WMO/ICSU, 121-275.

Machenhauer, B., and R. Daley, 1972: A baroclinic primitive equation model with a spectral representation in three dimensions. Report No. 4, Institut for Teoretisk Meteorologi, Kobenhavns Universitet, 62 pp.

McCrory, R. L., and S. A. Orszag, 1980: Spectral methods for multi-dimensional diffusion problems. J. Comp. Phys., 37, 93-112.

Merilees, P. E., and S. A. Orszag, 1979: The pseudospectral method. In Numerical Methods Used in Atmospheric Models, vol. 2, GARP Publication Series No. 17, WMO/ICSU, 276-299.

Mesinger, F., and A. Arakawa, 1976: Numerical Methods Used in Atmospheric Models, vol. 1. GARP Publication Series No. 17, WMO/ICSU, 64 pp.

Oliger, J., and A. Sundström, 1978: Theoretical and practical aspects of some initial boundary value problems in fluid dynamics. SIAM J. Appl. Math., 35, 419-446.

Orlanski, I., 1976: A simple boundary condition for unbounded hyperbolic flows. J. Comp. Phys., 21, 251-269.

Orszag, S. A., 1970: Transform method for the calculation of vector-coupled sums: application to the spectral form of the vorticity equation. J. Atmos. Sci., 27, 890-895.

Orszag, S. A., 1971a: Galerkin approximations to flows within slabs, spheres, and cylinders. Phys. Rev. Lett., 26, 1100-1103.

Orszag, S. A., 1971b: Numerical simulation of incompressible flows within simple boundaries. I. Galerkin (spectral) representations. Stud. Appl. Math., 50, 293-327.

Orszag, S. A., 1971c: Numerical simulation of incompressible flows within simple boundaries: accuracy. J. Fluid Mech., 49, 75-112.

Orszag, S. A., 1972: Comparison of pseudospectral and spectral approximation. Stud. Appl. Math., 51, 253-259.

Orszag, S. A., 1974: Fourier Series on Spheres. Mon. Wea. Rev., 102, 56-75.

Orszag, S. A., 1980: Spectral methods for problems in complex geometries. J. Comp. Phys., 37, 70-92.

Orszag, S. A., and M. Israeli, 1974: Numerical simulation of viscous incompressible flows. Ann. Rev. Fluid Mech., 6, 281-318.

Pearson, R. A., 1974: Consistent boundary conditions for numerical models of systems that admit dispersive waves. J. Atmos. Sci., 31, 1481-1489.

Peters, G., and J. H. Wilkinson, 1969: Eigenvalues of $Ax=\lambda Bx$ with band symmetric A and B. Comp. Journal, 12, 398-404.

Pierce, J. G., and R. S. Varga, 1972: Higher order convergence results for the Rayleigh-Ritz method applied to eigenvalue problems. I: Estimates relating Raleigh-Ritz and Galerkin approximations to eigenfunctions. SIAM J. Numer. Anal., 9, 137-151.

Phillips, N. A., 1959: An example of nonlinear computational instability. In The Atmosphere and the Sea in Motion. Rockefeller Institute Press, New York, 501-504, 509 pp.

Prenter, P. M., 1975: Splines and Variational Methods. Wiley, New York, 323 pp.

Rivlin, T., 1969: An Introduction to the Approximation of Functions. Dover, New York, 150 pp.

Schubert, W. H., J. J. Hack, P. L. Silva Dias and S. R. Fulton, 1980: Geostrophic adjustment in an axisymmetric vortex. J. Atmos. Sci., 37, 1464-1484.

Schubert, W. H., G. D. Taylor, S. R. Fulton and M. DeMaria, 1984: A Chebyshev spectral method for boundary-layer models. Arch. Met. Geoph. Biocl., Ser. A, in press.

Schubert, W. H., and M. DeMaria, 1984: Axisymmetric, primitive equation, spectral hurricane model. J. Atmos. Sci., in press.

Siebert, M., 1961: Atmospheric tides. In Advances in Geophysics, 7, 105-187.

Silva Dias, P. L., W. H. Schubert and M. DeMaria, 1983: Large-scale response of the tropical atmosphere to transient convection. J. Atmos. Sci., 40, 2689-2707.

Sneddon, I. N., 1972: The Use of Integral Transforms. McGraw-Hill, New York, 539 pp.

Snyder, M. A., 1966: Chebyshev Methods in Numerical Approximation. Prentice-Hall, Englewood Cliffs, NJ, 109 pp.

Stakgold, I., 1979: Green's Functions and Boundary Value Problems. Wiley, New York, 638 pp.

Staniforth, A. N., and H. L. Mitchell, 1977: A semi-implicit finite-element barotropic model. Mon. Wea. Rev., 105, 154-169.

Staniforth, A. N., and R. W. Daley, 1977: A finite-element formulation for the vertical discretization of sigma-coordinate primitive equation models. Mon. Wea. Rev., 105, 1108-1118.

Stoer, J., and R. Bulirsch, 1980: Introduction to Numerical Analysis. Springer-Verlag, New York, 609 pp.

Strang, G. W., and G. J. Fix, 1973: An Analysis of the Finite Element Method. Prentice-Hall, Englewood Cliffs, NJ, 306 pp.

Sui, C.-H., and M. Yanai, 1984: Vorticity budget of the GATE A/B area and its interpretation. Proceedings of the 15th Conference on Hurricanes and Tropical Meteorology, Miami, January 9-13, 1984. American Meteorological Society.

Taylor, G. I., 1936: The oscillations of the atmosphere. Proc. Roy. Soc., A156, 318-326.

Temperton, C., 1983a: Self-sorting mixed-radix fast Fourier transforms. J. Comp. Phys., 52, 1-23.

Temperton, C., 1983b: A note on prime factor FFT algorithms. J. Comp. Phys., 52, 198-204.

Temperton, C., 1983c: Fast mixed-radix real Fourier transforms. J. Comp. Phys., 52, 340-350.

Wurtele, M. G., J. Paegle and A. Sielecki, 1971: The use of open boundary conditions with the storm-surge equations. Mon. Wea. Rev., 99, 537-544.

Wendroff, B., 1965: Bounds for eigenvalues of some differential operators by the Rayleigh-Ritz method. Math. Comp., 19, 218-224.

Wiin-Nielsen, A., 1971a: On the motion of various vertical modes of transient, very long waves, part I. Beta plane approximation. Tellus, 23, 87-98.

Wiin-Nielsen, A., 1971b: On the motion of various vertical modes of transient, very long waves, part II. The spherical case. Tellus, 23, 207-217.

Yanai, M., S. Esbensen and J.-H. Chu, 1973: Determination of bulk properties of tropical cloud clusters from large-scale heat and moisture budgets. J. Atmos. Sci., 30, 611-627.

Yanai, M., J.-H. Chu, T. E. Stark and Ts. Nitta, 1976: Response of deep and shallow tropical maritime cumuli to large-scale processes. J. Atmos. Sci., 33, 976-991.

Young, J. A., 1968: Comparative properties of some time differencing schemes for linear and nonlinear oscillations. Mon. Wea. Rev., 96, 357-364.

Zang, T. A., Y. S. Wong and M. Y. Hussaini, 1982: Spectral multigrid methods for elliptic equations. J. Comp. Phys., 48, 485-501.

Zang, T. A., Y. S. Wong and M. Y. Hussaini, 1984: Spectral multigrid methods for elliptic equations II. J. Comp. Phys., in press.